

Aus dem Bereich Theoretische Medizin und Biowissenschaften,
der Medizinischen Fakultät der Universität des Saarlandes,
Homburg/Saar

**Modeling the Effects of Nanoparticles on Neuronal Cells:
From Ionic Channels to Network Dynamics**

*Dissertation zur Erlangung des Grades eines
Doktors der theoretischen Medizin und Biowissenschaften
an der Medizinischen Fakultät
der Universität des Saarlandes
2014*

vorgelegt von:

Dipl.-Wirtsch.-Ing.(FH) Michael Busse, M.Sc.

geb. am: 11. Februar 1980 in Saarbrücken, Deutschland

Dekan: Prof. Dr. med. Michael D. Menger

Referent: Prof. Dr. rer. nat. Dr. rer. med. Daniel J. Strauss

Auf den Schultern von Riesen

...dedicated to my passed away mother

Abstract

Background: Besides the promising application potential of nanotechnologies in engineering, the use of nanomaterials in medicine is growing. New therapies employing innovative nanocarrier systems to increase specificity and efficacy of drug delivery schemes to reach non-operable structures are already in clinical trials. However the influence of the nanoparticles (NPs) themselves is still unknown in medical applications, especially for complex interactions in least investigatable neural systems. The aim of this study was to investigate *in vitro* effects of coated silvernanoparticles (cAg-NPs) on the excitability of single neuronal cells and to integrate those findings into an *in silico* model to predict possible effects from single cells up to neuronal circuits and finally to neural field potentials generated by those circuits.

Methods: First, patch-clamp measurements were performed to investigate the effects of nano-sized silver particles, surrounded by an organic coating, on excitability of single cells. Second, it was determined which parameters were altered by exposure to those nanoparticles using the Hodgkin-Huxley model of the sodium current. As a third step those findings were integrated into a well defined neuronal circuit of thalamocortical interactions to predict possible changes in network signaling due to the applied cAg-NPs, *in silico*. Fourthly, the model was extended to observe neural fields originating from Hodgkin-Huxley type neurons. Therefore it was investigated how the neural field potentials influence the spike generation in neurons that are physically located within these fields, if this feedback causes relevant changes in the underlying neuronal signaling within the circuit, and most important if the cAg-NPs effects on single neurons of the network are strong enough to cause observable changes in the generated field potentials themselves.

Results: A rapid suppression of sodium currents was observed after exposure to cAg-NPs in the *in vitro* recordings. In numerical simulations of sodium currents the parameters most likely affected by cAg-NPs were identified. The effects of such changes on the activity of networks were then examined. *In silico* network modeling indicated effects of local cAg-NP application on firing patterns in all neurons in the circuit. It has been shown that field potentials have strong effects on the action potential generation of neurons that are exposed to those fields. Furthermore, it was also shown that this is also affecting the underlying neuronal signaling. The assumed cAg-NPs presence in the circuit's thalamic cells were finally found to also have distinctive effects on the emerging

neural field potentials.

Conclusion: The sodium current measurements and simulations show that suppression of sodium currents by cAg-NPs results primarily in a reduction in the current amplitude right after a few seconds of particle addition. The network simulations on larger scale show that locally cAg-NPs induced changes result in diversification of activity in the entire circuit. This was also found for the field potential simulations on a more larger scale. The results indicated that local application of cAg-NPs may influence the activity throughout the network and may cause distortions in cortical field potentials *in vivo*. This multiscale model may subserve as basic approach to estimate the NPs affected spatiotemporal dynamics of cortical field potentials on a very small cortical patch. The electrophysiological detection of this simulated effect by utilizing the voltage sensitive dyes technique is part of the future work that will be carried out by the group "Systems Neuroscience and Neurotechnology Unit".

Zusammenfassung

Hintergrund: Neben den vielversprechenden Anwendungsmöglichkeiten von Nanotechnologien in Ingenieurwissenschaften steigt die Verwendung von Nanomaterialien in medizinischen Anwendungen exponentiell. Neue Therapieformen, welche sich bereits in klinischen Tests befinden, bedienen sich innovativer Nanocarrier-Systeme um sowohl die Spezifität als auch die Effektivität von gezielter Pharmakotherapie zum Erreichen inoperabler Strukturen zu verbessern. Hinsichtlich medizinischer Anwendungen sind jedoch die physiologischen Einflüsse von Nanopartikeln (NPs) noch weitestgehend unbekannt, dies gilt vor allem im Hinblick auf komplexe Interaktionen solcher nanoskaliger Partikel mit nur schwer untersuchbaren neuronalen Systemen im Organismus. Das Ziel dieser Studie war die Untersuchung von *in vitro* Einflüssen von ummantelten Silber-Nanopartikeln (cAg-NPs) auf die Erregbarkeit einzelner neuronaler Zellen. Anschließend sollten diese Effekte in ein *in silico* Modell übertragen werden um mögliche Auswirkungen, angefangen bei Einzelzellen über neuronale Schaltkreise bis hin zu neuronalen Feldpotenzialen, welche durch diese Schaltkreise generiert werden, vorausszusagen.

Methoden: In einem ersten Schritt wurden Patch-Clamp Untersuchungen durchgeführt, mit Hilfe derer die Effekte nanoskaliger Silberpartikel mit organischer Ummantelung auf die elektrophysiologische Erregbarkeit von einzelnen Zellen erforscht werden sollten. Im zweiten Schritt wurden unter Einbeziehung des elektrophysiologischen Modells von Hodgkin und Huxley für Natriumströme diejenigen (Modell-)Parameter bestimmt, welche durch die Hinzugabe von cAg-NPs verändert werden. Als drittes wurden diese Resultate in ein etabliertes Modell thalamo-kortikaler Interaktion integriert, um damit mögliche cAg-NPs basierte Veränderungen in der korrespondierenden Netzwerkkommunikation vorherzusagen. Im vierten Schritt erfolgte die Erweiterung des entwickelten Modells um die Simulation neuronaler Feldpotenziale, welche durch die Hodgkin-Huxley Neuronen des oben aufgeführten Modells verursacht werden. Zu diesem Zweck wurde untersucht, wie neuronale Feldpotenziale das Feuerverhalten von Neuronen, welche physisch in den generierten Feldern gelegen sind, beeinflussen. Die Frage, ob dieses Feedback relevante Veränderungen in den unterliegenden neuronalen Kommunikation innerhalb des Schaltkreises hervorruft wurde genauso adressiert wie schließlich die Fragestellung, ob die durch cAg-NPs verursachten Effekte auf einzelne thalamische Zellen ausreichen, um tatsächlich Veränderungen in den höherskaligen kortikalen Feldpotenzialen hervorzurufen.

Ergebnisse: Nach der Zugabe von cAg-NPs konnte *in vitro* eine schnelle Suppression der Natriumströme beobachtet werden. Die numerische Simulation von Natriumkanälen ließ die Identifizierung von denjenigen Hodgkin-Huxley Parametern zu, welche durch die cAg-NPs beeinträchtigt wurden. Nachfolgend konnten auf dieser Basis die Effekte der NPs induzierten Änderungen der Aktivität von Zellnetzwerken im Modell untersucht werden. Das entwickelte *in silico* Neuronenmodell war in der Lage, die Effekte durch die lokale cAg-NPs Applikation (ausschließlich thalamische Zellen) im Netzwerk auf das Feuerverhalten aller im Schaltkreis befindlichen Neuronen abzubilden. Weiter konnte gezeigt werden, dass Feldpotenziale einen starken Einfluss auf die Generierung von Aktionspotenzialen von Neuronen haben, welche innerhalb dieser Feldern lokalisiert sind und dass sich diese Beeinflussung ebenfalls auf die neuronale Reizweiterleitung im gesamten Neuronenverbund auswirkt. Schließlich konnte anhand des um neuronale Feldpotenziale erweiterten Modells auch gezeigt werden, dass die angenommene lokale cAg-NPs Präsenz im Schaltkreis eindeutig observierbare Effekte auf die höherskaligen neuronalen Feldpotenziale haben.

Zusammenfassung: Die elektrophysiologischen Messungen, wie auch die Simulation von Natriumströme haben gezeigt, dass die cAg-NPs bedingte Suppression sich primär in einer Reduktion der Amplitude dieser Ströme wenige Sekunden nach Zugabe der Partikel darstellt. Die höherskaligen Simulationen von Netzwerkkommunikation und Feldpotenzialen offenbaren, dass eine lokale, cAg-NPs bedingte Modifikation des Feuerverhaltens weniger Zellen eine Änderung des gesamten neuronalen Schaltkreises und der damit korrespondierenden neuronalen Feldpotenziale zur Folge hat. Bezüglich einer Transferierung dieser Ergebnisse *in vivo* indizieren diese, dass die lokale Applikation von cAg-NPs die Aktivität des gesamten Netzwerks beeinflussen kann und dies könnte eine Verzerrung damit verbundener kortikaler neuronaler Feldpotenziale bedingen. Das entwickelte Multiskalenmodell stellt somit eine erste grundlegende Methode dar, um die NPs bedingte Änderung der Dynamik kortikaler Feldpotenziale eines sehr kleinen Kortexausschnitts abzuschätzen. Eine elektrophysiologische Erfassung dieses simulierten Effekts unter Nutzung von Voltage Sensitive Dyes im Tiermodell ist Ziel der Folgearbeiten innerhalb der Arbeitsgruppe "Systemische Neurowissenschaften und Neurotechnologie Unit".

Notation

ADHD	attention deficit hyperactivity disorder
ADP	afterdepolarization
AEP	auditory evoked potential
Ag	silver
Ag ⁺	silver-ions
Ag-NPs	silver-nanoparticles
AHP	after hyperpolarization
AMPA	α -amino-3-hydroxyl-5-methyl-4-isoxazole-propionate
AP	action potential
cAg-NPs	coated silvernanoparticles
C_m	membrane capacitance
CuO	copperoxide
DE	differential evolution
EEG	electroencephalography
FS	fast spiking
GABA _A	γ -aminobutyric acid-A
GABA _B	γ -aminobutyric acid-B
GPi	internal segment of the globus pallidus
G-protein	guanine nucleotide-binding protein
HH-model	Hodgkin-Huxley-Model
I_{Ca}	calcium current
I_D	dendritic current
I_K	potassium current

I_{K-AHP}	long-lasting calcium-dependent AHP potassium current
I_{K-C}	calcium-dependent potassium current
I_{K-DR}	delayed rectifier potassium current
IN	interneuron
I_{Na}	sodium-current
I_S	somatic current
ISI	interspike interval
I_{SYN}	synaptic current
LFP	local field potential
MUA	multi unit activity
Na^+	sodium-ions
NMDA	N-methyl-D-aspartate
NPs	Nanoparticles
NSTC	non-specific thalamic cell
ODE	ordinary differential equation
PDE	partial differential equation
PIR	post-inhibitory rebound
PY	pyramidal neuron
RS	regular spiking
RTN	reticular thalamic nucleus
STC	specific thalamic cell
TC	thalamocortical
V_D	dendritic voltage
V_S	somatic voltage
ZnO	Zincoxide

Contents

Abstract	iv
Zusammenfassung	vi
Notation	viii
1 Introduction	1
1.1 Nanoparticles in Medicine	1
1.2 Computational Modeling	2
1.2.1 Single Neuron Models	2
1.2.2 Neuronal Circuit Models	4
1.2.3 Neural Field Oscillation Models	5
1.3 Contribution of this Work	9
2 Methodologies	13
2.1 Coated Silver-Nanoparticles	14
2.2 Chromaffin Cell Model	14
2.3 Patch-Clamp Measurements	15
2.4 HH fitting employing Differential Evolution Algorithm	16

2.5	Thalamocortical Interactions	19
2.6	The Llinás-Model as Basis for the developed Corticothalamic Network	20
2.7	The Applied Thalamocortical Network	22
2.8	The Amari Neural Field Model	44
2.9	Linking Hodgkin-Huxley Neuronal Circuit Activity to Neural Field Potentials	46
2.10	Backpropagation of the Neural Field Potentials on the Cortical Neurons	48
3	Results	51
3.1	cAg-NPs Effects on Neuronal Cells <i>in vitro</i> and <i>in silico</i>	51
3.2	cAg-NPs Effects on the chosen Neuronal Feedback Circuit	56
3.3	cAg-NPs Effects on 2D Neural Field Oscillations	58
4	Discussion	69
4.1	cAg-NPs Effects on Neuronal Cells <i>in vitro</i> and <i>in silico</i>	69
4.2	cAg-NPs Effects on the Neuronal Feedback Circuit	70
4.3	cAg-NPs Effects on 2D Neural Field Oscillations	70
5	Conclusion	74
	Bibliography	75
	List of Publications	86
	Acknowledgements	89
	Curriculum Vitae	91

Chapter 1

Introduction

1.1 Nanoparticles in Medicine

The areas of application of nanomaterials have increased in the last decade and are not easy to grasp any more. They range from the application in paints and cosmetics to textiles, foods, food grade packaging, and various other technical products. The use of nanomaterials in medicine is notable since it comes with high expectations and hopes for treatment of hitherto untreatable diseases. Nanoparticles (NPs) offer a wide range of sizes, morphologies, and surface features that assure potential implementation in drug delivery, diagnostics, and therapy (Gupta and Gupta 2005). A big challenge in current research is to overcome existing drug delivery barriers such as biomembranes and the blood-brain barrier employing nonviral vectors functioning at the nano-to-micro scale. Those systems could be utilized for the systemic delivery of drugs or genes to target cells for therapy of cancer, inflammation or for the intended modulation of neural activity in brain tissue, e.g., see Zhang et al. 2012; Lamarre and Ryadnov 2011.

Regarding nanotoxicology, research is in its infancy and many questions remain unanswered and unaddressed. Studies in biological systems show that the physical parameters of nanosized particles influence their non-specific absorption in cells and their potential to induce cellular responses (Chithrani et al. 2006). Existing studies provide limited information in terms of the cellular processes affected by exposure to NPs and their subsequent impact. To understand how NPs of different material, size, and geometry interact with cells it is necessary to explore the

1.2 Computational Modeling

NP-membrane interaction processes on the molecular scale, i.e., receptor-binding, endocytosis, and signaling activation (Jiang et al. 2008; Unfried et al. 2007). Regarding excitable cells, a starting point is the electrophysiological behavior of cells exposed to NPs. Recent nanotoxicology studies (Oberdörster 2010; El-Ansary and Al-Daihan 2009; Wijnhoven et al. 2009) identified (pure) silver nanoparticles (Ag-NPs) as potentially toxic in tissue, especially in neurons. Xu et al. 2009; Zhao et al. 2009b; Liu et al. 2009 examined the influence of nano-sized CuO, ZnO, and Ag on single neurons *in vitro* using the patch-clamp method. They observed effects of Ag-NPs on the amplitude and the time course of the sodium current (I_{Na}). The underlying mechanism of the changes in I_{Na} was not determined.

1.2 Computational Modeling

Mathematical and computational neuronal models are powerful and important tools for the exploration and the comprehension of the evolution and structure organization of the nervous system, and in particular the dynamic processes in mammalian brains. A wide spectrum of neuronal models have been developed within the last decades. They capture and describe processes ranging from single cell dynamics in the microscopic level, up to large-scale neuronal population activity. As models can be employed as bridges between different levels of complexity, they must be detailed enough to capture the dynamics at the lower level of complexity, yet simple enough to provide clear results at the higher level. Hence, the smart integration of single neuron models into large-scale computational network models possess the promise of boosting studies of the brain by providing potentialities to test hypotheses, while it simultaneously allows to employ models of complex biological processes where experiments are not longer feasible.

1.2.1 Single Neuron Models

The biophysically most meaningful mathematical representation of a single neuron was introduced by Alan Hodgkin and Andrew Huxley, developed in the 50s of last century, see Hodgkin and Huxley 1952. The so called Hodgkin-Huxley model

1.2 Computational Modeling

(HH-model), that combines a set of nonlinear ordinary differential equations, is suitable to exhibit the neuronal behavior and properties of the nerve cells depending on measurable electrophysiological parameters such as the maximal conductance, steady-state (in)activation functions and time constants and thus has the best spatiotemporal resolution (Hodgkin and Huxley 1952; Izhikevich 2004; Nelson 2004).

Such models are important not only because their parameters are biophysically meaningful and measurable, but they allow us to investigate issues related to synaptic integration, effects of dendritic morphology, the interplay between ionic currents, and other issues related to single cell dynamics (Hodgkin and Huxley 1952). Because of its complex formalism, the disadvantage of this model in the recent years was that its calculation is of extremely high computational cost (1200 operations/1ms), hence, it is time consuming. But since computational power increases steadily, this one returns and moves more and more into the focus of modern modeling for questions where largest spatiotemporal resolutions are needed, see Hodgkin and Huxley 1952; Izhikevich 2004; Nelson 2004 for detailed discussions.

Although more than 50 years after Hodgkin and Huxley analyzed the squid axon, simple neuron models still offer surprises, many following studies criticized that the standard Hodgkin-Huxley formalism neglect the neuron's spatial structure and focus entirely on how its various ionic currents contribute to sub threshold behavior and spike generation (Izhikevich 2004; Rinzel and Ermentrout 1989; Herz et al. 2006). Therefore, in order to analyze the behavior of the cell precisely, it is sometimes useful to consider the different parts of the neuron separately, i.e., via compartmental models. One of the significant and more realistic models that were also applied for the pyramidal neurons (PY) in this study's utilized circuit is the mathematical two compartment model of the HH-formalism, which consists of the dendrite and the soma plus axonal initial segments described in (Pinsky and Rinzel 1994). In this model, the dendrite receives synaptic inputs and is coupled to the soma where the neuron's response is generated (Herz et al. 2006). As a consequence, this model is also able for the exploration of how neurons adapt their intrinsic properties to represent stimuli (Stemmler and Koch 1999).

Up to now, there are also a couple of other single neuron models that have shown to be valid to fit neural firing patterns from (*in vivo* and *in vitro*) recordings in different spatial resolutions. Clearly, the challenge for all such studies is to find the least complex neuron model with which the observed phenomena can

1.2 Computational Modeling

still be recreated (Herz et al. 2006). However, since most of those models are preferably developed to mimic the more macroscopic effects of neuronal firing by concomitantly neglecting paying attention to smaller details, these techniques are not discussed within this thesis. Please follow Izhikevich 2007 for a detailed discussion of such models.

1.2.2 Neuronal Circuit Models

Extensive synaptic connectivity is a characteristic property of neural circuitry: an exemplary neuron, for instance, which is located in the mammalian neocortex, receives thousands of synaptic inputs. The computational potential of such connectivity can be explored by analysis and simulations of network models (Dayan and Abbott 2001). Detailed investigations on cerebral neuronal circuits have provided further evidence that these circuits exhibit fascinating stereotypical characteristics, but that these stereotypical circuit patterns are quite complex (Gupta et al. 2000; Thomson et al. 2002; Gupta 2003). The reason for this complexity originates from the fact that stereotypical cortical microcircuits are composed of a fairly large number of different types of neurons and synapses that are combined in rather regular circuit patterns. In terms of numerical modeling, this provides in addition the challenge to accomplish the organization of computations in such complex microcircuits. Therefore it needs to be addressed how the variety of those microcircuits' components and their connection patterns complexity could contribute - or even be elemental - for the enormous computational power of biological neural systems.

At present time it seems to be hopeless to analyze realistic models for biological neural microcircuits including all elements that are known to play a functional key role within those by theoretical methods. However, computer simulations provide the most promising tool for that challenge (Natschläger et al. 2003; Faber 2011). They are very helpful for deducing causal connections and testing hypotheses about individual aspects of neuronal processing and interactions.

As introduced in the subsections before, mathematical models allow neuronal processes to be studied at several scales, from molecular interactions over single neural models up to communication in neuronal circuits. The critical decision when creating such simulation tools is again determining the right balance between

1.2 Computational Modeling

detail and abstraction and in terms of multiscale modeling how to connect scale specific models.

Taken now the advantage of a biologically high resolved neuron model like the one introduced by Hodgkin and Huxley, modern computer technology makes it possible to interconnect such neuron models into a neuronal circuit (even though the required computational power is expected to be huge).

Detailed anatomical and physiological studies about the neural interactions of particular networks discovered the intrinsic variables (synaptic interconnectivity, transmitter release processes, reaction times) that open the door for the consideration of building a biophysically meaningful computational model of those.

A neuronal circuitry that gained a lot of attention in the last decades and that is therefore well explored is the thalamocortical loop system, studied to explore conscious states in the brain and the famous 'binding problem' (a detailed description can be found in subsection 2.5 in the methods part). Models of consciousness that attribute a role to the thalamic system are no recent development. Almost 30 years ago, Crick 1984 offered one of the first hypotheses about consciousness, the so called *thalamic searchlight hypothesis*. This hypothesis described for the first time that the thalamus is in charge to control which region of the cortex becomes the focal point for consciousness. Ten years later, a similar but more sophisticated idea has been proposed by Llinás and Ribary 1993 and Llinás et al. 1994 which hypothesized that the oscillations of certain neurons in the thalamus serve as a sort of basic rhythm with which the cortical oscillations of the various sensory modalities synchronize themselves to form a unified image of the environment.

These thalamocortical loops have come to play an important role in practically all of the neurobiological theories that attempt to explain the higher states of consciousness. Therefore, and due to their wide acceptance in the scientific society, they were chosen to build the quantitative basis for the multiscale simulations on Ag-NPs cell-interactions that are discussed in this thesis.

1.2.3 Neural Field Oscillation Models

Accurately representing both the architecture and functions of the human cerebral cortex bears an interesting challenge; most of neuronal phenomena are not directly observable. Due to the complexity of neural networks, simplifications are applied

1.2 Computational Modeling

to their parameters, in order to keep neuronal representations as simple as possible with as little as possible compromising their realism. This can insofar be solved through a series connection of different modeling approaches. Here, each model would consider a different spatiotemporal scale, reaching from single ion channels over neurons up to neuronal populations and into neural fields, spike distributions or single elements, all pointed to describe the complex dynamics in neuronal activity (due to the interaction between different neuron types). One of the most singular breakthroughs in modeling the neuronal behavior was done by Hodgkin & Huxley, with their model of the giant squid neuron (Hodgkin and Huxley 1952), providing a quantitative description of membrane dynamics, most specifically current interactions due to ionic conductance. HH-single-neuron ensemble dynamics have been studied in the microscopic domain, showing for example, how sporadic firing is caused by background stochastic inputs (e.g., from brainstem spontaneous activity) and how uniform sensory inputs (i.e., constant synaptic currents) lead to a stable limit cycle dynamics and phase locking within the whole ensemble (Deco et al. 2008).

Spiking dynamics have also been implemented in similar one-compartment, point-source neuronal models as the leaky integrate-and-fire (LIF) (Knight 1972). Together, the HH and the LIF models, among others, have been the basis for studies based on spike-generating events. Due to the high computational requirements of modeling single-neuron ensembles (in particular HH), for investigations on larger scales, research focused only on the mean of their dynamics. In the past, neural mass modeling allows representing a large population of spiking neurons through a probability distribution function; the ensemble density of the population is replaced by a point mass (e.g., a delta function) and the dynamics are location-dependent. Moreover, temporary uncorrelated stochastic firing is reduced (e.g., ensemble mean dynamics are linearly stable).

Another approach is the study of neural fields. Unlike neural mass modeling, neural field models do not consider the neurons as single units, compartments or point sources, but instead they examine the macroscopic (e.g., a cortical layer, spatial gradients and horizontal spreading) result of the interaction within neuronal masses. Its field of study resides in a continuum (time-space) or field, in which neuronal dynamics such as depolarization can be observed. Parameters such as synaptic time, signal propagation, volume conduction, among others, become relevant for approaching EEG generation (according to the desired modeling scope) and are therefore used within neural field models (see Deco et al. 2008 for a

1.2 Computational Modeling

summary).

Both neural mass and field approaches are known as valid dimensional reductions, see Luck 2005 or David and Friston 2003 for detailed discussions of those. In such, the activity of the cortex is modeled based on the sum of synchronized neuron columns, instead of modeling each neuron by itself. To be mentioned here is the work done by Wilson and Cowan 1973, who established a concrete framework for spatiotemporal interaction of excitatory and inhibitory neurons; considering a two-dimensional layer with homogeneously distributed neurons (due to cortical columns providing redundancy, useful for data integrity). In such a planar array, both neuron types react in function of a distance-controlled lateral inhibition. As a consequence of recurrent excitatory iterations, three dynamical response modes were described: those were able to relate active transient behavior to sensorial activity (such as the primary visual cortex), oscillatory responses to thalamic neuron clusters and generation of EEG rhythms, and finally stable steady states of activity related to short term memory within prefrontal connections.

A few years later a simplified form of the neural field equation was proposed by Amari 1977, who studied the dynamics of excitation patterns in neural fields within both excitatory and inhibitory layers (as well as both excitatory and inhibitory neurons in a single, homogeneous layer). Lateral inhibition was implemented with predominant excitatory connections for proximate neurons and inhibitory connections with increasing distance. Amari discussed the interaction between excitation patterns, as well as the dynamic patterns within two-layered fields (oscillatory and traveling waves). His neural field equation presents a simple and basic model, yet accurate enough to represent neural field dynamics.

Since then, such framework has been used in a variety of ways; Freestone et al. 2011 developed a framework in which they tried to adjust a continuum neural field model (such as Amari 1977 and Wilson and Cowan 1973) to patient-specific clinical data (such as epilepsy surgery patients) through finite-element method of the neural field, transforming the PDE neural field equations into a finite-dimensional system. Applications of such works is seen in epilepsy treatment, by tracking parameter combinations that lead to seizures in the model and apply them for patients, hopefully preventing the onset of an attack. Pinpointing the mechanisms of abnormal excitatory and/or inhibitory behavior within the cortex (i.e., parametric estimation within such scenarios) would also allow for improved therapies. Prominent investigations on neural mass models were undertaken by da Silva et al. 1976 and Jansen and Rit 1995. They observed phase synchronization by coupling

1.2 Computational Modeling

two identical neuronal columns and alpha/beta oscillations by stimulating two different columns; Those researchers were also able to address the role of synaptic delay and inter-column connectivity on the appearance of evoked potentials within their model. As of lately, the Wilson-Cowan model, together with such neural mass models, have been thoroughly studied and used to describe localized neuronal populations, e.g., David and Friston 2003 in which a alpha-oscillatory model was expanded to produce rhythms ranging from the beta to the gamma band.

However, the Amari model for neural fields is still relevant and presents opportunities to implement cortical dynamics, and more specifically, to study the behavior of neural fields once the dynamics of neuronal masses are known (Potthast and beim Graben 2009; Doubrovinski and Herrmann 2009; Aram et al. 2013).

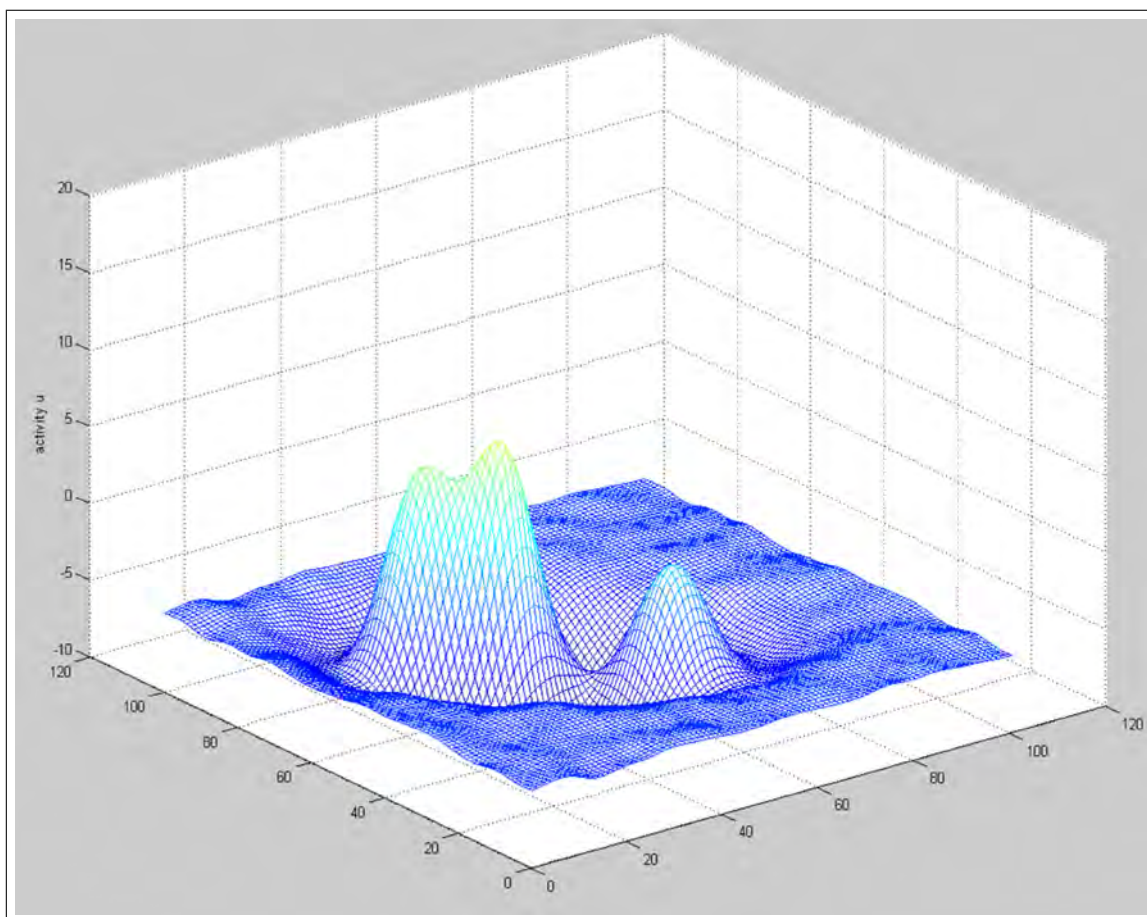


Figure 1.1: Example for a modeled neural field based on the equations of Amari 1977.

Figure 1.1 shows an example of an Amari modeled field at an example timepoint. One of the most common features describing neural field activity is the firing rate.

1.3 Contribution of this Work

It is represented usually as a sigmoidal function, not actually derived from biological properties but from physical convenience. Adding a coupling weight, defining a domain (e.g., cortical layer) and integrating over such domain leads to equations such as the ones proposed by Wilson and Cowan 1973 and Amari 1977. Interaction between neurons is mediated through firing rates, or explicitly through action potentials. As Roxin et al. 2011 studied, this firing rate has some interesting properties. A time-averaged firing rate distribution presents a non-linearity, which can be accounted as a biological inherent property of neuronal activity due to neuronal noise for example extracellular current elicited by the dynamics of the neuronal fields in which a cell is embedded, (which is now firmly believed to convey important information as well; it has been sometimes neglected for large-scale networks, thus making firing rate deterministic in nature). Such non-linearity produces a right-skewed, long-tailed Gauss-like distribution. Single-cell spike trains are highly non-linear (Poisson distributed) *in vivo*. Both *in vivo*, *in vitro*, and in neuronal models of neuronal networks (and both IF and conductance-based networks) present a skewed distribution due to noise contribution. Only in the case of linear synaptic inputs would a firing rate be represented by a normal distribution. This would be the case, e.g., when a constant input current is being injected to the neurons or for a randomly connected network where the number of neurons tend to infinity (central limit theorem).

1.3 Contribution of this Work

The main purpose of this work is to introduce for the first time a multiscale computational model to simulate the effects of NPs, which were applied to few single neurons at a small scale, on network rhythms, and finally on large scale neural field potentials.

Applying neuronal circuits that are located deep in the brain makes it impossible to observe and study those effects *in vivo* or *in vitro*. Moreover, as a basic approach to feed the computational model with data, this work was focused on the following question: are there instant observable effects in the electrophysiology of excitable cells when they are exposed to NPs and what kind of interaction mechanisms lead to such effects?

We have first taken a systems approach to the question what are the effects of NPs

1.3 Contribution of this Work

brought into contact to a few cells of a neuronal circuit on network activity of neuronal populations. To do so, patch-clamp recordings in neuroendocrine cells were carried out and the effects of coated silvernanoparticles (cAg-NPs) on excitability were examined. An established model of dynamic changes in membrane conductance was employed to model the observed changes in I_{Na} . Based on the fitting results, the observed changes in I_{Na} parameters in individual neurons were computationally reproduced. Later on, the work was focused on transferring the small scale findings into the next larger scale through testing the effects of the cAg-NPs induced changes in a neuronal network model. The outcome of this simplified *in silico* model served as initial approximation of *in vivo* neuromodulatory effects of cAg-NPs in neuronal circuits.

Subsequently the goal was to expand the quantitative model and take another step in spatial scale by adding the domain of neural field potentials that are generated by the applied neural circuitry. The model of neural field potentials focuses a very small cortical patch and includes the implementation of feedback loops from the largest spatial domain (neural field potentials) back to the smallest spatial scale (single neuron) in the model. This step also requires the transition from a discrete to a continuous domain and could be first time realized by the application of the biophysically most meaningful HH-model as elemental unit. As a consequence, the influence of the field potentials on single neurons can be adopted by the model in the best physiological way.

Based on this, the final approach was targeting to link together three computational models, each at a different spatial scale. Figure 1.2 depicts a schematic description of the final model's different scales.

More in detail, the HH-model of Hodgkin and Huxley 1952 describes the ionic current dynamics temporally in a single cell. The well explored neuronal circuit of Llinás and Ribary 1993; Llinás et al. 1994, 1998, 2002 is used to estimate the performance of the thalamocortical activity and finally the neural field model of Amari 1977 offers the corresponding spatiotemporal dynamics of field potentials. The field potentials caused by the neuronal generators (cortical pyramidal neurons) were estimated for the physical spot where every single generator is located and feed back to those neurons as an inhibitory or excitatory somatic current within the next time increment. These cortical cells are a part of the elaborate activity of synchronized thalamocortical columns at the quasi-microscopic level which is based on the model of Llinás and Ribary 1993; Llinás et al. 1994, 1998, 2002, where the involved neurons are gathered together in units. Indeed, these coupling are based

1.3 Contribution of this Work

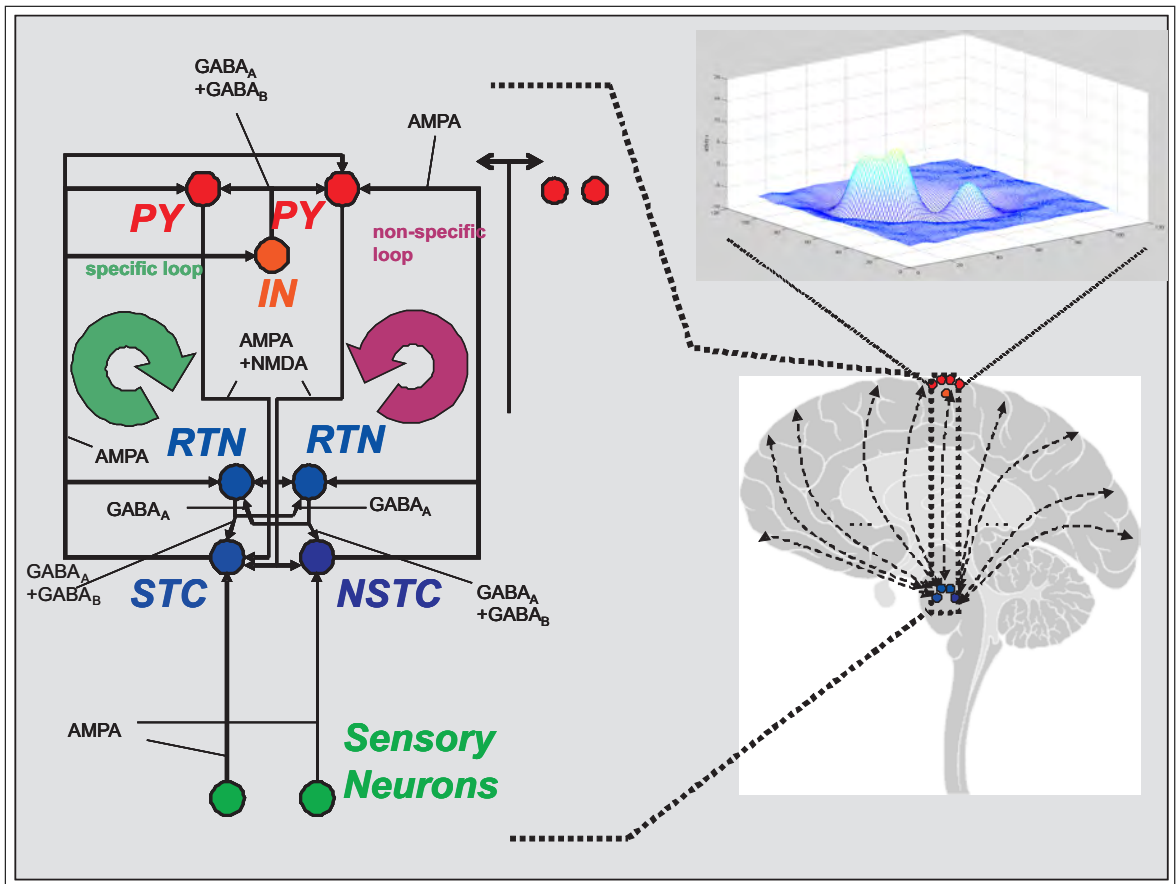


Figure 1.2: Schematic representation of the final models different scales: from single neuron up to the chosen neuronal circuit up to the cortical neural field potentials.

1.3 Contribution of this Work

on a two compartment scheme derived from the Hodgkin-Huxley model. The spatiotemporal field potential is converted into injected current to excite the somatic compartment of a cell model. After that, the somatic and dendritic activities are used as inputs for field estimations through the Amari field equation consisting of two homogenous layers. The resulting field area that reflects the network's activity is located within an exceedingly limited local domain.

Organization of the Work:

The information is organized as follows: In Chapter 2 the employed Nanoparticles, the applied chromaffin cells, as well as the conducted patch clamp measurements are explained. Also the algorithm for the Hodgkin-Huxley fitting process is presented here. Moreover, the explanation of thalamocortical interactions, the Llinás model as basis for the developed thalamocortical circuit, the applied thalamocortical network and the Amari neural field model are explained in this Chapter as well. Finally the linking of the Hodgkin-Huxley neural circuit activity to the neural field potentials as well as the already mentioned cyclical process of closing the feedback loop between neural field potentials and cortical neurons are described in Chapter 2. Chapter 3 presents then the results of the developed approach. This includes the NPs induced effects on neuronal cells from the *in vitro* patch-clamp recordings and their *in silico* simulations, the modeled NPs induced effects on the chosen neuronal feedback circuit and also the modeled effects of NPs on neuronal field oscillations. Chapter 4 offers a detailed discussion of the reported results. The conclusions as well as future works that can follow this study are finally proposed in Chapter 5.

Chapter 2

Methodologies

The first objective of the thesis was to determine the electrophysiological effects of cAg-NPs on single excitable cells. For this purpose Ag-NPs with an organic coating that prevents particle agglomeration and release of free Ag^+ , which is suitable for drug delivery were applied. Patch-clamp recordings on chromaffin-cells were carried out to evaluate the effects of cAg-NPs on the voltage gated sodium channels (isoform $\text{Na}_v1.7$). The Hodgkin-Huxley model of dynamic changes in membrane conductance was employed (Hodgkin and Huxley 1952) and this model was computationally fitted to the measured patch-clamp data. The utilization of the Differential-Evolution-Algorithm (DE) (Price et al. 2005) allowed an efficient fit of the model to the recorded data. As a consequence, changes in components of the HH-model were observed which shed light on the NPs-membrane interactions. The altered parameters were applied to modeled neurons within a neuronal feedback circuit. Thus the possible effects of those cAg-NPs on network dynamics were explored *in silico*, i.e., modeling intrinsic single cell dynamics and network oscillations in a circuit by reverting to an extended Hodgkin-Huxley-type formalism and dynamic synaptic coupling based on an example of the thalamocortical model introduced by Llinàs et al. (Llinàs and Ribary 1993; Llinàs et al. 1994, 1998, 2002) that served as theoretical fundament for the computational implementation. Consequently, the neuronal response dynamics of the network neurons assuming with and without the interference of cAg-NPs in specific and non-specific thalamic cells (STC/NSTC) and in reticular thalamic cells (RTN)(all of isoform $\text{Na}_v1.2$) could have been compared.

2.1 Coated Silver-Nanoparticles

cAg-NPs were prepared by thermal decomposition of silver oleate and stabilized by oleyamine. These hydrophobic NPs had a mean diameter of $5nm \pm 2nm$. The particles were capped with an amphiphilic polymer (Polyethylenglycol) for transfer in aqueous phase and steric stabilization, see Pellegrino et al. 2004 for further explanation. Prior to use, particles were suspended in ultrapure water and then filtered through a sterile $0.22\mu m$ membrane. ICP-AES (Horiba Jobin Yvon GmbH, Munich, Germany) determination found a total silver content of $1.3mMol$ in the resulting nanoparticle dispersion, including a fraction of $0.4\mu Mol$ free Ag^+ . The concentration and the type of molecules and ions on the particle surface lead to electrostatic interaction in the dilution medium and this changes the coated particles' hydrodynamic diameter to a mean value of $13nm \pm 2nm$ in pure water, $16nm \pm 4nm$ in Roswell Park Memorial Institute cell culture medium (Life Technologies, Carlsbad, CA, USA) (RPMI cell culture medium) and $9nm \pm 1nm$ in 10 x phosphate-buffered saline (PBS buffer solution)(Life Technologies). A Dyna Pro Titan instrument (Wyatt Technology Europe GmbH, Dernbach, Germany) was used to perform dynamic light scattering with a laser wavelength of $831nm$. The measured zeta-potential (Zetasizer Nano, Malvern Instruments, Malvern, UK) of the nanoparticles was $\sim 69mV$ in pure water (steric stabilized). Because the solution ingredients bind to the negatively charged particle surfaces, the zeta-potential was significantly reduced when dispersed in 10 x PBS buffer ($-6mV$) and RPMI medium ($-16mV$).

2.2 Chromaffin Cell Model

Chromaffin cells are neuroendocrine cells which are well characterized electrophysiologically and are ideally suited for voltage clamp analysis of membrane currents due to their small size and spherical shape (Fenwick et al. 1982; Kobayashi et al. 2002; Tischler 2002). The study focused on voltage-gated sodium currents which initiate action potentials and propagation in excitable cells (Goldin et al. 2000). Xu et al. 2009, Zhao et al. 2009a, and Liu et al. 2009 tested the influences of CuO, ZnO, and uncoated Ag-NPs on sodium currents in hippocampal neurons ($Na_v1.2$)

2.3 Patch-Clamp Measurements

by using the patch-clamp method. They found effects of Ag-NPs on the amplitude and the time course of the sodium current (I_{Na}) in their experiments. Since the author observed similar findings on chromaffin $Na_v1.7$ channels it is likely that this effect is not Na_v isoform specific. This is consistent with the fact that the Na_v isoforms in hippocampal cells ($Na_v1.1$ & 1.2) and in chromaffin cells ($Na_v1.7$) have an amino acid sequence similarity of about 95% and show nearly identical electrophysiological behavior (Goldin et al. 2000; Catterall et al. 2005; Goldin 2001; Lorincz and Nusser 2010; Royeck et al. 2008; Toledo-Aral et al. 1997). Those findings on $Na_v1.7$ channels were employed for the modeling approach, in which the measured effects of cAg-NPs on chromaffin cell voltage-gated sodium currents were devolved to voltage-gated sodium channels of thalamic neurons (STC, NSTC, RTN).

For cell preparation, the adrenal glands from 1-3-day-old mice were collected and digested with 20 units of papain (Worthington Biochemical Corp., Lakewood, NY, USA) at $37^\circ C$ for 25 – 30min. After trituration, cells were plated on 25mm cover glasses and then incubated at $37^\circ C$ and 8% CO_2 . Chromaffin cells were kept in culture medium (ITS-X, DMEM with GlutaMax and 100 U Penicillin/Streptomycin; Invitrogen, Life Technologies GmbH, Darmstadt, Germany) prior to recordings 12 – 48hrs later.

2.3 Patch-Clamp Measurements

Patch-clamp measurements in the whole-cell configuration were carried out with 3–6M Ω pipettes using an EPC-9 patch-clamp amplifier controlled by PULSE software (HEKA Instruments Inc, Lambrecht, Germany). Sodium current measurements were performed on both cAg-NPs exposed and naive cells at a holding potential of $-70mV$ at room temperature. The measurement procedure was the following: In a new dish, 4 control cells were recorded first; each recording comprised around 10 depolarizations to $-10mV$ with the step duration of 30ms. While the last control cell patch was still active the cAg-NPs dispersion was pipetted into the chamber and then effects on the patched cell could be measured. Afterwards, the sodium currents of 3 to 5 more cells from the treated dish were collected. This procedure was repeated for concentrations of 13 μMol , 16 μMol , 43 μMol , 130 μMol and 1.3mMol respectively. As diluent, the extracellular solution (Hepes buffered saline solution) was utilized. Altogether, the current traces of 70 control and 45 cAg-NPs exposed

2.4 HH fitting employing Differential Evolution Algorithm

chromaffin-cells were recorded. The extracellular solution contained 145mM NaCl, 2.4mM KCl, 10mM HEPES, 1.2mM MgCl₂, 2.5mM CaCl₂, 10mM glucose (pH 7.5). The pipette solution contained 135mM Cs-aspartate, 10mM Cs-HEPES, 5mM Cs-EGTA, 3mM CaCl₂, 1mM MgCl₂, 2mM Mg-ATP, 0.3mM Na₂-GTP, (pH 7.2).

2.4 HH fitting employing Differential Evolution Algorithm

The original model of Hodgkin and Huxley 1952 was based on experimental data of the notorious squid's giant axon. All the parameters in that model's equations were at that time fixed based on this specific type of neurons. Therefore, to gain a HH-model that is capable to adapt the electrophysiological behavior of chromaffin cells, it becomes necessary to adjust all the model parameters to be characteristic for chromaffin cells. A way to adjust these parameters is to fit the HH-model output, e.g., a particular ion flux, to a measured ion flux by mutating the model's particular parameters. A sophisticated algorithm can facilitate this scheme. If this fitting process is done for the recorded ionic sodium currents before cAg-NPs addition and the HH-model is capable to exactly simulate those, another fitting procedure for the I_{Na} after cAg-NPs addition makes it is possible to compare the resulting differences in the particular model parameters. Based on these thoughts, the I_{Na} from the recorded patch clamp data was fitted to the HH-model (Hodgkin and Huxley 1952) to determine which parameters might be modified under the influence of cAg-NPs. Those factors directly link to physiological mechanisms involved in action potential generation. The basic Hodgkin-Huxley equations used (Malmivuo and Plonsey 1995) are given by

$$\begin{aligned} G_{Na} = G_{Namax}m^3h \quad \frac{dm}{dt} &= \alpha_m(1 - m) - \beta_m m & (2.4.1) \\ \frac{dh}{dt} &= \alpha_h(1 - h) - \beta_h h \end{aligned}$$

for the conductance of sodium ions at the experimental conditions of Hodgkin and Huxley 1952 with a maximum sodium conductance of

$$G_{Namax} = 120mS/cm^2. \quad (2.4.2)$$

2.4 HH fitting employing Differential Evolution Algorithm

The corresponding empirical theorems for the transfer rate coefficients are

$$\begin{aligned}
 \alpha_m &= \frac{2.5 - 0.1V'}{e^{2.5-0.1V'} - 1} \frac{1}{ms} \\
 \beta_m &= \frac{4}{e^{V'/18}} \frac{1}{ms} \\
 \alpha_h &= \frac{0.07}{e^{V'/20}} \frac{1}{ms} \\
 \beta_h &= \frac{1}{e^{30-V'/10} + 1} \frac{1}{ms}
 \end{aligned} \tag{2.4.3}$$

with $V' = V_m - V_r$ [mV], where V_m is the actual membrane voltage and V_r is the resting voltage. Using voltage clamp, for a voltage step, the transfer rate coefficients α_m , β_m , α_h , and β_h change instantly to new values (in steady state, Malmivuo and Plonsey 1995). As in steady state, the transfer rate coefficients in Equation 2.4.3 are constant, so the primary differential equation can be readily solved for m and h , giving

$$m(t) = m_\infty - (m_\infty - m_0)e^{\frac{-t}{\tau_m}}, \tag{2.4.4}$$

where

$$m_\infty = \frac{\alpha_m}{\alpha_m + \beta_m} \tag{2.4.5}$$

represents the value of m and

$$\tau_m = \frac{1}{\alpha_m + \beta_m} \tag{2.4.6}$$

defines the time constant in [s] in steady state. The mathematical term of h is similar to the m in Equation 2.4.4. By applying voltage clamp, a voltage step initiates an exponential change in m (and h) from its initial value of m_0 or h_0 (at $t = 0$) toward the steady state value of m_∞ or h_∞ (at $t = \infty$). Finally, the sodium current I_{Na} that has to be fitted is then given by

$$I_{Na} = G_{Na}(V_m - V_{Na}) \frac{nA}{cm^2}, \tag{2.4.7}$$

2.4 HH fitting employing Differential Evolution Algorithm

where V_{Na} [mV] expresses the resulting Nernst- or also called reversal-potential following the equation of Nernst, simplified for this issue to

$$V_{Na} = \phi_i - \phi_o \quad (2.4.8)$$

with ϕ_i = intracellular and ϕ_o = extracellular potential (ion concentration dependent).

Various problems in applied mathematics have target functions that are non-continuous, non-linear, non-differentiable, noisy, multi-dimensional or have many local minima, constraints or stochasticity. Fitting the steady-state HH-model (Equation 2.4.1–2.4.7) to the measured patch-clamp data requires the solution of a high dimensional multivariate inverse problem: since the essential HH-model-equations that need to be taken into account for the fitting consist of 13 independent parameters (constants evaluated by Hodgkin & Huxley for the squid axon) that have to be estimated, this problem cannot be solved analytically.

Approximate solutions can be achieved by the Differential-Evolution (DE) algorithm, a technique that originates from the genetic annealing algorithm, introduced by Price et al. 2005. This invention offers a global optimization method by stochastic, population-based optimization. The General problem formulation is:

For an objective function $f : \mathcal{X} \subset \mathbb{R}^D \rightarrow \mathbb{R}$ where the feasible region $\mathcal{X} \neq \emptyset$, the minimization problem is to find $x^* \in \mathcal{X}$ such that $f(x^*) \leq f(x) \forall x \in \mathcal{X}$.

This methodology can be utilized to optimize real parameters and real valued functions such as the 13 parameters in the HH-model fitting problem. A detailed description of the algorithm can be found in Price et al. 2005. In terms of the introduced fitting problem, the DE-algorithm was implemented to minimize the distance between the measured sodium current and the one iteratively calculated by the HH-model. As a consequence, the parameters for the best fit were evaluated. The 13 parameters, that give the freedom for the curve fitting process, represent all the empirical coefficients in Equation 2.4.1–2.4.7 that were estimated by Hodgkin & Huxley in their experiments in 1952 (Hodgkin and Huxley 1952). The following equations indicate again the applied HH-formulations, but now with the 13 free parameters expressed by $\xi.1 - 13$:

2.5 Thalamocortical Interactions

$$\begin{aligned}
 \alpha_h &= \frac{\xi.1}{e^{V'/\xi.2}} \frac{1}{ms} \\
 \beta_h &= \frac{1}{e^{\xi.3-V'/\xi.4} + \xi.5} \frac{1}{ms} \\
 \alpha_m &= \frac{\xi.6 - \xi.7 \cdot V'}{e^{\xi.6-\xi.7 \cdot V'} - \xi.8} \frac{1}{ms} \\
 \beta_m &= \frac{\xi.9}{e^{V'/\xi.10}} \frac{1}{ms}
 \end{aligned} \tag{2.4.9}$$

$$\begin{aligned}
 G_{Na} &= \xi.11 \cdot m^3 h \\
 I_{Na} &= G_{Na} \cdot (V_m - \xi.12)
 \end{aligned} \tag{2.4.10}$$

and lastly the point of time for the start of the depolarization t_{stim} as $\xi.13$.

2.5 Thalamocortical Interactions

The thalamus provides the major route for afferents to the neocortex and extracortical sensory regions of the brain. The traditional concept treating the thalamus as the sensory gateway to the cortex is an oversimplification, because the cerebral cortex receives input not only from the sense-specific nuclei, but also from the non-specific thalamic nuclei, which have multimodal connections to the cortex, probably governing overall arousal (Shepherd 2001).

With respect to the interactions between the specific and non-specific thalamic loops, Llinás suggested that rather than a gate, the thalamus is a hub from which any area in the cortex can communicate with any other (Llinás et al. 1998). Bidirectionality is the most remarkable feature of this thalamocortical connectivity. Thalamic nuclei receive reciprocal connections from the cortical areas that they project to, though the number of corticothalamic fibres is significantly greater than the number of thalamocortical axons (Shepherd 2001; Jones 2002). These reciprocal thalamocortical connections create bidirectional neuronal loops between the thalamus and the cortex.

Consequently, distributed neural representations of simultaneous perceptual events or features could be related to each other within the thalamocortical system. Binding input from different sensory modalities into a single cognitive event is assumed

2.6 The Llinás-Model as Basis for the developed Corticothalamic Network

to be a consequence. The underlying mechanism has been proposed as temporal binding, a process based on the synchronization of neural signals (Singer 1999). Different studies have shown that certain types of cognitive functions are intimately related to synchronized neuronal oscillations at both low ($4 - 7/8 - 13Hz$) and high ($18 - 35/30 - 70Hz$) frequencies (Llinás et al. 2002; Hughes et al. 2008; Gray and Singer 1989; Ribary et al. 1991b; Singer 1993; Gregoriou et al. 2009). The activity patterns of these oscillations are formed within one or more bounded areas (corresponding to cortical columns)(Llinás et al. 1998, 2002; Ribary et al. 1991a). A subset of the employed cortical neurons can generate repetitive, high frequency burst discharges referred to as chattering cells. Those can generate bursts with intraburst frequencies of $300 - 750Hz$ and interburst frequencies of $8 - 80Hz$ (Gray and McCormick 1996; Steriade et al. 1998; Brumberg et al. 2000). We focused on the thalamocortical activity of those chattering cells since their firing patterns in burst mode contain more information to evaluate impact of NPs on the circuit's activity.

2.6 The Llinás-Model as Basis for the developed Corticothalamic Network

Rodolfo Llinás and his group suggested a reasonably detailed model of thalamocortical interaction and binding (Llinás and Ribary 1993; Llinás et al. 1994, 1998, 2002), see section before. Its principal finding is that the intrinsic electrical properties of neurons and the dynamic events resulting from their connectivity cause global resonant states. Resonant states in the network will change by just small alterations in the neural signaling characteristics. The Llinás et al. model exposing the thalamocortical circuit is depicted in Figure 2.1.

For the purpose of this thesis, the focus was on two types of thalamic cells: 1^{st} specific thalamic cells, also known as thalamic core cells due to their focused projection to an individual cortical area and 2^{nd} intralaminar non-specific thalamic cells, also known as thalamic matrix cells as they project across larger neocortical areas in a more dispersed way (Shepherd 2001). Two thalamocortical resonant loops were utilized for the model development. The description of neural interactions and dynamics can be found in the subsequent section. It was proposed by Llinás et al.

2.6 The Llinás-Model as Basis for the developed Corticothalamic Network

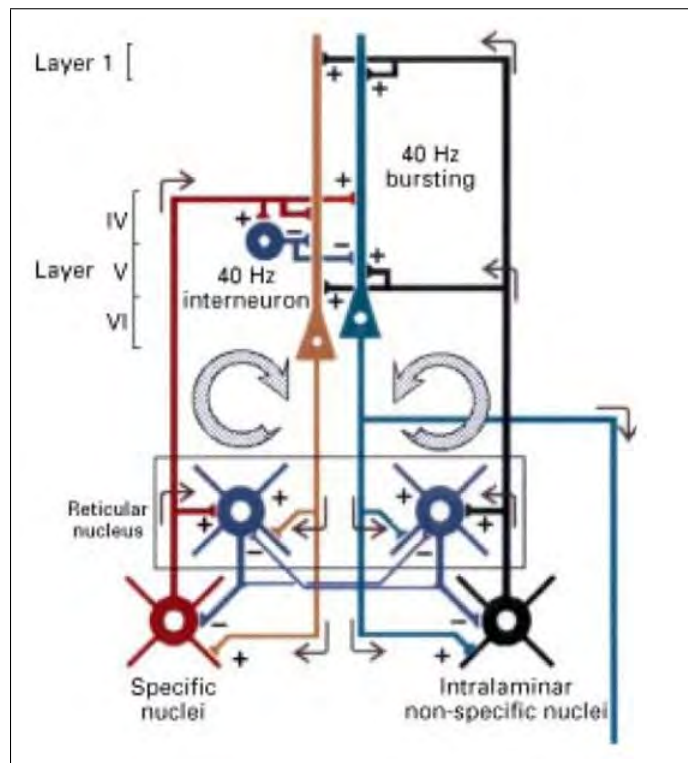


Figure 2.1: Thalamocortical circuit. The Llinás et al. model (Adopted from Llinás et al. 1998).

that none of these two systems alone is able to generate cognition, and consistent with this model, damage to the non-specific thalamus induces deep disturbances of consciousness while damage to the specific systems causes loss of particular modality (Llinás et al. 1998). Their statement implies that these two systems can only generate a cognitive experience synced, based on the summation of non-specific and specific activity along the dendritic tree of the cortical element, by coincidence detection at the pyramidal neuron (Llinás et al. 1998, 2002).

To conclude, the system operates on the basis of thalamocortical resonant columns that can support global cognitive experiences. In this context, the specific system provides the content that relates to the external world while the non-specific system would give rise to the temporal conjunction (binding circuit). This well explored and accepted model served as the theoretical fundament for the investigations on NPs' induced signaling modifications in neuronal circuits.

2.7 The Applied Thalamocortical Network

The simplified *in silico* model that we used to predict *in vivo* behavior is based on the principle of thalamocortical interaction and binding as elucidated before. The principal result is that the intrinsic electrical properties of neurons and the dynamic events resulting from their connectivity cause global resonant states. Resonant states in the network will change due to small alterations in the neural signaling characteristics. The applied circuit is based on kinetic models of pyramidal neurons (here: chattering cells, PY) (Wang et al. 1995; Wang 1998; Golomb et al. 1996, 2006), inhibitory cortical interneurons (IN)(Golomb et al. 1996; Wang and Buzsáki 1996), thalamic cells (TC) including specific thalamic cells (STC) and non-specific thalamic cells (NSTC)(Destexhe et al. 1996a; Bazhenov et al. 1998; Golomb and Amitai 1997), and reticular thalamic neurons (RTN)(Wang et al. 1995; Golomb et al. 1996; Destexhe et al. 1994a, 1996b). Each single neuron model is considered as one compartment (except PY, modeled as two-compartments) and is represented by coupled differential equations according to an extended Hodgkin-Huxley-type scheme (Hodgkin and Huxley 1952). A schematic representation of the two-compartment model that was put into use for each of the PY-neurons is given in Figure 2.2. It shows the ionic currents present in each compartment, with the direction of current represented by an arrow. The two compartments are coupled through a conductance parameter.

The applied currents (I_S, I_D) are shown, as well as the synaptic current (I_{SYN}). The difference in potential across the membrane is denoted by V_S and V_D for the somatic and dendritic compartments respectively, and represents the deviation (in mV) from the resting membrane potential of $-60mV$ (Ferguson and Campbell 2009). The somatic compartment consists of five ionic current channels: sodium and calcium are the inward currents (I_{Na_S} and I_{Ca_S} respectively), and the outward currents are the delayed rectifier potassium current (I_{K-DR_S}), long-lasting calcium-dependent AHP potassium current (I_{K-AHP_S}), which is associated with the slow after hyperpolarization (AHP) (Herz et al. 2006), and short-duration voltage and calcium-dependent potassium current(I_{K-C_S}). The dendrite compartment has three ionic current channels: inward calcium current (I_{Ca_D}), and the outward I_{K-AHP_D} and I_{K-C_D} whose activation depends on the calcium concentration inside the cell. Although it isn't shown in the schematic model, there is a small leak current in both the soma and dendrite compartments. The membrane capacitance is represented

2.7 The Applied Thalamocortical Network

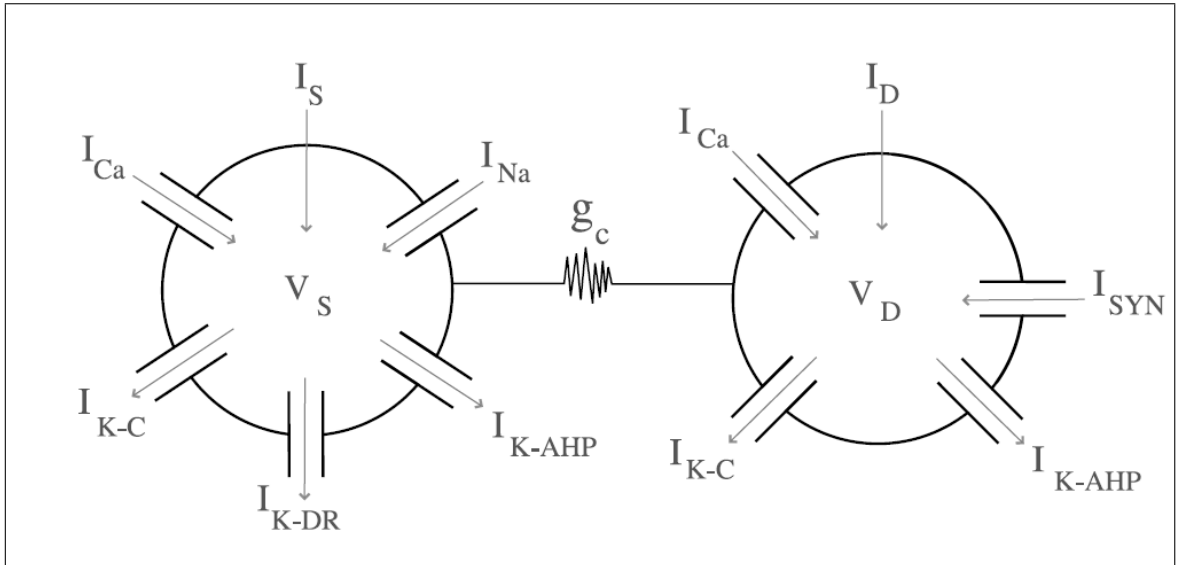


Figure 2.2: Scheme of an example two-compartment model showing applied currents, outward and inward active currents to soma and dendrite compartments (adopted from Ferguson and Campbell 2009).

by C_m (in units $\mu F/cm^2$). All currents in this model have the unit $\mu A/cm^2$ and all conductances have the unit mS/cm^2 (Ferguson and Campbell 2009). After using Kirchoff's Law, the current balance equations for the ionic currents for the somatic and dendritic membrane potentials and voltage change across the membrane of each compartment are obtained (Ferguson and Campbell 2009).

The scheme of synaptic connectivity in the developed simplified thalamocortical network model is represented by Figure 2.3. In this model, specific thalamic inputs are represented by a thalamic neuron (STC) that projects to both PY neuron and inhibitory IN located in cortical layer IV after sending an axon collateral to the RTN neuron. A second thalamic neuron (NSTC) represents intralaminar, non-specific thalamic inputs and projects to neocortical layer I after sending axon collaterals to the RTN neuron. STC and NSTC neurons generate excitatory postsynaptic potentials that are mediated by fast excitatory receptors in the model. RTN neurons project with inhibitory characteristic to specific and intralaminar nucleus neurons. Inhibitory fast and slow receptors in the thalamic neurons both mediate the inhibitory postsynaptic potentials of those cells. The RTN neurons also have reciprocal inhibitory synaptic connectivity. The corresponding activity is mediated by fast inhibitory receptors. In the model, the cerebral cortex was considered as a simple network model of inhibitory IN and excitatory PY neurons (Llinás and Ribary 1993; Llinás et al. 1994, 1998, 2002). Although this is a highly simplified

2.7 The Applied Thalamocortical Network

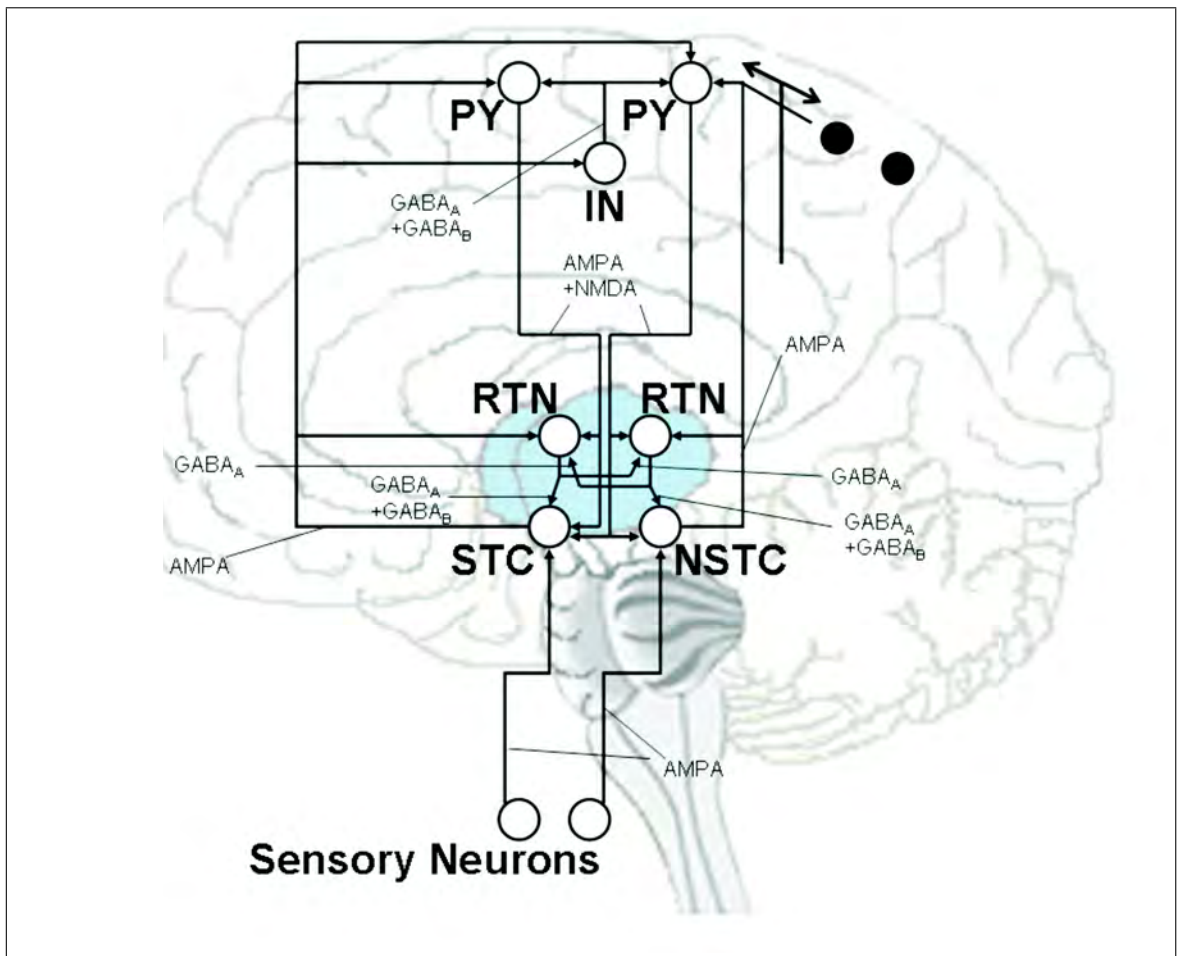


Figure 2.3: Schematic description of synaptic interconnections in the simplified computational model of the thalamocortical network.

2.7 The Applied Thalamocortical Network

representation of the neocortex's multilayered structure, no additional complexity was required for the theoretical modeling. Consequently, the pyramidal neurons in the layers IV and V are described by single neurons (Figure 2.3, PY) that receive inputs and project to both STC and NSTC cells and have axon collaterals to the RTN neurons. In the model, four PY neurons were included, two of which receive input from the STC to provide specific sensory input to the cortex. This structure represents the specific resonant loop as is shown in Figure 2.3 on the left. The right side of Figure 2.3 indicates the non-specific resonant loop, where three PY neurons receive their inputs in a more diffuse way from NSTC to provide the multimodal connectivity to the cortex. The two black spots represent two PY neurons that receive inputs and project back to the NSTC. In this model, the corticofugal excitation of the PY is mediated by both fast and slow excitatory receptors. In the circuit, all PY neurons receive axons from the cortical inhibitory IN, in which the inhibitory postsynaptic potential elicited by this cell is also mediated by both fast and slow excitatory receptors. Lastly, the essential sensory inputs to activate STC and NSTC are provided by including two sensory neurons in the present model (see Figure 2.3). Thus, the synaptic projections from those sensory neurons activate the fast receptors of the thalamic nuclei. Every neuron of the simplified thalamocortical model receives various synaptic inputs that are modeled as the sum over all synaptic currents that each cell receives (Destexhe et al. 1998a; Bazhenov et al. 2002). Accordingly, every neuron is described by the generic membrane equation

$$C_m \frac{dV_i}{dt} = - \underbrace{\bar{g}_L(V_i - E_L)}_{\text{leakage term}} - \sum_j I_{ji}^{int} - \sum_k I_{ki}^{syn} \quad (2.7.11)$$

where C_m is the specific membrane capacity and V_i is the postsynaptic membrane potential. I_{ji}^{int} and I_{ki}^{syn} signify the intrinsic (ionic) and synaptic currents. The generic form of the intrinsic currents (generalization of Equation 2.4.7) is represented by

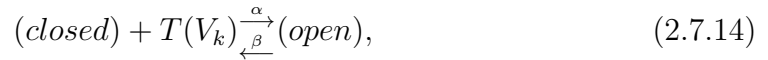
$$I_{ji}^{int} = \bar{g}_j m_j^M h_j^N (V_i - E_j), \quad (2.7.12)$$

Here, i connotes the postsynaptic neuron and j represents for the specific ionic type. Further, \bar{g}_j is the maximal conductance, m the time and voltage dependent activation variable, h is the corresponding (time and voltage dependent) inactivation variable and finally $(V_i - E_j)$ is the difference between membrane potential and reversal potential of each ion. The following generic equation represents the synaptic currents in the system:

$$I_{ki}^{syn} = \bar{g}_{ki} s_{ki} (V_i - E_{ki}) \quad (2.7.13)$$

2.7 The Applied Thalamocortical Network

Where ki designates the synaptic junction from the presynaptic neuron k to the postsynaptic neuron i , g_{ki} is the maximal conductance of the postsynaptic receptors and E_{ki} is the reversal potential. The fraction of open receptors is specified by s_{ki} according to the simple two state scheme



For computational efficiency, a reduced transmitter release model is used, assuming all intervening reactions in the release process are relatively fast and thus, can be considered in steady state (instantaneous) (Destexhe et al. 1998b). Consequently, the stationary relationship between the transmitter concentration $[T]$ and presynaptic voltage is described by a simple sigmoidal function (Destexhe et al. 1998b)

$$[T](V_{pre}) = \frac{Tmax}{1 + exp(-(V_{pre} - V_p)/K_p)} \quad (2.7.15)$$

where T_{max} is the maximal concentration of transmitter in the synaptic cleft, V_{pre} is the presynaptic voltage, K_p gives the steepness and V_p sets the value at which the function is half activated. This form, in conjunction with simple kinetic models of postsynaptic channels, provides a model of synaptic interaction based on autonomous differential equations with only one or two variables (Wang and Rinzel 1992; Golomb et al. 1994).

In the model, all initial conditions and set parameters representing a single cell or synaptic connection originate from electrophysiological measurements on the specific neurons taken from cited references. Please see Wang et al. 1995; Wang and Rinzel 1992, Golomb et al. 2006, and Destexhe et al. 1998b, 1994b for a detailed description of the particular equations and the corresponding cell- and transmitter specific parameters. According to Destexhe et al. 1998a, different values of I_h and I_{KL} would cause heterogeneity in the intrinsic properties of the cells. Therefore the intrinsic conductance of g_h and g_{KL} for the STC and the NSTC and g_{KL} for the RTN neuron models are slightly different in the present model.

To simulate the effects of cAg-NPs in contact with thalamic cells, i.e., STC, NSTC, and RTN, respectively, the changes of the intrinsic currents that were identified by fitting the patch-clamp data to the HH-model were applied to those cells. The kinetics and voltage dependence of the modeled currents are very similar to the currents measured in patch clamp experiments (see section Chromaffin Cell Model). MATLAB was used as simulation environment in which the differential equations were solved by employing a fourth-order Runge-Kutta method.

2.7 The Applied Thalamocortical Network

The following equations provide a detailed description of each single neuron model that was developed to be utilized in the applied Llinás circuit that is based on the generic single-cell membrane equations (see also Vukelic 2010 for a basic discussion of the model's equations). The particular parameters for each individual cell type are originating from patch clamp measurements of cited literature.

Neocortical PY neurons

Current Balance Equations

$$C_m \frac{dV_{S_i}}{dt} = + I_{app} - \bar{g}_L(V_{S_i} - E_L) - I_{Na}(V_{S_i}, h) - I_K(V_{S_i}, n) - I_{Ca}(V_{S_i}) - I_{AHP}(V_{S_i}, [Ca^{2+}]_i) - \frac{g_c}{p}(V_{S_i} - V_{D_i}) \quad (2.7.16)$$

$$C_m \frac{dV_{D_i}}{dt} = - \bar{g}_L(V_{D_i} - E_L) - I_{Ca}(V_{D_i}) - I_{AHP}(V_{D_i}, [Ca^{2+}]_i) - \frac{g_c}{1-p}(V_{D_i} - V_{S_i}) - I_{AMPA}^{TCPY}(V_{D_i}, \{s_{AMPA,k}^{TC}\}) - I_{GABAA}^{INPY}(V_{D_i}, \{s_{GABAA,k}^{IN}\}) - I_{GABAB}^{INPY}(V_{D_i}, \{s_{GABAB,k}^{IN}\}) \quad (2.7.17)$$

where $C_m = 1 \mu\text{F}/\text{cm}^2$, $\bar{g}_L = 0.1 \text{ mS}/\text{cm}^2$, $E_L = -65 \text{ mV}$ Wang 1998.

Intrinsic Currents

The delayed rectifier potassium current I_K and the sodium current I_{Na} are described according to Wang 1998.

$$I_{Na}(V_{S_i}, h) = \bar{g}_{Na} m_\infty^3(V_{S_i}) h (V_{S_i} - E_{Na}) \quad (2.7.18)$$

where the fast activation variable is replaced by its steady state form

$$m_\infty(V_{S_i}) = \alpha_m(V_{S_i}) / (\alpha_m(V_{S_i}) + \beta_m(V_{S_i})) \quad (2.7.19)$$

$$\alpha_m(V_{S_i}) = \frac{-0.1(V_{S_i} + 33)}{\exp(-0.1(V_{S_i} + 33)) - 1} \quad (2.7.20)$$

$$\beta_m(V_{S_i}) = 4 \exp(-(V_{S_i} + 58)/12) \quad (2.7.21)$$

2.7 The Applied Thalamocortical Network

$$\frac{dh}{dt} = \phi_h [\alpha_h(V_{S_i})(1 - h) - \beta_h(V_{S_i})h] \quad (2.7.22)$$

$$\alpha_h(V_{S_i}) = 0.07 \exp(-(V_{S_i} + 50)/10) \quad (2.7.23)$$

$$\beta_h(V_{S_i}) = \frac{1}{\exp(-0.1(V_{S_i} + 20)) + 1} \quad (2.7.24)$$

$$I_K(V_{S_i}, n) = \bar{g}_K n^4 (V_{S_i} - E_K) \quad (2.7.25)$$

$$\frac{dn}{dt} = \phi_n [\alpha_n(V_{S_i})(1 - n) - \beta_n(V_{S_i})n] \quad (2.7.26)$$

$$\alpha_n(V_{S_i}) = \frac{-0.01(V_{S_i} + 34)}{\exp(-0.1(V_{S_i} + 34)) - 1} \quad (2.7.27)$$

$$\beta_n(V_{S_i}) = 0.125 \exp(-(V_{S_i} + 44)/25) \quad (2.7.28)$$

with $\bar{g}_{Na} = 45 \text{ mS/cm}^2$, $E_{Na} = 55 \text{ mV}$, $\bar{g}_K = 18 \text{ mS/cm}^2$, $E_K = -80 \text{ mV}$ and $\phi_h = \phi_n = 4$ is a temperature factor Wang 1998.

The high-threshold calcium current I_{Ca} is defined by Wang 1998

$$I_{Ca}(V_i) = \bar{g}_{Ca} m_\infty^2(V_i)(V_i - E_{Ca}) \quad (2.7.29)$$

where m is replaced by its steady state form

$$m_\infty(V_i) = \frac{1}{1 + \exp(-(V_i + 20)/9)} \quad (2.7.30)$$

where usually $\bar{g}_{Ca} = 1 \text{ mS/cm}^2$ in the dendritic part and $\bar{g}_{Ca} = 0 \text{ mS/cm}^2$ in the somatic part (if not stated otherwise), $E_{Ca} = 120 \text{ mV}$.

The voltage-independent, calcium-activated potassium current I_{AHP} is defined in Wang 1998

$$I_{AHP}(V_i, [Ca^{2+}]_i) = \bar{g}_{AHP} ([Ca^{2+}]_i / ([Ca^{2+}]_i + K_D)) (V_i - E_K) \quad (2.7.31)$$

where usually $\bar{g}_{AHP} = 5 \text{ mS/cm}^2$ in the dendritic part and $\bar{g}_{AHP} = 0 \text{ mS/cm}^2$ in the somatic part (if not stated otherwise) and $K_D = 30 \text{ }\mu\text{M}$.

2.7 The Applied Thalamocortical Network

The intracellular calcium dynamics is governed by a leaky-integrator in Wang 1998

$$\frac{d[Ca^{2+}]_{i,D}}{dt} = -\alpha_D I_{Ca,D} - [Ca^{2+}]_{i,D} / \tau_{Ca,D} \quad (2.7.32)$$

if the calcium conductances were also included at the soma then an additional equation for the calcium dynamics is needed

$$\frac{d[Ca^{2+}]_{i,S}}{dt} = -\alpha_S I_{Ca,S} - [Ca^{2+}]_{i,S} / \tau_{Ca,S} \quad (2.7.33)$$

where α is proportional to the surface/volume (S/V) ratio, thus it should be much smaller for the somatic part than for the dendritic part. τ_{Ca} is a time constant (decay process) which describes the various extrusion and buffering mechanisms and it is expected to be increased at the somatic than at the dendritic part Wang 1998.

$\alpha_D = 0.002 \mu\text{M} (m\text{S}\mu\text{A})^{-1} \text{cm}^2$ and $\tau_{Ca,D} = 80 \text{ms}$ are chosen so that the calcium influx per spike is approximately 200 nM, whereas the values for the somatic part a the right-hand side of equation 2.7.33 is multiplied by a factor 1/3, so that $\alpha_S = 0.000667 \mu\text{M} (m\text{S}\mu\text{A})^{-1} \text{cm}^2$ and $\tau_{Ca,S} = 240 \text{ms}$ Wang 1998.

Synaptic Currents

The AMPA current I_{AMPA}^{TCPY} from TC to PY is defined in Golomb et al. 1996

$$I_{AMPA}^{TCPY}(V_{D_i}, \{s_{AMPA,k}^{TC}\}) = \bar{g}_{AMPA} s (V_{PY,D} - E_{AMPA}) \quad (2.7.34)$$

with $E_{AMPA} = 0 \text{mV}$, the gating variable s depends on V_{TC} , and \bar{g}_{AMPA} in units mS/cm^2 .

The AMPA gating variable s is given as

$$\begin{aligned} \frac{ds}{dt} &= k_{fA} X_\infty(V_{TC})(1 - s) - k_{rA} s \\ X_\infty(V_{TC}) &= \frac{1}{1 + \exp(-(V_{TC} - \theta_{syn})/\sigma_{syn})} \end{aligned} \quad (2.7.35)$$

where $k_{fA} = 2.0 \text{ms}^{-1}$, $k_{rA} = 0.1 \text{ms}^{-1}$, $\theta_{syn} = -40 \text{mV}$, $\sigma_{syn} = 2 \text{mV}$ Golomb et al. 1996.

The GABA_A current $I_{GABA_A}^{INPY}$ from IN to PY is defined by Golomb et al. 2006

$$I_{GABA_A}^{INPY}(V_{D_i}, \{s_{GABA_A,k}^{IN}\}) = \bar{g}_{GABA_A} s (V_{PY,D} - E_{GABA_A}) \quad (2.7.36)$$

2.7 The Applied Thalamocortical Network

with $E_{GABA_A} = -70$ mV, the gating variable s depends on V_{IN} , and \bar{g}_{GABA_A} in units mS/cm^2 varies in simulations (see results).

The $GABA_A$ gating variable s is given as

$$\begin{aligned} \frac{ds}{dt} &= k_{fG}X_{\infty}(V_{IN})(1-s) - k_{rG}s \\ X_{\infty}(V_{IN}) &= \frac{1}{1 + \exp(-(V_{IN} - \theta_{syn})/\sigma_{syn})} \end{aligned} \quad (2.7.37)$$

where $k_{fG} = 1.0 \text{ ms}^{-1}$, $k_{rG} = 0.1 \text{ ms}^{-1}$, $\theta_{syn} = -20$ mV, $\sigma_{syn} = 2$ mV Golomb et al. 2006.

The $GABA_B$ current $I_{GABA_B}^{INPY}$ from IN to PY is given by Wang et al. 1995

$$I_{GABA_B}^{INPY}(V_{D_i}, \{s_{GABA_B,k}^{IN}\}) = \bar{g}_{GABA_B} s^q (V_{PY,D} - E_{GABA_B}) \quad (2.7.38)$$

with $E_{GABA_B} = -100$ mV, the gating variable s depends on V_{IN} , $q = 4$, and \bar{g}_{GABA_B} in units mS/cm^2 varies in simulations (see results). The equations and parameters for gating variables are

$$\begin{aligned} \frac{dx}{dt} &= \alpha_x X_{\infty}(V_{IN})(1-x) - \beta_x x \\ \frac{ds}{dt} &= \alpha_s x(1-s) - \beta_s s \end{aligned} \quad (2.7.39)$$

$$X_{\infty}(V_{IN}) = \frac{1}{1 + \exp(-(V_{IN} - \theta_{syn})/\sigma_{syn})} \quad (2.7.40)$$

where $\theta_{syn} = -45$ mV, $\sigma_{syn} = 2$ mV Wang et al. 1995.

Inhibitory neocortical INs

Current Balance Equations

$$C_m \frac{dV_i}{dt} = + I_{app} - \bar{g}_L(V_i - E_L) - I_{Na}(V_i, h) - I_K(V_i, n) - I_{AMPA}^{TCIN}(V_i, \{s_{AMPA,k}^{TC}\}) \quad (2.7.41)$$

where $C_m = 1 \mu\text{F}/\text{cm}^2$, $\bar{g}_L = 0.1 \text{ mS}/\text{cm}^2$, $E_L = -65 \text{ mV}$ according to Wang and Buzsáki 1996.

Intrinsic Currents

The sodium current I_{Na} and the delayed rectifier potassium current I_K are described according to Wang and Buzsáki 1996

$$I_{Na}(V_i, h) = \bar{g}_{Na} m_\infty^3(V_i) h(V_i - E_{Na}) \quad (2.7.42)$$

where the activation variable m is assumed to be fast and substituted by its steady state form

$$m_\infty(V_i) = \alpha_m(V_i) / (\alpha_m(V_i) + \beta_m(V_i)) \quad (2.7.43)$$

$$\alpha_m(V_i) = \frac{-0.1(V_i + 35)}{\exp(-0.1(V_i + 35)) - 1} \quad (2.7.44)$$

$$\beta_m(V_i) = 4 \exp(-(V_i + 60)/18) \quad (2.7.45)$$

$$\frac{dh}{dt} = \phi_h [\alpha_h(V_i)(1 - h) - \beta_h(V_i)h] \quad (2.7.46)$$

$$\alpha_h(V_i) = 0.07 \exp(-(V_i + 58)/20) \quad (2.7.47)$$

$$\beta_h(V_i) = \frac{1}{\exp(-0.1(V_i + 28)) + 1} \quad (2.7.48)$$

$$I_K(V_i, n) = \bar{g}_K n^4 (V_i - E_K) \quad (2.7.49)$$

$$\frac{dn}{dt} = \phi_n [\alpha_n(V_i)(1 - n) - \beta_n(V_i)n] \quad (2.7.50)$$

2.7 The Applied Thalamocortical Network

$$\alpha_n(V_i) = \frac{-0.01(V_i + 34)}{\exp(-0.1(V_i + 34)) - 1} \quad (2.7.51)$$

$$\beta_n(V_i) = 0.125 \exp(-(V_i + 44)/80) \quad (2.7.52)$$

with $\bar{g}_{Na} = 35 \text{ mS/cm}^2$, $E_{Na} = 55 \text{ mV}$, $\bar{g}_K = 9 \text{ mS/cm}^2$, $E_K = -90 \text{ mV}$ and $\phi_h = \phi_n = 5$ is a temperature factor Wang and Buzsáki 1996.

Synaptic Currents

The AMPA current I_{AMPA}^{TCIN} from TC to IN is Golomb et al. 1996

$$I_{AMPA}^{TCIN}(V_i, \{s_{AMPA,k}^{TC}\}) = \bar{g}_{AMPA}s(V_{IN} - E_{AMPA}) \quad (2.7.53)$$

with $E_{AMPA} = 0 \text{ mV}$, the gating variable s depends on V_{TC} , and \bar{g}_{AMPA} in units mS/cm^2 .

The AMPA gating variable s is defined as

$$\begin{aligned} \frac{ds}{dt} &= k_{fA}X_\infty(V_{TC})(1 - s) - k_{rA}s \\ X_\infty(V_{TC}) &= \frac{1}{1 + \exp(-(V_{TC} - \theta_{syn})/\sigma_{syn})} \end{aligned} \quad (2.7.54)$$

where $k_{fA} = 2.0 \text{ ms}^{-1}$, $k_{rA} = 0.1 \text{ ms}^{-1}$, $\theta_{syn} = -40 \text{ mV}$, $\sigma_{syn} = 2 \text{ mV}$ Golomb et al. 1996.

RTN neurons

Current Balance Equation

$$\begin{aligned} C_m \frac{dV_i}{dt} &= + I_{app} - \bar{g}_L(V_i - E_L) - I_{Na}(V_i, m, h) - I_K(V_i, n) \\ &\quad - I_T(V_i, m, h, [Ca^{2+}]_i) - I_{KL}(V_i) - I_{GABAA}^{RTNRTN}(V_i, \{s_{GABAA,k}^{RTN}\}) \\ &\quad - I_{AMPA}^{TCRTN}(V_i, \{s_{AMPA,k}^{TC}\}) - I_{AMPA}^{PYRTN}(V_i, \{s_{AMPA,k}^{PY}\}) \\ &\quad - I_{NMDA}^{PYRTN}(V_i, \{s_{NMDA,k}^{PY}\}) \end{aligned} \quad (2.7.55)$$

where $C_m = 1 \text{ } \mu\text{F/cm}^2$, $\bar{g}_L = 0.05 \text{ mS/cm}^2$, $E_L = -77 \text{ mV}$ Destexhe et al. 1994a.

2.7 The Applied Thalamocortical Network

Intrinsic Currents

The sodium current I_{Na} and the delayed rectifier potassium current I_K are defined according to Traub and Miles 1991.

$$I_{Na}(V_i, m, h) = \bar{g}_{Na} m^3 h (V_i - E_{Na}) \quad (2.7.56)$$

$$\frac{dm}{dt} = \alpha_m(V_i)(1 - m) - \beta_m(V_i)m \quad (2.7.57)$$

$$\frac{dh}{dt} = \alpha_h(V_i)(1 - h) - \beta_h(V_i)h \quad (2.7.58)$$

$$\alpha_m(V_i) = \frac{0.32(V_i + vtraubrtn - 13)}{1 - \exp(-(V_i + vtraubrtn - 13)/4)} \quad (2.7.59)$$

$$\beta_m(V_i) = \frac{0.28(V_i + vtraubrtn - 40)}{\exp(-(V_i + vtraubrtn - 40)/5) - 1} \quad (2.7.60)$$

$$\alpha_h(V_i) = 0.128 \exp(-(V_i + vtraubrtn - 17)/18) \quad (2.7.61)$$

$$\beta_h(V_i) = \frac{4}{1 + \exp(-(V_i + vtraubrtn - 40)/5)} \quad (2.7.62)$$

$$I_K(V_i, n) = \bar{g}_K n^4 (V_i - E_K) \quad (2.7.63)$$

$$\frac{dn}{dt} = \alpha_n(V_i)(1 - n) - \beta_n(V_i)n \quad (2.7.64)$$

$$\alpha_n(V_i) = \frac{0.032(V_i + vtraubrtn - 15)}{1 - \exp(-(V_i + vtraubrtn - 15)/5)} \quad (2.7.65)$$

$$\beta_n(V_i) = 0.5 \exp(-(V_i + vtraubrtn - 10)/40) \quad (2.7.66)$$

where $\bar{g}_{Na} = 100 \text{ mS/cm}^2$, $E_{Na} = 50 \text{ mV}$, $\bar{g}_K = 10 \text{ mS/cm}^2$, $E_K = -100 \text{ mV}$ and $vtraubrtn = 50 \text{ mV}$ (gating kinetics adjusted to 36C).

2.7 The Applied Thalamocortical Network

The low-threshold calcium current I_T is defined according to Destexhe et al. 1994a, Destexhe et al. 1996b, Bazhenov et al. 1998.

$$I_T(V_i, m, h, [Ca^{2+}]_i) = \bar{g}_T m^2 h (V_i - E_{Ca}) \quad (2.7.67)$$

$$\frac{dm}{dt} = (m_\infty(V_i) - m) / \tau_m(V_i) \quad (2.7.68)$$

$$\frac{dh}{dt} = (h_\infty(V_i) - h) / \tau_h(V_i) \quad (2.7.69)$$

$$m_\infty(V_i) = \frac{1}{1 + \exp(-(V_i + 52)/7.4)} \quad (2.7.70)$$

$$h_\infty(V_i) = \frac{1}{1 + \exp(-(V_i + 80)/5)} \quad (2.7.71)$$

$$\tau_m(V_i) = 1 + \frac{0.33}{\exp((V_i + 27)/10) + \exp(-(V_i + 102)/15)} \quad (2.7.72)$$

$$\tau_h(V_i) = 22.7 + \frac{0.27}{\exp((V_i + 48)/4) + \exp(-(V_i + 407)/50)} \quad (2.7.73)$$

where $\bar{g}_T = 2 \text{ mS/cm}^2$ and the reversal potential strongly depends on the intracellular calcium concentration $[Ca^{2+}]_i$ and is determined by the Nernst equation

$$E_{Ca} = k' \frac{RT}{2F} \log \frac{[Ca^{2+}]_o}{[Ca^{2+}]_i} \quad (2.7.74)$$

where $k' = 1,000$ (constant for unit conversion for E_{Ca} in millivolts),

$R = 8,31441 \text{ mJ/(K}\cdot\text{Mol)}$, $F = 96,480 \text{ coulombs/Mol}$, $T = 309,15\text{K}$, and $[Ca^{2+}]_o = 2 \text{ mM}$ is the extracellular calcium concentration corresponding to a temperature of 36C and the intracellular calcium dynamic obeys a first order differential equation

$$\frac{d[Ca^{2+}]_i}{dt} = -AI_T - ([Ca^{2+}]_i - [Ca^{2+}]_\infty) / \tau \quad (2.7.75)$$

where $[Ca^{2+}]_\infty = 2.4 \cdot 10^{-4} \text{ mM}$ denotes the equilibrium calcium concentration, $A = 5.18 \cdot 10^{-5} \text{ (mM}\cdot\text{cm}^2)/(\text{ms}\cdot\mu\text{A})$ and $\tau = 5 \text{ ms}$ Bazhenov et al. 1998.

2.7 The Applied Thalamocortical Network

The leak potassium current I_{KL} is represented as follows McCormick and Huguenard 1992

$$I_{KL} = \bar{g}_{KL}(V_i - E_{KL}) \quad (2.7.76)$$

$\bar{g}_{KL} = 0.005 \text{ mS/cm}^2$ and $E_{KL} = -95 \text{ mV}$.

Synaptic Currents

The AMPA current I_{AMPA}^{TCRTN} from TC to RTN is defined by Golomb et al. 1996

$$I_{AMPA}^{TCRTN}(V_i, \{s_{AMPA,k}^{TC}\}) = \bar{g}_{AMPA}s(V_{RTN} - E_{AMPA}) \quad (2.7.77)$$

with $E_{AMPA} = 0 \text{ mV}$, the gating variable s depends on V_{TC} , and \bar{g}_{AMPA} in units mS/cm^2 .

The AMPA gating variable s obey the same parameters and equations as in Equation 2.7.35.

The AMPA current I_{AMPA}^{PYRTN} from PY to RTN is defined by Golomb and Amitai 1997

$$I_{AMPA}^{PYRTN}(V_i, \{s_{AMPA,k}^{PY}\}) = \bar{g}_{AMPA}s(V_{RTN} - E_{AMPA}) \quad (2.7.78)$$

with $E_{AMPA} = 0 \text{ mV}$, the gating variable s depends on V_{PY} , and \bar{g}_{AMPA} in units mS/cm^2 .

The AMPA gating variable s is as follows

$$\begin{aligned} \frac{ds}{dt} &= k_{fA}X_{\infty}(V_{PY})(1 - s) - k_{rA}s \\ X_{\infty}(V_{PY}) &= \frac{1}{1 + \exp(-(V_{PY} - \theta_{syn})/\sigma_{syn})} \end{aligned} \quad (2.7.79)$$

where $k_{fA} = 1.0 \text{ ms}^{-1}$, $k_{rA} = 0.2 \text{ ms}^{-1}$, $\theta_{syn} = -20 \text{ mV}$, $\sigma_{syn} = 2 \text{ mV}$ Golomb and Amitai 1997.

2.7 The Applied Thalamocortical Network

The *NMDA* current I_{NMDA}^{PYRTN} from PY to RTN is defined by Golomb et al. 2006

$$I_{NMDA}^{PYRTN}(V_i, \{s_{NMDA,k}^{PY}\}) = I_{syn} = \bar{g}_{NMDA} s f(V_{RTN})(V_{RTN} - E_{NMDA}) \quad (2.7.80)$$

with $E_{NMDA} = 0$ mV, the gating variable s depends on V_{PY} , and \bar{g}_{NMDA} in units mS/cm^2 .

Additional dependence on postsynaptic membrane potential V_{RTN} is given by Dayan and Abbott 2001

$$f(V_{RTN}) = \frac{1}{1 + \frac{[Mg^{2+}]_o}{3.57\text{mM}} \cdot \exp(-V_{RTN}/16.13\text{mV})} \quad (2.7.81)$$

normal $[Mg^{2+}]_o$ concentration is in the range of 1 to 2 mM Dayan and Abbott 2001. The *NMDA* gating variables are defined according to the model of Golomb et al. Golomb et al. 2006

$$\begin{aligned} \frac{dx_{NMDA}}{dt} &= k_{xN} X_\infty(V_{PY})(1 - x_{NMDA}) - [1 - X_\infty(V_{PY})] x_{NMDA} / \tilde{\tau}_{NMDA} \\ \frac{ds_{NMDA}}{dt} &= k_{fN} x_{NMDA}(1 - s_{NMDA}) - s_{NMDA} / \tau_{NMDA} \end{aligned} \quad (2.7.82)$$

where $X_\infty(V_{PY})$ is calculated by equation 2.7.79 (same parameters). $k_{xN} = 1 \text{ ms}^{-1}$, $\tilde{\tau}_{NMDA} = 14.3 \text{ ms}$, $k_{fN} = 1 \text{ ms}^{-1}$, $\tau_{NMDA} = 100 \text{ ms}$.

The *GABA_A* current $I_{GABA_A}^{RTNRTN}$ from RTN to RTN is given by Golomb et al. 1996

$$I_{GABA_A}^{RTNRTN}(V_i, \{s_{GABA_A,k}^{RTN}\}) = \bar{g}_{GABA_A} s (V_{RTN} - E_{GABA_A}) \quad (2.7.83)$$

with $E_{GABA_A} = -75$ mV, the gating variable s depends on V_{RTN} , and \bar{g}_{GABA_A} in units mS/cm^2 .

The *GABA_A* gating variable s is given as

$$\begin{aligned} \frac{ds}{dt} &= k_{fG} X_\infty(V_{RTN})(1 - s) - k_{rG} s \\ X_\infty(V_{RTN}) &= \frac{1}{1 + \exp(-(V_{RTN} - \theta_{syn})/\sigma_{syn})} \end{aligned} \quad (2.7.84)$$

where $k_{fG} = 2.0 \text{ ms}^{-1}$, $k_{rG} = 0.08 \text{ ms}^{-1}$, $\theta_{syn} = -40$ mV, $\sigma_{syn} = 2$ mV Golomb et al. 1996.

TC neurons

The model of TC neurons include STC and NSTC from the simplified thalamocortical network model in Figure 2.3.

Current Balance Equation

$$\begin{aligned}
 C_m \frac{dV_i}{dt} = & + I_{app} - \bar{g}_L(V_i - E_L) - I_{Na}(V_i, m, h) - I_K(V_i, n) \\
 & - I_T(V_i, m, h, [Ca^{2+}]_i) - I_A(V_i, m, h) \\
 & - I_h(V_i, m, [Ca^{2+}]_i, P) - I_{KL}(V_i) \\
 & - I_{GABA_A}^{RTNTC}(V_i, \{s_{GABA_A,k}^{RTN}\}) - I_{GABA_B}^{RTNTC}(V_i, \{s_{GABA_B,k}^{RTN}\}) \\
 & - I_{GABA_A}^{GPiTC}(V_i, \{s_{GABA_A,k}^{GPi}\}) - I_{GABA_B}^{GPiTC}(V_i, \{s_{GABA_B,k}^{GPi}\}) \\
 & - I_{AMPA}^{SensTC}(V_i, \{s_{AMPA,k}^{Sens}\}) - I_{AMPA}^{PYTC}(V_i, \{s_{AMPA,k}^{PY}\}) \\
 & - I_{NMDA}^{PYTC}(V_i, \{s_{NMDA,k}^{PY}\}) \tag{2.7.85}
 \end{aligned}$$

where $C_m = 1 \mu\text{F}/\text{cm}^2$, $\bar{g}_L = 0.01 \text{ mS}/\text{cm}^2$, $E_L = -70 \text{ mV}$ Destexhe et al. 1996a.

Intrinsic Currents

The sodium current I_{Na} and the delayed rectifier potassium current I_K according to Traub and Miles 1991, are defined by

$$I_{Na}(V_i, m, h) = \bar{g}_{Na} m^3 h (V_i - E_{Na}) \tag{2.7.86}$$

$$\frac{dm}{dt} = \alpha_m(V_i)(1 - m) - \beta_m(V_i)m \tag{2.7.87}$$

$$\frac{dh}{dt} = \alpha_h(V_i)(1 - h) - \beta_h(V_i)h \tag{2.7.88}$$

$$\alpha_m(V_i) = \frac{0.32(V_i + vtraubtc - 13)}{1 - \exp(-(V_i + vtraubtc - 13)/4)} \tag{2.7.89}$$

$$\beta_m(V_i) = \frac{0.28(V_i + vtraubtc - 40)}{\exp(-(V_i + vtraubtc - 40)/5) - 1} \tag{2.7.90}$$

$$\alpha_h(V_i) = 0.128 \exp(-(V_i + vtraubtc - 17)/18) \tag{2.7.91}$$

$$\beta_h(V_i) = \frac{4}{1 + \exp(-(V_i + vtraubtc - 40)/5)} \tag{2.7.92}$$

2.7 The Applied Thalamocortical Network

$$I_K(V_i, n) = \bar{g}_K n^4 (V_i - E_K) \quad (2.7.93)$$

$$\frac{dn}{dt} = \alpha_n(V_i)(1 - n) - \beta_n(V_i)n \quad (2.7.94)$$

$$\alpha_n(V_i) = \frac{0.032(V_i + vtraubtc - 15)}{1 - \exp(-(V_i + vtraubtc - 15)/5)} \quad (2.7.95)$$

$$\beta_n(V_i) = 0.5 \exp(-(V_i + vtraubtc - 10)/40) \quad (2.7.96)$$

where $\bar{g}_{Na} = 90 \text{ mS/cm}^2$, $E_{Na} = 50 \text{ mV}$, $\bar{g}_K = 10 \text{ mS/cm}^2$, $E_K = -95 \text{ mV}$ and $vtraubtc = 30 \text{ mV}$ (gating kinetics adjusted to 36C).

The low-threshold calcium current I_T according to Destexhe et al. 1996a, Bazhenov et al. 1998, is defined by

$$I_T(V_i, m, h, [Ca^{2+}]_i) = \bar{g}_T m^2 h (V_i - E_{Ca}) \quad (2.7.97)$$

$$\frac{dm}{dt} = (m_\infty(V_i) - m)/\tau_m(V_i) \quad (2.7.98)$$

$$\frac{dh}{dt} = (h_\infty(V_i) - h)/\tau_h(V_i) \quad (2.7.99)$$

$$m_\infty(V_i) = \frac{1}{1 + \exp(-(V_i + 59)/6.2)} \quad (2.7.100)$$

$$h_\infty(V_i) = \frac{1}{1 + \exp(-(V_i + 83)/4)} \quad (2.7.101)$$

$$\tau_m(V_i) = 0.13 + \frac{0.22}{\exp(-(V_i + 132)/16.7) + \exp((V_i + 16.8)/18.2)} \quad (2.7.102)$$

$$\tau_h(V_i) = 8.2 + \left[56.6 + \frac{0.27 \exp((V_i + 115.2)/5)}{1 + \exp((V_i + 86)/3.2)} \right] \quad (2.7.103)$$

where $\bar{g}_T = 2.2 \text{ mS/cm}^2$ and the reversal potential strongly depends on the intracellular calcium concentration $[Ca^{2+}]_i$ and is determined by the Nernst equation

$$E_{Ca} = k' \frac{RT}{2F} \log \frac{[Ca^{2+}]_o}{[Ca^{2+}]_i} \quad (2.7.104)$$

where $k' = 1,000$ (constant for unit conversion for E_{Ca} in millivolts),

$R = 8,31441 \text{ mJ/(K}\cdot\text{Mol)}$, $F = 96,480 \text{ coulombs/Mol}$, $T = 309,15 \text{ K}$, and $[Ca^{2+}]_o = 2 \text{ mM}$ is the extracellular calcium concentration corresponding to a temperature of 36C and the intracellular calcium dynamic obeys a first order differential equation

$$\frac{d[Ca^{2+}]_i}{dt} = -AI_T - ([Ca^{2+}]_i - [Ca^{2+}]_\infty) / \tau \quad (2.7.105)$$

2.7 The Applied Thalamocortical Network

where $[Ca^{2+}]_{\infty} = 2.4 \cdot 10^{-4}$ mM denotes the equilibrium calcium concentration, $A = 5.18 \cdot 10^{-5}$ (mM·cm²)/(ms·μA) and $\tau = 5$ ms Bazhenov et al. 1998.

The transient potassium current I_A according to Bazhenov et al. 1998; Huguenard and McCormick 1992 can be denoted by

$$I_A(V_i, m, h) = \bar{g}_A m^4 h (V_i - E_K) \quad (2.7.106)$$

$$\frac{dm}{dt} = (m_{\infty}(V_i) - m) / \tau_m(V_i) \quad (2.7.107)$$

$$\frac{dh}{dt} = (h_{\infty}(V_i) - h) / \tau_h(V_i) \quad (2.7.108)$$

$$m_{\infty}(V_i) = \frac{1}{1 + \exp(-(V_i + 60)/8.5)} \quad (2.7.109)$$

$$h_{\infty}(V_i) = \frac{1}{1 + \exp(-(V_i + 78)/6)} \quad (2.7.110)$$

$$\tau_m(V_i) = 0.1 + \frac{0.27}{\exp((V_i + 35.8)/19.7) + \exp(-(V_i + 79.7)/12.7)} \quad (2.7.111)$$

if $V_i < -63$ mV

$$\tau_h(V_i) = \frac{0.27}{\exp((V_i + 46)/5) + \exp(-(V_i + 238)/37.5)} \quad (2.7.112)$$

if $V_i > -63$ mV

$$\tau_h = 5.1 \quad (2.7.113)$$

where $\bar{g}_A = 1$ mS/cm² and $E_K = -95$ mV.

The hyperpolarization-activated cation current I_h according to Destexhe et al. 1996a, Bazhenov et al. 1998, Huguenard and McCormick 1992, is defined as

$$I_h = \bar{g}_h ([O] + k_h [O_L]) (V_i - E_h) \quad (2.7.114)$$

with a maximal conductance of $\bar{g}_h = 0.02$ mS/cm² and $E_h = -40$ mV. Because of the factor $k_h = 2$, the conductance of the calcium-bound open state is twice that of the unbound open state Destexhe et al. 1996a.

The full kinetic scheme according to Destexhe et al. 1996a is



2.7 The Applied Thalamocortical Network

$$O + P_1 \xrightleftharpoons[k_4]{k_3} O_L, \quad (2.7.117)$$

where $k_1 = 2.5 \times 10^7 \text{ mM}^{-4} \text{ ms}^{-1}$, $k_2 = 4 \times 10^{-4} \text{ ms}^{-1}$ (half-activation of 0.002 mM Ca^{2+}), $k_3 = 0.1 \text{ ms}^{-1}$, $k_4 = 0.001 \text{ ms}^{-1}$ are constants and $\alpha(V_i)$ and $\beta(V_i)$ are the voltage-dependent transition rates Bazhenov et al. 1998

$$\alpha(V_i) = m_\infty(V_i)/\tau(V_i) \quad (2.7.118)$$

$$\beta(V_i) = (1 - m_\infty(V_i))/\tau(V_i) \quad (2.7.119)$$

$$m_\infty(V_i) = \frac{1}{1 + \exp(-(V_i + 74)/5.5)} \quad (2.7.120)$$

$$\tau(V_i) = 5.3 + \frac{267}{\exp((V_i + 71.5)/14.2) + \exp(-(V_i + 89)/11.6)} \quad (2.7.121)$$

A non-regulated calcium version of I_h (with only voltage dependency) is also incorporated where the equations are adopted from Huguenard and McCormick 1992

$$I_h(V_i, m) = \bar{g}_h m (V_i - E_h) \quad (2.7.122)$$

$$\frac{dm}{dt} = (m_\infty(V_i) - m)/\tau_m(V_i) \quad (2.7.123)$$

$$m_\infty(V_i) = \frac{1}{1 + \exp(-(V_i + 75)/5.5)} \quad (2.7.124)$$

$$\tau_m(V_i) = \frac{1}{\exp(-0.086 \cdot V_i - 14.6) + \exp(0.07 \cdot V_i - 1.87)} \quad (2.7.125)$$

with $\bar{g}_h = 0.1 \text{ mS/cm}^2$ and $E_h = -40 \text{ mV}$.

The leak potassium current I_{KL} is represented according to McCormick and Huguenard 1992 by

$$I_{KL} = \bar{g}_{KL} (V_i - E_{KL}) \quad (2.7.126)$$

$\bar{g}_{KL} = 0.012 \text{ mS/cm}^2$ and $E_{KL} = -95 \text{ mV}$.

Synaptic Currents

The AMPA current I_{AMPA}^{PYTC} from PY to TC is defined by Golomb and Amitai 1997

$$I_{AMPA}^{PYTC}(V_i, \{s_{AMPA,k}^{PY}\}) = \bar{g}_{AMPA} s(V_{TC} - E_{AMPA}) \quad (2.7.127)$$

2.7 The Applied Thalamocortical Network

with $E_{AMPA} = 0$ mV, the gating variable s depends on V_{PY} , and \bar{g}_{AMPA} in units mS/cm^2 .

The AMPA gating variable s is given as

$$\begin{aligned} \frac{ds}{dt} &= k_{fA} X_{\infty}(V_{PY})(1 - s) - k_{rA}s \\ X_{\infty}(V_{PY}) &= \frac{1}{1 + \exp(-(V_{PY} - \theta_{syn})/\sigma_{syn})} \end{aligned} \quad (2.7.128)$$

where $k_{fA} = 1.0 \text{ ms}^{-1}$, $k_{rA} = 0.2 \text{ ms}^{-1}$, $\theta_{syn} = -20$ mV, $\sigma_{syn} = 2$ mV Golomb and Amitai 1997. The AMPA current I_{AMPA}^{SensTC} from sensory neurons to TC is defined as Golomb and Amitai 1997

$$I_{AMPA}^{SensTC}(V_i, \{s_{AMPA,k}^{Sens}\}) = \bar{g}_{AMPA}s(V_{TC} - E_{AMPA}) \quad (2.7.129)$$

with the very same parameters as in 2.7.127 and gating variable s obey the same equations as Equation 2.7.128.

The NMDA current I_{NMDA}^{PYTC} from PY to TC is defined by Golomb et al. 2006

$$I_{NMDA}^{PYTC}(V_i, \{s_{NMDA,k}^{PY}\}) = I_{syn} = \bar{g}_{NMDA}s f(V_{TC})(V_{TC} - E_{NMDA}) \quad (2.7.130)$$

with $E_{NMDA} = 0$ mV, the gating variable s depends on V_{PY} , and \bar{g}_{NMDA} in units mS/cm^2 . Additional dependence on postsynaptic membrane potential $f(V_{TC})$ are the same as in Equation 2.7.81.

The NMDA gating variables according to the model according to Golomb et al. Golomb et al. 2006 are the same as in Equation 2.7.82.

The $GABA_A$ current $I_{GABA_A}^{RTNTC}$ from RTN to TC Golomb et al. 1996 is defined by

$$I_{GABA_A}^{RTNTC}(V_i, \{s_{GABA_A,k}^{RTN}\}) = \bar{g}_{GABA_A}s(V_{TC} - E_{GABA_A}) \quad (2.7.131)$$

with $E_{GABA_A} = -85$ mV, the gating variable s depends on V_{RTN} , and \bar{g}_{GABA_A} in units mS/cm^2 .

$GABA_A$ gating variable s using the same equations and parameters as in Equation 2.7.84.

The $GABA_A$ current $I_{GABA_A}^{GPiTC}$ from GPi to TC is defined by Golomb et al. 1996

$$I_{GABA_A}^{GPiTC}(V_i, \{s_{GABA_A,k}^{GPi}\}) = \bar{g}_{GABA_A}s(V_{TC} - E_{GABA_A}) \quad (2.7.132)$$

with $E_{GABA_A} = -85$ mV, the gating variable s depends on V_{GPi} , and \bar{g}_{GABA_A} in units mS/cm^2 .

$GABA_A$ gating variable s using the same as in Equation 2.7.84.

2.7 The Applied Thalamocortical Network

The $GABA_B$ current $I_{GABA_B}^{RTNTC}$ from RTN to TC is defined by Wang et al. 1995

$$I_{GABA_B}^{RTNTC}(V_i, \{s_{GABA_B,k}^{RTN}\}) = \bar{g}_{GABA_B} s^q (V_{TC} - E_{GABA_B}) \quad (2.7.133)$$

with $E_{GABA_B} = -100$ mV, the gating variable s depends on V_{RTN} , $q = 4$, and \bar{g}_{GABA_B} in units mS/cm^2 .

The $GABA_B$ gating variables are the same as in Equation 2.7.39 and Equation 2.7.40.

$\alpha_x = 5.0 \text{ ms}^{-1}$, $\beta_x = 0.007 \text{ ms}^{-1}$, $\alpha_s = 0.03 \text{ ms}^{-1}$, and $\beta_s = 0.005 \text{ ms}^{-1}$, parameters are chosen in the way that the rise time (≈ 100 ms) and decay time (≈ 200 ms) matches with experimental data Otis et al. 1993.

The $GABA_B$ current $I_{GABA_B}^{GPiTC}$ from GPi to TC Wang et al. 1995

$$I_{GABA_B}^{GPiTC}(V_i, \{s_{GABA_B,k}^{GPi}\}) = \bar{g}_{GABA_B} s^q (V_{TC} - E_{GABA_B}) \quad (2.7.134)$$

Same parameters as in Equation 2.7.38, the gating variable s depends on V_{GPi} and the parameters and equations for gating variables are the same as in Equation 2.7.39 and Equation 2.7.40.

The **sensory neurons** in the schematic description of synaptic interconnection in the simplified thalamocortical network model Figure 2.3 are both modeled as simple as possible, thereby providing only rhythmic inhibitory and excitatory spike or burst activity to TC neurons. The current balance equation only considers spike generating ionic currents.

Current Balance Equations

$$C_m \frac{dV_i}{dt} = + I_{app} - \bar{g}_L (V_i - E_L) - I_{Na}(V_i, m, h) - I_K(V_i, n) \quad (2.7.135)$$

where $C_m = 1 \mu\text{F}/\text{cm}^2$, $\bar{g}_L = 0.05 \text{ mS}/\text{cm}^2$, $E_L = -60$ mV.

Intrinsic Currents

The sodium current I_{Na} and the delayed rectifier potassium current I_K are described according to Hadipour-Niktarash 2006

$$I_{Na}(V_i, h) = \bar{g}_{Na} m^3 h (V_i - E_{Na}) \quad (2.7.136)$$

2.7 The Applied Thalamocortical Network

$$\frac{dm}{dt} = \alpha_m(V_i)(1 - m) - \beta_m(V_i)m \quad (2.7.137)$$

$$\frac{dh}{dt} = \alpha_h(V_i)(1 - h) - \beta_h(V_i)h \quad (2.7.138)$$

$$\alpha_m(V_i) = \frac{0.38(V_i + 29.7)}{1 - \exp(-0.1(V_i + 29.7))} \quad (2.7.139)$$

$$\alpha_h(V_i) = 0.266 \exp(-0.05(V_i + 48)) \quad (2.7.140)$$

$$\beta_m(V_i) = 15.2 \exp(-0.0556(V_i + 54.7)) \quad (2.7.141)$$

$$\beta_h(V_i) = \frac{3.8}{1 + \exp(-0.1(V_i + 18))} \quad (2.7.142)$$

$$I_K(V_i, n) = \bar{g}_K n^4 (V_i - E_K) \quad (2.7.143)$$

$$\frac{dn}{dt} = \alpha_n(V_i)(1 - n) - \beta_n(V_i)n \quad (2.7.144)$$

$$\alpha_n(V_i) = \frac{0.02(V_i + 45.7)}{1 - \exp(-0.1(V_i + 45.7))} \quad (2.7.145)$$

$$\beta_n(V_i) = 0.25 \exp(-0.125(V_i + 55.7)) \quad (2.7.146)$$

with $\bar{g}_{Na} = 90 \text{ mS/cm}^2$, $E_{Na} = 50 \text{ mV}$, $\bar{g}_K = 10 \text{ mS/cm}^2$, $E_K = -95 \text{ mV}$.

2.8 The Amari Neural Field Model

After creating an *in silico* model considering the cell membrane dynamics based on an extended Hodgkin and Huxley formalism, the study of neural networks as a population of a few HH-like cortical neurons becomes extremely interesting. This domain is directly connected to tissue level models that describe the spatiotemporal evolution of coarse-grained variables such as synaptic or firing rate activity in populations of neurons. These equations are known as neural field equations (Amari 1977).

The first studies about such more macroscopic neural activity were developed by Beurle 1956 with concentration on networks of excitatory neurons with no refractory component and then later by Wilson and Cowan 1973 which included both inhibitory and excitatory neurons. Later in the 1970's, Amari considered an effective model for a mixed population of interacting inhibitory and excitatory neurons with typical cortical connections under natural assumptions on the connectivity and firing rate function (commonly referred to as Mexican hat connectivity) (Amari 1977). Amari has used mathematical analyses to study the mechanism of formation and interaction of firing patterns and their response to input stimuli in homogenous fields. According to his assumptions, a neural oscillation occurs in a system consisting of excitatory and inhibitory neurons. Thus, the study of dynamic pattern formation related to neural oscillation is possible through a field consisting of at least two layers (Amari 1977). Amari considered the neural field consisting of m types of neurons, which can be arranged in m layers, each layer includes one type of neuron (Figure 2.4). In his model, the neurons are connected in a random manner. By considering small portions of each layer as homogeneous random subnets, one can treat the entire field as a net composed of these homogeneous subnets (Amari 1977).

As first approach, the basic 1D Amari model, extended by a secondary inhibitory layer, was applied for first time coupling the Llinás model of thalamocortical interaction to a model representing the corresponding neural field potentials. This one dimensional neural field model was then extended to two dimensions: Amari's general idea to express and estimate a neural field F which consists of two or more layers, can be mathematically noted as

$$\tau_i \frac{\partial u_i(x, t)}{\partial t} = -u_i + \sum_{j=1}^m \int_F w_{ij}(x, x'; t - t') Z_j(x', t') dx' dt' + h_i + s_i(x, t), \quad (2.8.147)$$

2.8 The Amari Neural Field Model

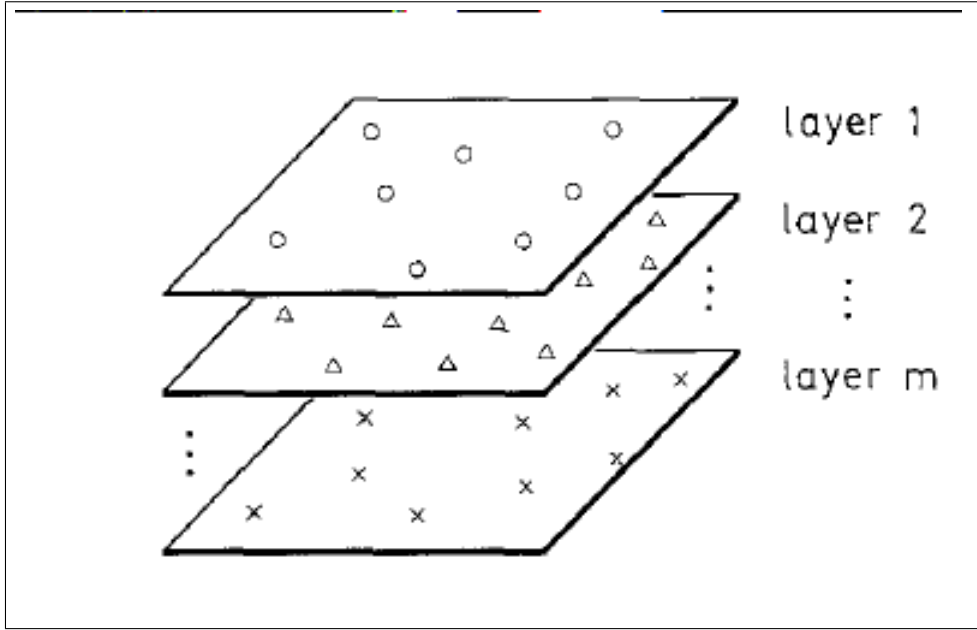


Figure 2.4: The neuron layers of Amari 1977.

where $\partial u_i(x, t)$ is the average membrane potential of the neurons located at position $x = (x_1, x_2)$ at time t on the i^{th} layer. $F = \{x \in \mathbb{R}^2 \mid |x| \leq R\}$. The average activity, i.e., the pulse emission rate of the neurons at x and t can be noted as

$$Z_j(x', t') = f_i[u_i(x', t')], \quad (2.8.148)$$

where f_i is an output function in the form of a non-linear sigmoid function and is monotonically nondecreasing, saturating to a constant for large u_i . The average intensity of connection from neurons in the j^{th} layer at place y to neurons of the i^{th} layer at place x is defined by $w_{ij}(x, y)$. The function $w_{ij}(x, y; t)$ represents the degree of stimulation of neurons at x in the i^{th} layer by the pulses emitted from neurons at place y of the j^{th} layer in t time units before.

This function is used when it is necessary to take pulse conduction time and synaptic delay into consideration. If there is an applied stimulus from outside the field to the neurons of the i^{th} layer, then its intensity at place x at time t will be shown by a component, which can be decomposed into $\bar{s}_i + s_i(x, t)$, where \bar{s}_i denotes the average stimulation level at the i^{th} layer and $s_i(x, t)$ is the deviation from the average \bar{s}_i . The level h_i is the difference between \bar{s}_i and resting potential r_i ($h_i = (\bar{s}_i - r_i)$). That means, if there is no deviational input $s_i(x, t)$, the potential u_i will converge to h_i with τ_i , where τ_i is the time constant for the dynamics of the i^{th} type of neuron. The level h_i is usually negative, depending on the average stimulation \bar{s}_i . Therefore the value of h_i can be controlled from outside the field

(Amari 1977; Kishimoto and Amari 1979).

2.9 Linking Hodgkin-Huxley Neuronal Circuit Activity to Neural Field Potentials

The developed neural field model consists of the introduced two-layer architecture: the excitatory (top) layer represents the mean firing rate of the two compartments of PY neurons, and the inhibitory (sub-) layer is substituting IN neurons, located over a wider spatial area possessing unspecific all-to-all connections (lateral inhibition). According to the Amari field model, a local excitation pattern is elicited by external time-invariant input stimuli, that is applied to the cortical neurons at position x . After excitation of the cortical neurons and achieving the action potentials, the oscillating activity of both, the dendritic tree's characteristic low-pass activity and also the somatic spiking activity are taken as mean firing rate inputs to the neural field model. To do that, it is necessary to map the 1D neuron model firing output (soma + dendrite) to a 2D Gaussian spatiotemporal signal distribution using Equation 2.9.149. Because the distribution of average single-cell activity which naturally arises in a randomly connected network is expected to be Gaussian by the central limit theorem, which states that, under certain conditions, the mean of a sufficiently large number of independent random variables, each with a well-defined mean and well-defined variance, will be approximately normally distributed. The spatiotemporal signal distribution is defined as

$$f(x) = a \exp\left(-\frac{(x - x_0)^2}{2\sigma^2}\right), \quad (2.9.149)$$

where a is the height of the curve's peak that is substituted by the amplitude of somatic and dendritic activity calculated. x_0 is the location parameter or a mean value which is replaced by a coordinate of the firing neurons (see Figure 3.10) for chosen coordinates), and σ^2 is the squared scale parameter which corresponds to the variance of the distribution. It should be noted that the developed 2D field model requires a two dimensional Gaussian function since the average value which stands at $x = (x_0, y_0)$ has two coordinates, so

$$f(x, y) = a \exp\left(-\frac{(x - x_0)^2}{2\sigma_x^2} + \frac{(y - y_0)^2}{2\sigma_y^2}\right) \quad (2.9.150)$$

2.9 Linking Hodgkin-Huxley Neuronal Circuit Activity to Neural Field Potentials

was applied in the 2D domain. Therefore, each stimulus in this model can be depicted for the somatic part as

$$S_{PY_{som}} = \frac{1}{C_m} (-\bar{g}_L(V_S - E_L) - I_{Na}(V_S, h) - I_K(V_S, n) - I_{Ca}(V_S) - I_{AHP}(V_S, [Ca^{2+}]_i) - \frac{g_c}{p}(V_S - V_D) + C_m V_m) \exp\left(-\frac{(y - y_0)^2}{2\sigma_y^2}\right) \quad (2.9.151)$$

and for the dendritic part as

$$S_{PY_{den}} = \frac{1}{C_m} (-\bar{g}_L(V_D - E_L) - I_{Ca}(V_D) - I_{AHP}(V_D, [Ca^{2+}]_i) - \frac{g_c}{1-p}(V_D - V_S) + I_{syn}) \exp\left(-\frac{(y - y_0)^2}{2\sigma_y^2}\right) \quad (2.9.152)$$

After arrival of the rated stimulation in the dynamics pattern as an input, the transformed current value of the field can be computed through Equation 2.9.153. As stated, the field is generated by a set of four pyramidal neurons. So eight inputs must be considered here, four to the dendritic and four to the somatic compartments:

$$\begin{aligned} \frac{du(x, t)}{dt} = & \frac{1}{\tau} (-u(x, t) + h_u + \int_F w_u(x - x') f[u(x', t)] dx' - \int_F w_v(x - x') f[v(x', t)] dx' \\ & + S_{PY1_{som}}(x, t) + S_{PY2_{som}}(x, t) + S_{PY3_{som}}(x, t) + S_{PY4_{som}}(x, t) \\ & + S_{PY1_{den}}(x, t) + S_{PY2_{den}}(x, t) + S_{PY3_{den}}(x, t) + S_{PY4_{den}}(x, t) \end{aligned} \quad (2.9.153)$$

Here, $\frac{du(x, t)}{dt}$ is the rate of each neuron's change of field activation level across the spatial dimension x as a function of time t . τ is the time scale of the dynamics and $u(x, t)$ is defined as the activation in the field at each position x at time t and is the first factor that advances the rate of change of activation and due to its negative term, the activation changes towards the activation level h_u , that is relevant for the threshold function f . $F = \{x \in \mathbb{R}^2 \mid |x| \leq R\}$.

Based on the Amari model introduced in 1977, the field in this model also consists of excitatory and inhibitory layers, in which the inhibitory neurons only target the excitatory neurons. Moreover, the excitatory neurons have very narrow fan-out connections to the inhibitory neurons so that the excitatory neurons at place x excite the inhibitory neurons at place x only (Amari 1977).

2.10 Backpropagation of the Neural Field Potentials on the Cortical Neurons

This local excitation and lateral inhibition is respectively defined by

$$\int_F w_u(x - x')f[u(x', t)]dx' \text{ and } \int_F w_v(x - x')f[v(x', t)]dx' \text{ in Equation 2.9.153.}$$

The intrafield interaction between the neurons of one layer takes the shape of a convolution over the threshold field $f(u)$ with a homogeneous convolution kernel w_u . The interfield interaction between the neurons placed at two layers follows the same scheme with the threshold field $f(v)$ and convolution kernel w_v .

The threshold function f can either be a step function or have a smoother sigmoidal pattern such as

$$f(u) = \frac{1}{1 + \exp[-\beta(u - u_0)]}. \quad (2.9.154)$$

This determines that in both cases only the field parts which are sufficiently activated are contributing to intrafield interactions. Here, β is determined as the sigmoidal function's slope and shows the degree to which neurons close to threshold contribute to the activation dynamics. u_0 is the inflection point, namely threshold point. Furthermore the connectivity w which is deduced from Gaussian kernel and is often referred to as lateral inhibition explains excitatory behavior over small distances, inhibitory over medium distances and either inhibitory or zero over larger distances (global inhibition). This interaction mode is widely applied in modeling, known as Mexican hat function:

$$w(x - x') = \exp\left(-0.5\frac{(x - x')^2}{\sigma^2}\right). \quad (2.9.155)$$

where σ denotes the width of the excitatory part of the kernel.

A detailed description of these functions and their parameters can be found in Toledo-Aral et al. 1997.

2.10 Backpropagation of the Neural Field Potentials on the Cortical Neurons

This part of the model describes how to incorporate the effect of neural field oscillations at position x and time t calculated by the Amari neural field model on the membrane potential of neurons by means of the single neuron's Hodgkin-Huxley formalism embedded in the neural circuit model of Llinás and his colleagues (Llinás and Ribary 1993; Llinás et al. 1994, 1998, 2002).

2.10 Backpropagation of the Neural Field Potentials on the Cortical Neurons

With regard to the Nernst model, the membrane potential V_m defined as the difference in electrical potential between the intracellular and the surrounding extracellular medium of a neuron is proportional to the current I_m passing into the cell at any given time. This current is determined by the membrane capacitance C_m as a multiplication factor and can be described via the basic equation for a single neuron:

$$C_m \cdot V_m = I_m. \quad (2.10.156)$$

In this way, it is possible to convert the neural field potentials to electric current at a given spatial point of a modeled neuron and to use that as an additional feedback input for the thalamocortical circuit in order to calculate the effects of the generated field potentials back on each pyramidal neuron. Because changes in the neural signaling properties will change the resonant states in the network, it is expected that this feedback is mandatory to gain a valid multiscale model.

Since we separated the PY neurons into a dendritic and a somatic compartment, the potential equations for each part are given by

$$\begin{aligned} \frac{dV_S}{dt} = & \frac{1}{C_m} (-\bar{g}_L(V_S - E_L) - I_{Na}(V_S, h) - I_K(V_S, n) \\ & - I_{Ca}(V_S) - I_{AHP}(V_S, [Ca^{2+}]_i) - \frac{g_c}{p}(V_S - V_D) + I_{app}), \end{aligned} \quad (2.10.157)$$

and

$$\begin{aligned} \frac{dV_D}{dt} = & \frac{1}{C_m} (-\bar{g}_L(V_D - E_L) - I_{Ca}(V_D) - I_{AHP}(V_D, [Ca^{2+}]_i) \\ & - \frac{g_c}{1-p}(V_D - V_S) + I_{syn}), \end{aligned} \quad (2.10.158)$$

where C_m is the membrane capacitance, V_S and V_D are the membrane potentials of somatic and dendritic compartment, respectively, and $\bar{g}_L(V_S - E_L)$ and $\bar{g}_L(V_D - E_L)$ depict the corresponding leakage conductance term for each compartment. The current flow between the soma and the dendrite is proportional to $(V_S - V_D)$ in A/cm^2 , with coupling conductance $g_c = 2mS/cm^2$ and the parameter $p = \text{somatic area/total area} = 0.5$. The cell can be either excited by an injected current I_{app} (in $\mu A/cm^2$) to the soma or by synaptic inputs to the dendrite (Wang 1998).

According to recent research in rat cortical pyramidal neuron stimulation, it has been found that extracellular fields cause changes in the exposed cell's somatic membrane potentials (Anastassiou et al. 2011). Therefore, the feedback current

2.10 Backpropagation of the Neural Field Potentials on the Cortical Neurons

caused by the neural fields is only modeled in the somatic part of the two compartment model as I_{app} .

Chapter 3

Results

3.1 cAg-NPs Effects on Neuronal Cells *in vitro* and *in silico*

The results of measurements of sodium current amplitudes are shown in Table 3.1. Averages (medians) (\tilde{x}) and standard deviations (σ) in I_{Na} amplitudes before and after cAg-NPs addition and differences in median ($\Delta\tilde{x}$) between controls and cAg-NPs exposed cells at different concentrations are represented there. Since the amplitudes of the controls (baseline) vary, the values have been normalized. Table 3.2 indicates the amplitudes of I_{Na} before and after cAg-NP addition as total values.

The attenuation of the amplitude occurred rapidly after the application of the cAg-NPs and was then recorded in another 3 to 5 cells in the treated dish. Suppression of I_{Na} was observed in 43 of 45 experiments. In another group of experiments, cAg-NPs ($16\mu M$) were applied locally via an application pipette to chromaffin cells after recording of control action potentials. Current voltage relationships were recorded under control conditions and after application of cAg-NPs. Figure 3.1 and 3.2 show a representative experiment. Figure 3.1 depicts the current-voltage relation fit and Figure 3.2 shows single depolarizations to $-0mV$ which were applied to track changes in sodium current amplitude. I_{Na} was reduced within seconds of application with maximal block occurring after about two minutes. In some cases substantial recovery occurred within 10 minutes of application. There was no significant shift

3.1 cAg-NPs Effects on Neuronal Cells *in vitro* and *in silico*

Table 3.1: Normalized amplitudes of I_{Na} before and after cAg-NPs addition (holding potential $-70mV$, depolarization potential $-20mV$).

cAg-NPs concentration	\tilde{x}^a before cAg-NPs normalized	\tilde{x} after cAg-NPs normalized	σ^b before cAg-NPs normalized	σ after cAg-NPs normalized	$\Delta\tilde{x}^c$ normalized
$13\mu Mol(1/100)$	1	0.91	0.14	0.12	0.09
$16\mu Mol(1/80)$	1	0.77	0.19	0.11	0.23
$43\mu Mol(1/30)$	1	0.52	0.18	0.09	0.48
$130\mu Mol(1/10)$	1	0.47	0.13	0.10	0.53
$1.3mMol(1/1)$	1	0.31	0.13	0.23	0.69

^a \tilde{x} = Normalized average amplitude

^b σ = Normalized standard deviation

^c $\Delta\tilde{x}$ = Normalized difference between controls and cAg-NPs exposed cells

Table 3.2: Amplitudes of I_{Na} before and after cAg-NPs addition as total values (holding potential -70 mV, depolarization potential -20 mV).

cAg-NPs concentration	\tilde{x}^a before cAg-NPs in pA	\tilde{x} after cAg-NPs in pA	σ^b before cAg-NPs in pA	σ after cAg-NPs in pA	$\Delta\tilde{x}^c$ in pA
$13\mu Mol(1/100)$	634.2	579.3	86	77.5	54.9
$16\mu Mol(1/80)$	613.4	472.3	116.6	67.5	141.1
$43\mu Mol(1/30)$	731.9	382.9	129.8	66.6	349
$130\mu Mol(1/10)$	824.7	384.9	105.6	84.3	439.9
$1.3mMol(1/1)$	609.3	190.4	81.4	141.3	418.9

^a \tilde{x} = Average amplitude expressed as median value in pA

^b σ = Standard deviation

^c $\Delta\tilde{x}$ = Difference in median between controls and cAgNP exposed cells.

3.1 cAg-NPs Effects on Neuronal Cells *in vitro* and *in silico*

in the voltage-dependence of the I_{Na} ($3.1 + 2.6mV$, mean + SD) and no significant shift in the Null potential of I_{Na} ($4.4 + 4.9mV$, mean + SD).

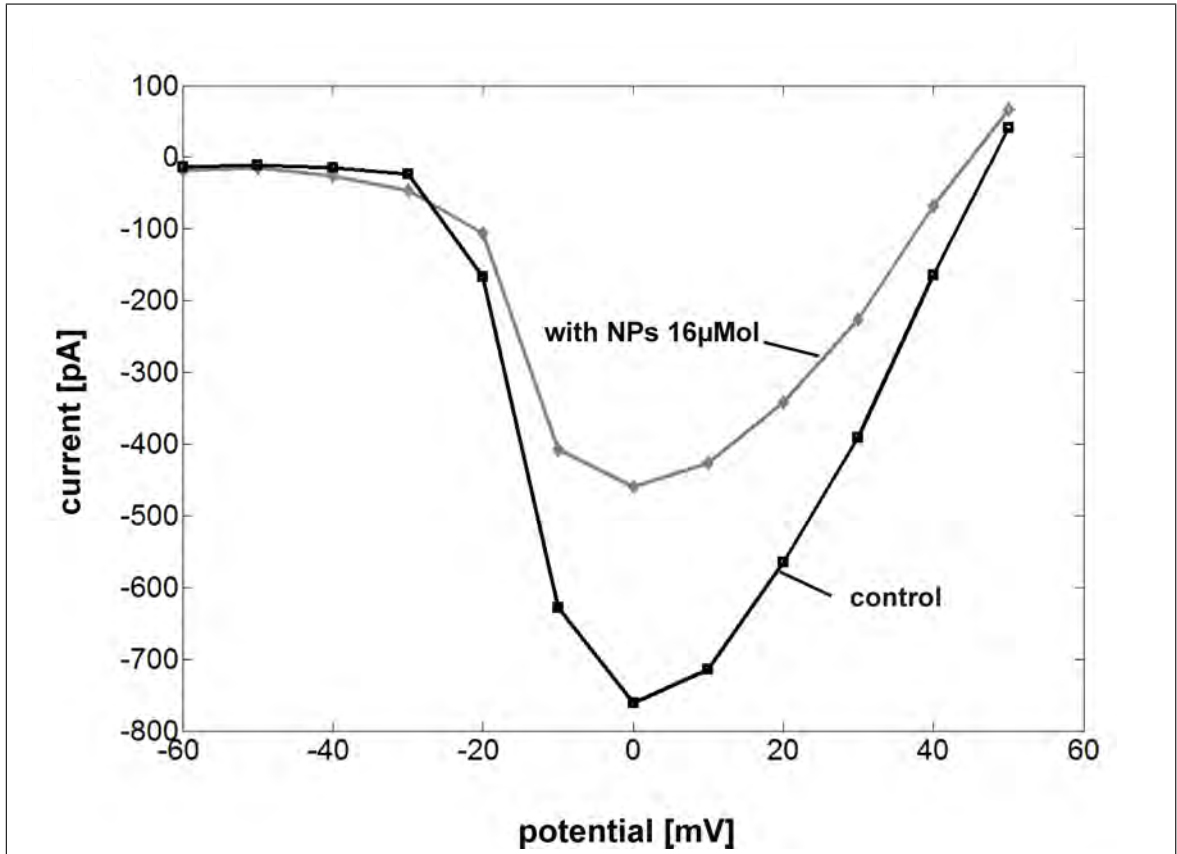


Figure 3.1: Local application of cAg-NPs to chromaffin cells. A representative IV-curve of a cell before and after application of cAg-NPs ($16\mu Mol$, grey, and corresponding control, black).

Five representative sodium current curves taken after the application of cAg-NPs and their corresponding controls from the $1.3mM$ dataset have been selected for the DE-fitting procedure. Before processing, a cubic spline interpolation was employed to smooth the curves, to reduce noise, and to produce consistent vector length. Figure 3.3 shows representative sodium currents as continuous lines: on top (a) is a control sodium current, the bottom (b) shows the sodium current of the same cell after the addition of cAg-NPs.

The dashed lines in Figure 3.3 represent the corresponding model fittings to these curves by the DE-algorithm. The fitting process generated estimates of the 13 free coefficients (ξ) in Equation 2.4.9 and 2.4.10. There were conspicuous changes

3.1 cAg-NPs Effects on Neuronal Cells *in vitro* and *in silico*

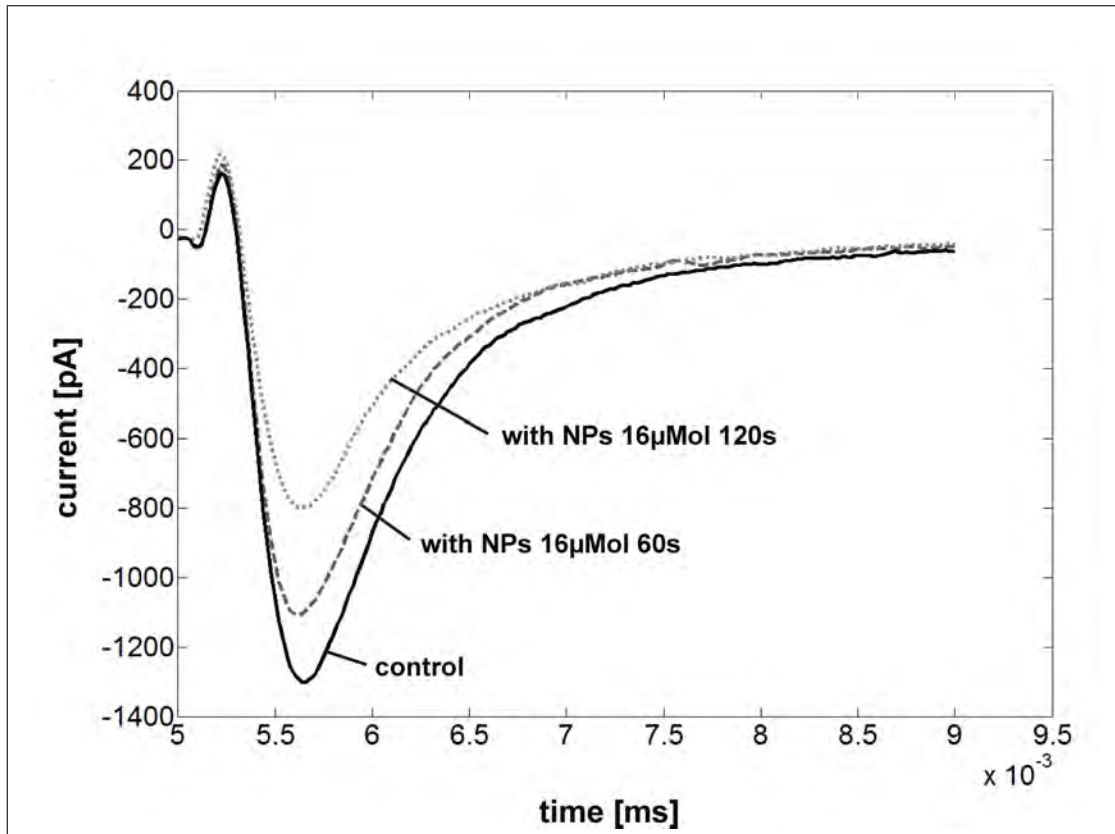


Figure 3.2: Local application of cAg-NPs to chromaffin cells. Records of I_{Na} before and after local application of cAg-NPs after 60s and 120s respectively.

in parameters $\xi_1, 2, 6, 7, 8, 9, 10$ & 12 (Equation 2.4.9 and 2.4.10). By transferring those findings back into a more macroscopic (transfer rate coefficients) level of the Hodgkin-Huxley equations, the transfer rate coefficients and the reversal potential V_{Na} (Equation 2.4.9 and 2.4.10) were found to be potentially modified. Since the reduction in amplitude of I_{Na} occurred without an appreciable shift in either activation voltage or null potential, it is unlikely that a change in V_{Na} is involved in the effects of cAg-NPs on I_{Na} . Therefore V_{Na} was fixed and the simulation was ran again. As expected, very good fits could be achieved when only changes in the transfer rate coefficients $\alpha_h, \alpha_m, \beta_m$ were allowed. Figure 3.4 shows the changes of these variables after particle exposition in a normalized bar diagram. Changes in these parameters were required for a good fit to the cAg-NPs data.

Figure 3.5 shows the output of a representative sodium current fit with the relevant parameters changes (dashed lines).

3.1 cAg-NPs Effects on Neuronal Cells *in vitro* and *in silico*

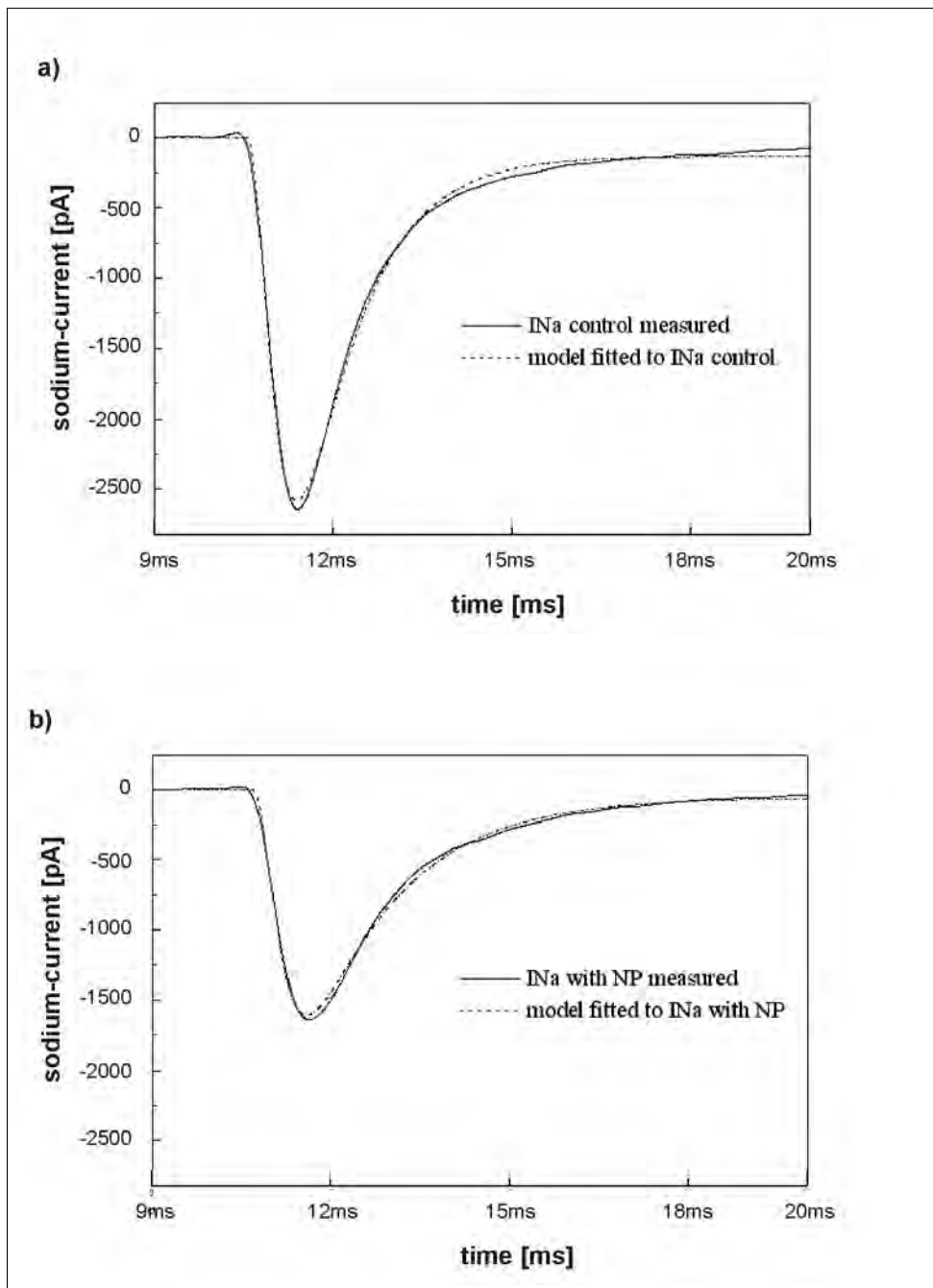


Figure 3.3: Measured sodium current without (a) and with (b) cAg-NPs (solid lines, holding potential $-70mV$, depolarization potential $-20mV$), and the curve fits by DE (dashed lines).

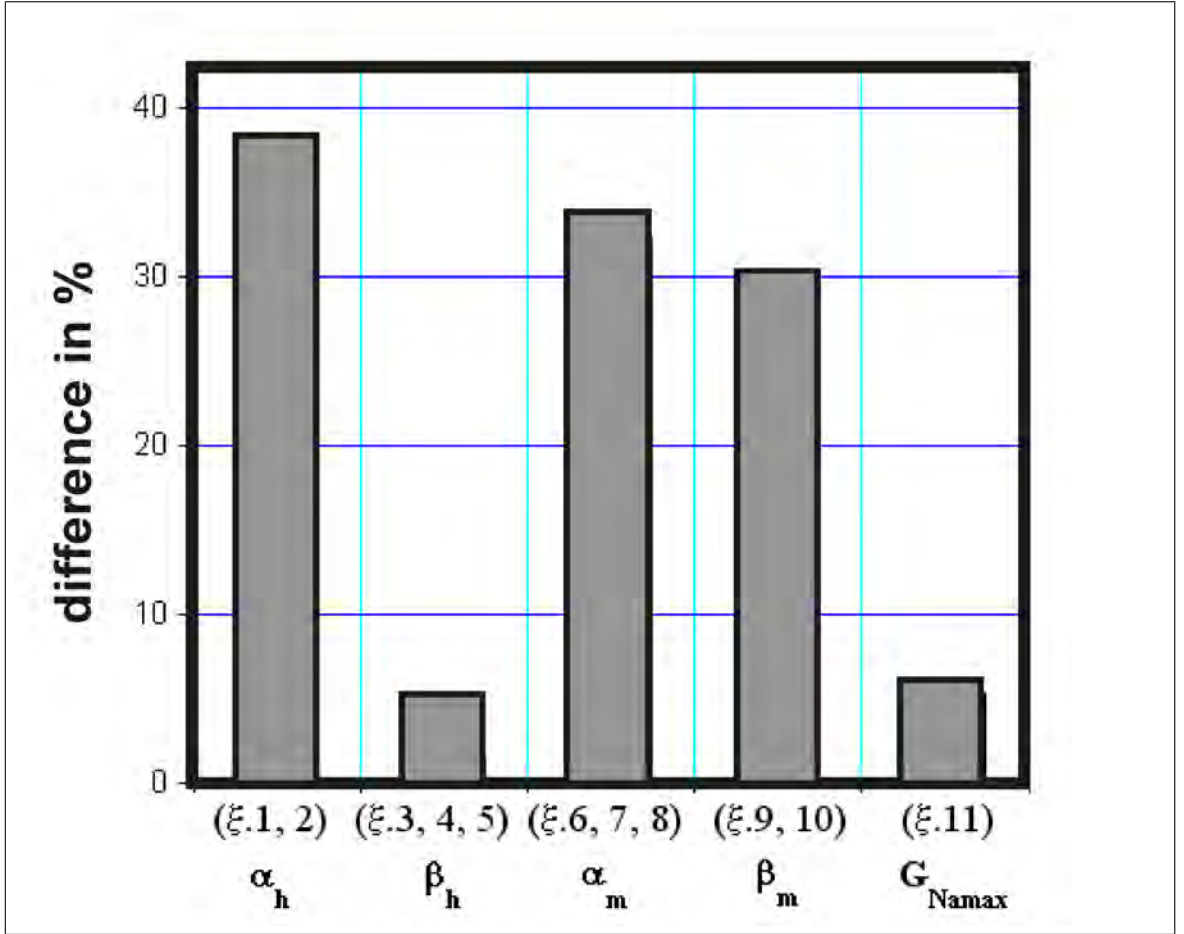


Figure 3.4: Differences of model fitted α_h , β_h , α_m , β_m , and G_{Namax} between the measured sodium current with cAg-NPs in $130\mu Mol$ concentration and the corresponding controls. $\xi.13$ (stim-time) is not considered.

3.2 cAg-NPs Effects on the chosen Neuronal Feedback Circuit

To estimate the impact of cAg-NPs on the activity in a neuronal feedback circuit, the simulated results of the first model were employed to modify the properties of I_{Na} of thalamic cells in the network model of corticothalamic interactions. The initial conditions for all gating variables of each neuron model involved were calculated according to their steady-state functions whereas the membrane potential's initial conditions were taken from cited references. To activate the feedback circuit, a single action potential (AP) was generated in the model sensory neuron which directly projects to STC by utilizing a brief depolarisation current pulse of $I_{app} = 6\mu A/cm^2$. This leads to a small depolarization in STC and as a consequence of the specific

3.2 cAg-NPs Effects on the chosen Neuronal Feedback Circuit

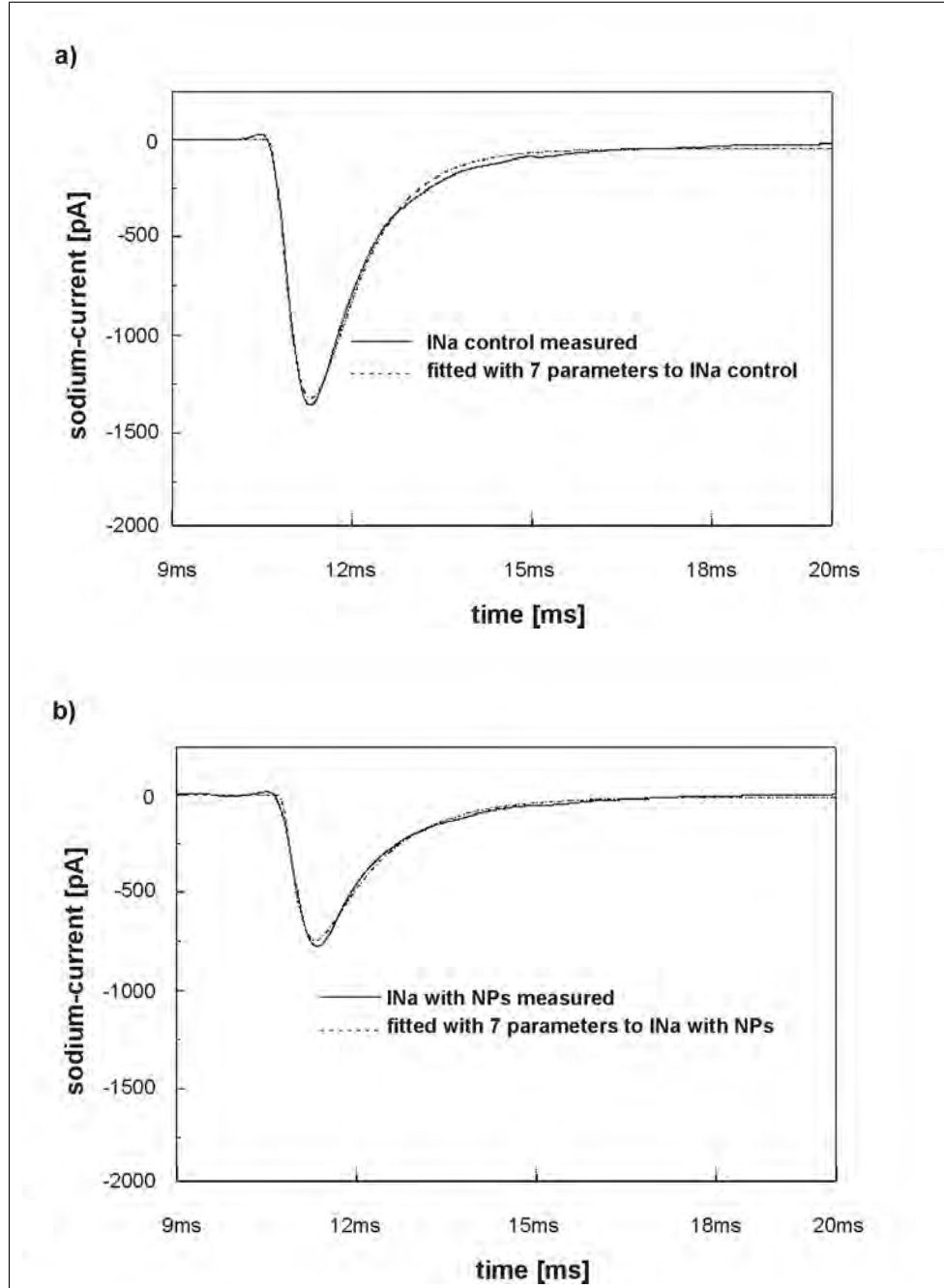


Figure 3.5: DE fittings (dashed lines) utilizing just the 7 identified Hodgkin-Huxley-Equation parameters (α_h , α_m , β_m) and the corresponding electrophysiologically measured currents for control (a) and cAg-NPs ($130\mu\text{Mol}$) transfected (b).

3.3 cAg-NPs Effects on 2D Neural Field Oscillations

synaptic parameters, all neurons fire in a $6 - 8Hz$ bursting oscillation mode. The resulting membrane potentials of the cortical PY neuron 1, 2, 3 & 4 are shown in Figure 3.6 for a time interval of $4s$.

Figure 3.7 illustrates the resulting membrane potentials of the cortical inhibitory IN, RTN1, RTN2, STC and the NSTC neuron for $4s$. The black graphs in both figures show the behavior of the engaged cells after the initial AP in the sensory neuron (see Figure 2.3) under normal physiological conditions.

The gray lines show the behavior of the same cells in the network after altering I_{Na} of thalamic cells, i.e., NSTC, STC & RTNs consistent with the changes in I_{Na} observed after cAg-NP application. Variations in the firing patterns of all cells embedded in the simplified network model were apparent after this manipulation. Changes in activity can be seen in Table 3.2 as mean values including the corresponding standard deviations (σ) for interburst intervals, the resulting interburst frequencies and the intraburst frequencies before and after hypothesized cAg-NPs presence in thalamic cells for $4s$ (only the bursting neurons were considered for the statistics).

Table 3.2 reveals that the interburst frequencies are slightly increased after cAg-NPs application in the thalamus core. The intraburst frequencies are found to be slightly decreased for PY1, PY2 and for IN. In contrast, the intraburst frequencies for both RTN1 and RTN2 are slightly increased whereas the intraburst frequency for PY4 is more than doubled after NPs addition.

3.3 cAg-NPs Effects on 2D Neural Field Oscillations

Before modeling the influences of cAg-NPs on neural field potentials, it was investigated how the neural field potentials influence the spike generation in neurons that are physically located within such fields. If the feedback changes in the underlying neuronal signaling within the circuit has the potential to cause observable changes in the generated field potentials themselves, this enhanced model will be the basis for the investigation of NPs induced modifications of neural field oscillations.

After initiating an action potential ($4\mu A/cm^2$) at the left sensory neuron of the

3.3 cAg-NPs Effects on 2D Neural Field Oscillations

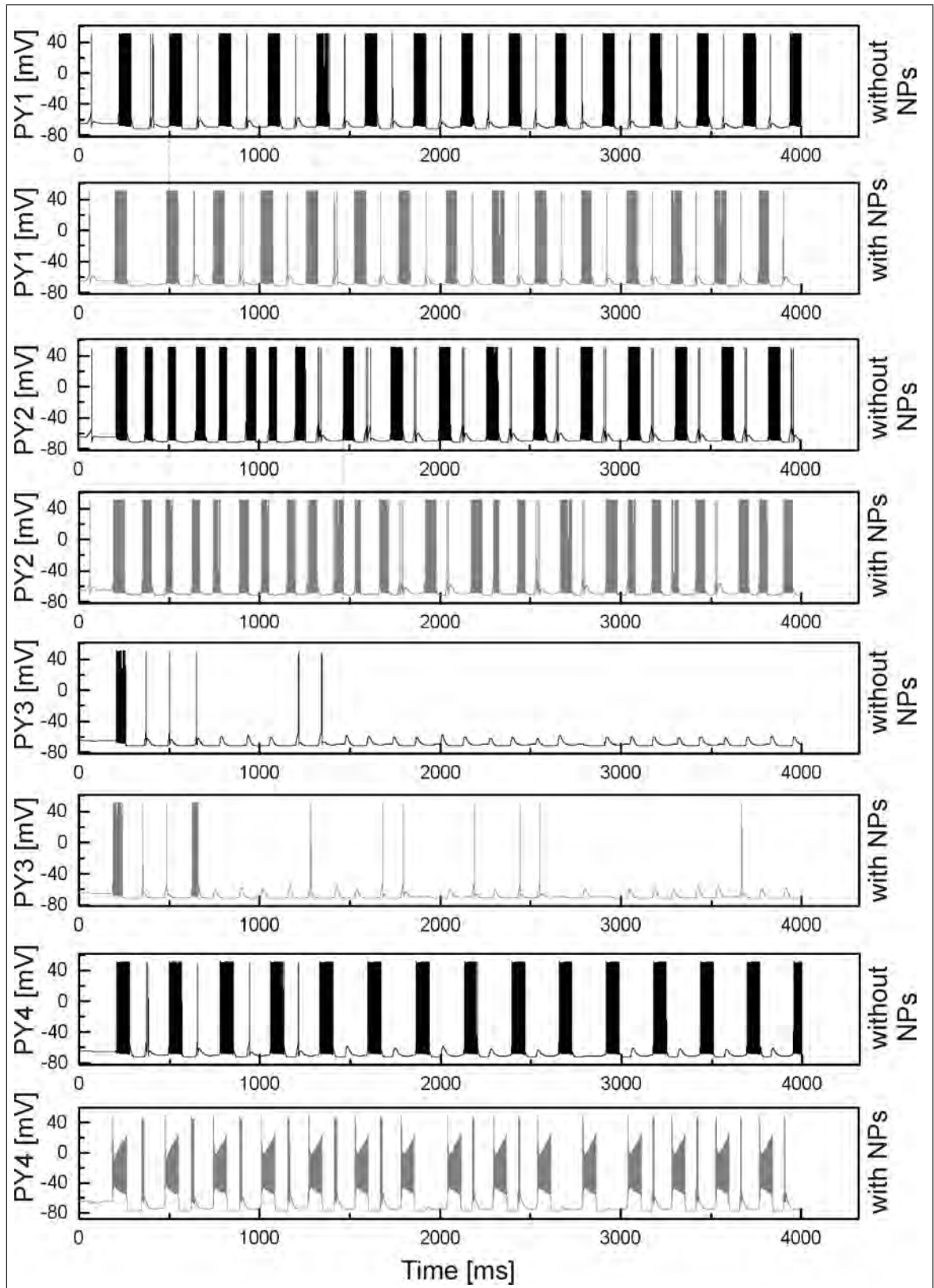


Figure 3.6: Differences in firing patterns of PY1-, PY2-, PY3 and PY4- neuron for 4s before and after cAg-NPs application in thalamic neurons.

3.3 cAg-NPs Effects on 2D Neural Field Oscillations

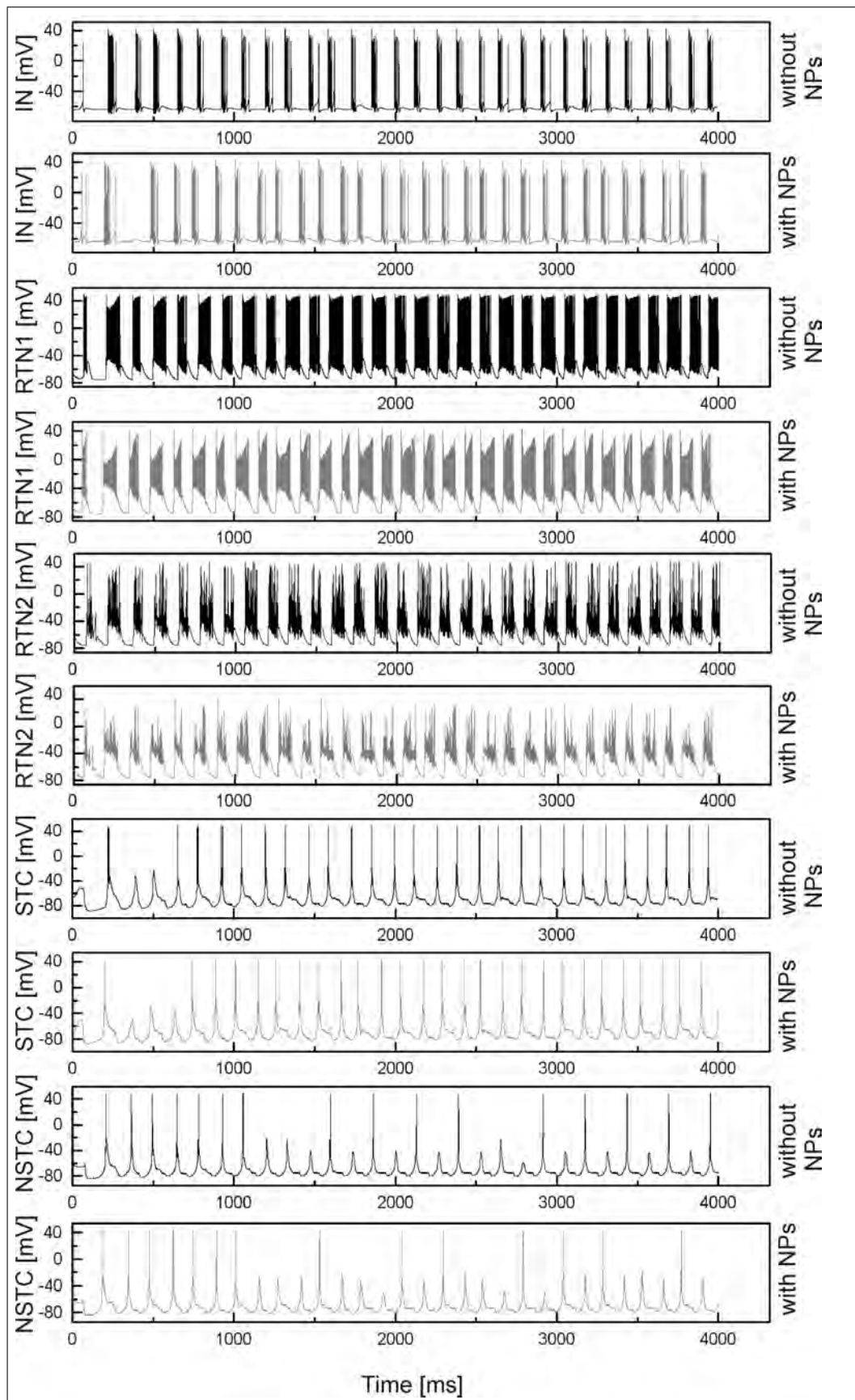


Figure 3.7: Differences in firing patterns of IN-, RTN1-, RTN2, STC- and NSTC- neuron for 4s before and after cAg-NPs application in RTN and STC neurons.

3.3 cAg-NPs Effects on 2D Neural Field Oscillations

utilized circuit (Figure 2.3, left), STC depolarizes and the thalamocortical network starts oscillating. To ease the identification and in order to compare the model output on a larger temporal scale, a likewise synchronized $5 - 12Hz$ bursting activity was again evoked instead of the synchronized $40Hz$ oscillations. Figure 3.8 shows the somatic firing activity of the involved PY neurons for $3000ms$ as black lines. The spiking activity of the thalamic neurons and the IN is depicted as well as black lines in Figure 3.9. The simulation of the neural field activity generated

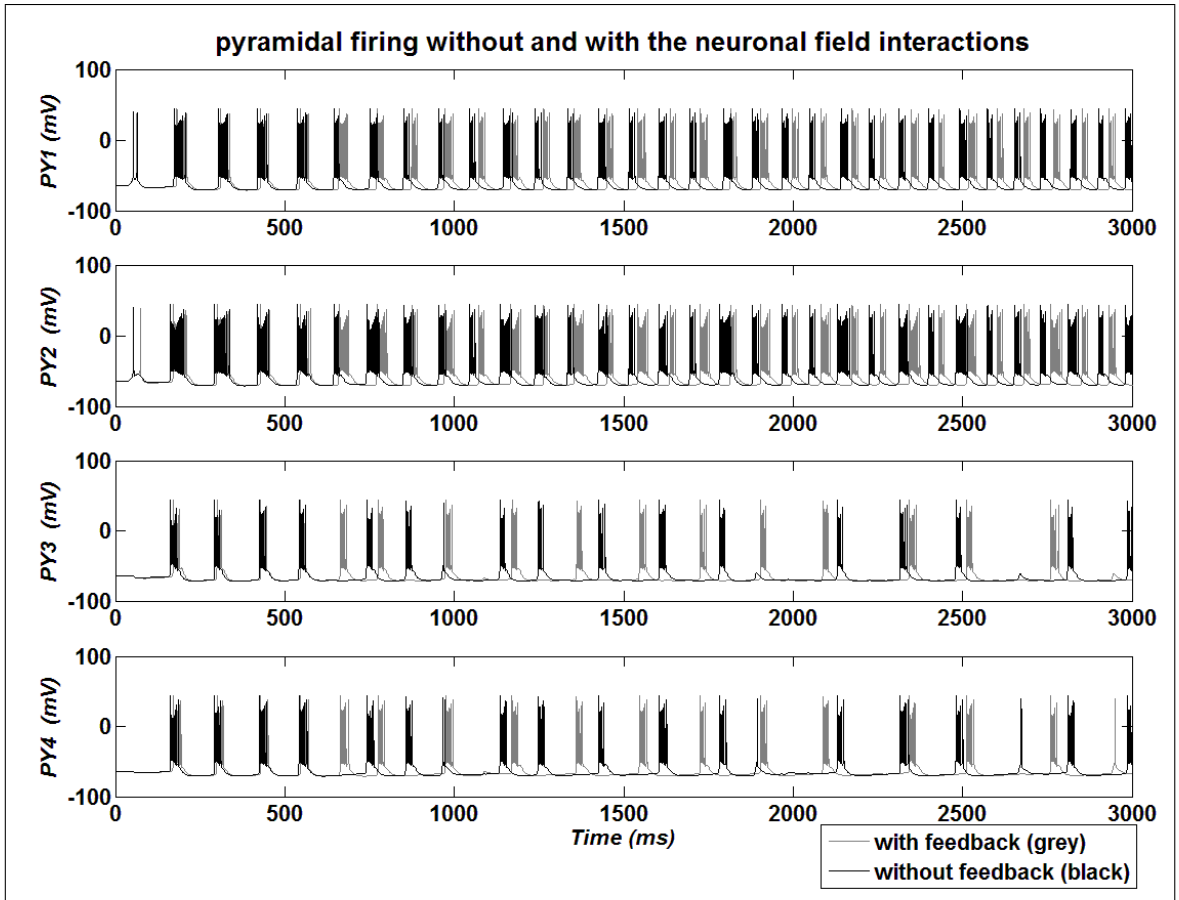


Figure 3.8: Comparison of the somatic membrane potentials (in mV) for all four PY neurons with and without neural field interactions as a function of time (ms). Black graphs depict the PY firing without field interactions, the grey graphs include field interactions.

by the cortical neurons was executed for $t = 3s$ with a resolution of $1ms$ ($= 3000$ time steps in the model), resulting in smooth dynamic changes in the top layer u . Dependent on the spatial and temporal pattern of the field u , the inhibitory layer demonstrates analog field activity v . Figure 3.10 shows the activity of the field u (top) and the field v (bottom) for an example point in time. The physical 2D configuration of the PY neurons that was chosen for all simulations can also be

3.3 cAg-NPs Effects on 2D Neural Field Oscillations

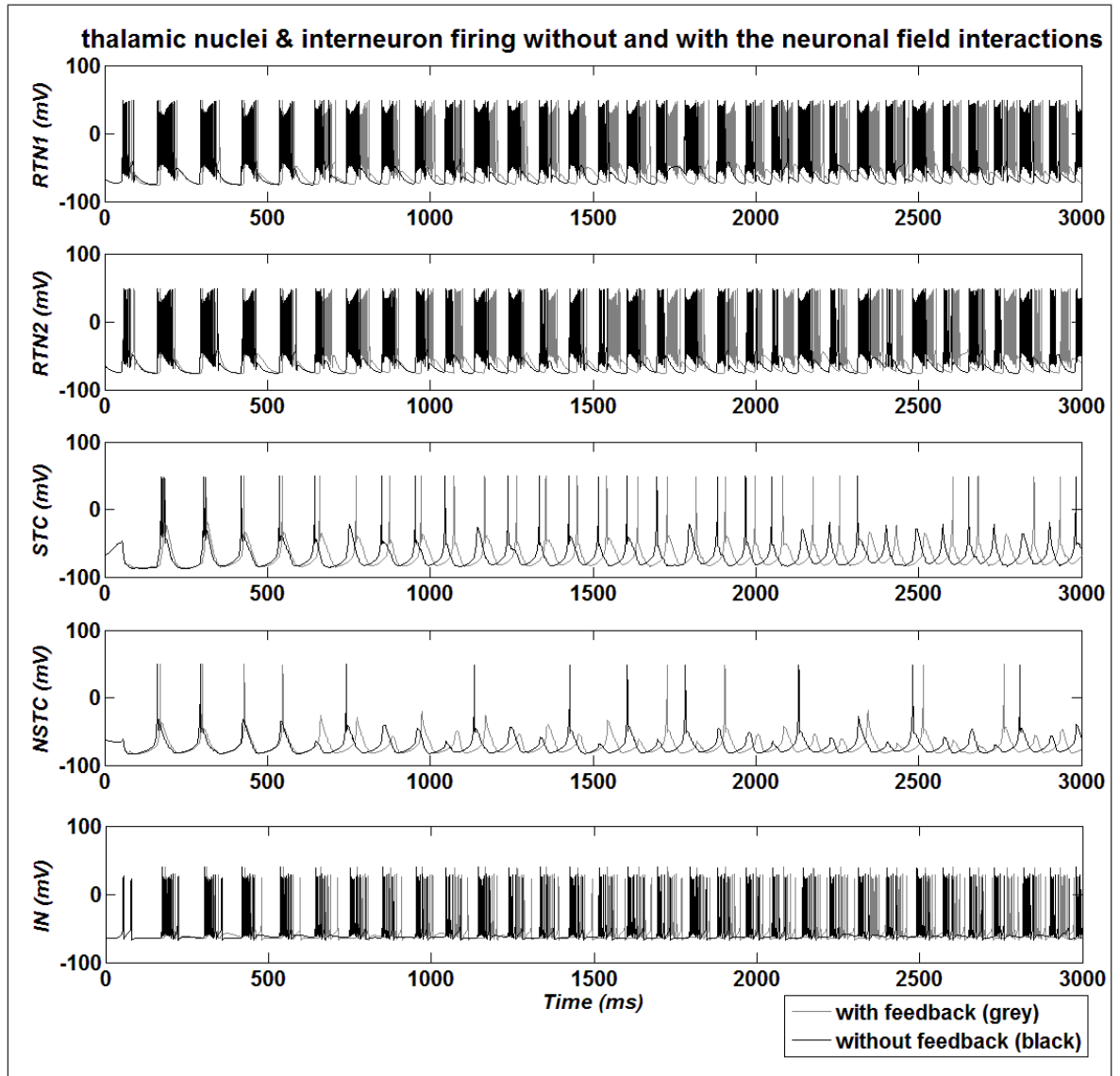


Figure 3.9: Comparison of the membrane potentials (in mV) for all involved thalamic neurons, i.e., RTN1, RTN2, STC and NSTC, with and without neural field interactions as a function of time (ms). Black graphs depict the firing without field interactions to PYs, grey graphs include field interactions.

3.3 cAg-NPs Effects on 2D Neural Field Oscillations

derived from this illustration.

After simulating the cortical field potentials emerging from thalamocortical inter-

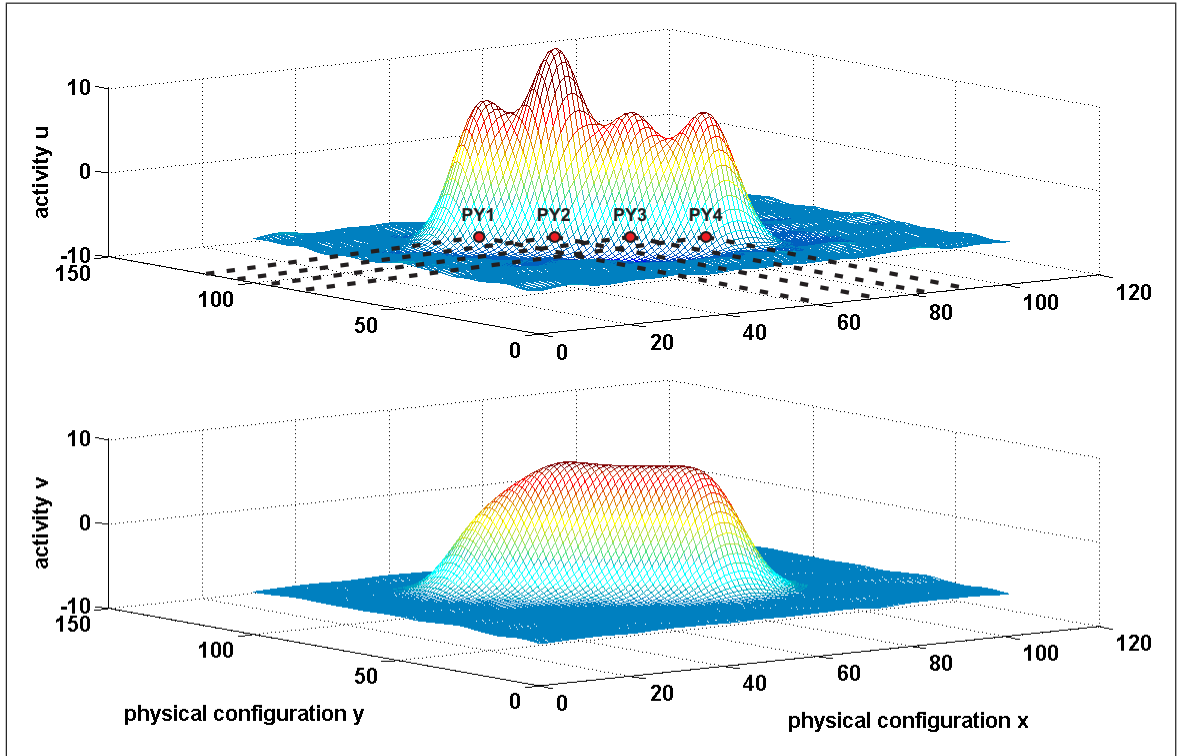


Figure 3.10: Example for the field activity of the 1st (excitatory) layer u (top) and the corresponding activity of the 2nd (inhibitory) layer v (bottom). The physical configuration of the PY neurons which was chosen for all simulations can also be derived from this illustration. All field potentials are in $10^1 \mu V$.

actions on a small cortical patch, it was examined how much those field potentials affect its generating neurons, i.e., how the field potentials feed back in real time to the two-compartment pyramidal neurons influence the circuit's signaling behavior. Thus it could be estimated if this closed loop effects have the potential to produce diversified neural field activity.

After superimposing the emerging spatiotemporal field potentials on the single neuron models, the simulations were restarted: The grey graphs show the somatic firing of the four PY neurons including field interactions in Figure 3.9 and the corresponding IN and thalamic neuron potentials in Figure 3.10.

Figure 3.11 is now illustrating the emerging field potentials in 2D of four pyramidal neurons without (left) and with (middle) the influence of the feedback to pyramidal neurons for an example time point. The right panel shows the difference of these two field potentials for the same time point. These results are illustrated again

3.3 cAg-NPs Effects on 2D Neural Field Oscillations

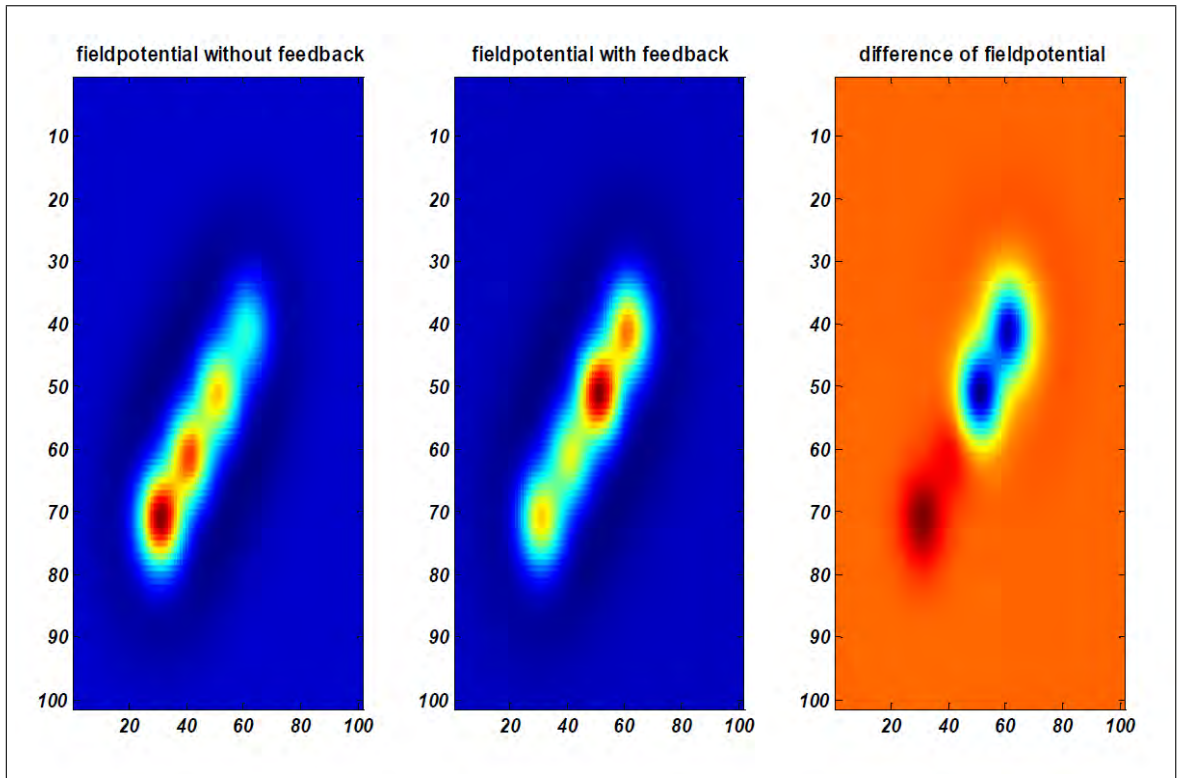


Figure 3.11: Emerging field potentials in 2D of four pyramidal neurons without (left) and with (middle) the influence of the feedback to pyramidal neurons and difference (right) of these two field potentials for the same example time point.

in Figure 3.12. In contrast, this one shows the neural field potentials generated by the PY neurons for four example points of time as 3D plots. The left column of Figure 3.12 illustrates the field potential patterns at those time points without feeding those back to the Hodgkin-Huxley domain and the right column depicts the corresponding potentials at the same time points including the feedback loop for comparison issues.

After successfully simulating the cortical field potentials emerging from a small cortical patch of synchronized Llinás-model based thalamocortical interactions, it was examined if it is possible to also observe effects in those field potentials engendered by NPs. Therefore, the presence of Ag-NPs in the referred thalamic neurons was considered and the resulting field activity was simulated again for $t=1500s$.

Figure 3.3 illustrates finally these neural field potentials including field interactions (feedback) in the domain of Hodgkin-Huxley and the interaction of cAg-NPs in thalamic cells for four representative points in time on the right. The right panel of 3.3 shows the corresponding field potentials without the presence of cAg-NPs in

3.3 cAg-NPs Effects on 2D Neural Field Oscillations

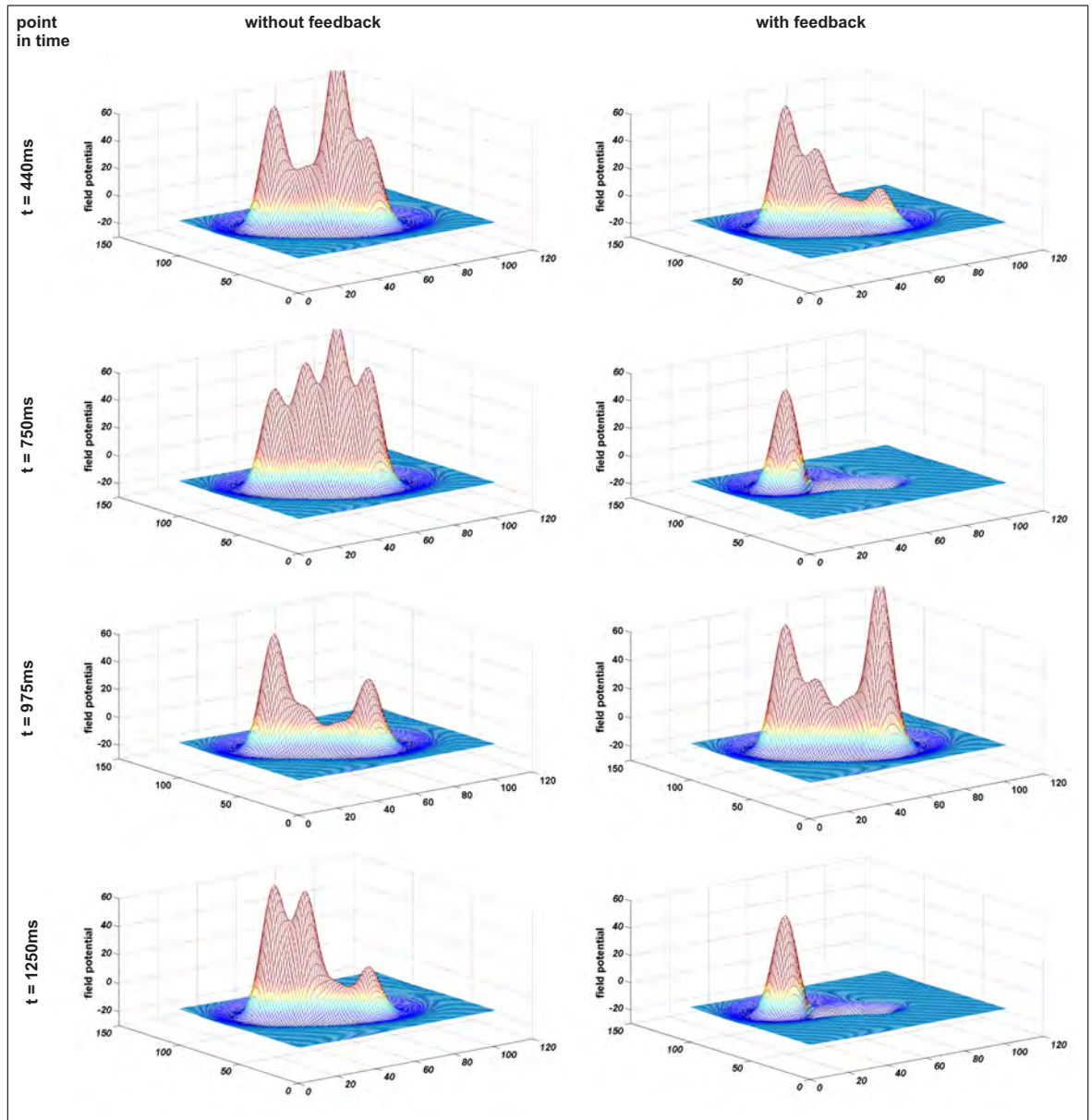


Figure 3.12: Comparison of the generated neural field potentials (1^{st} layer) at four randomly chosen points of time with and without feeding back the field potentials to the single neuron models. All field potentials are in $10^1\mu V$.

3.3 cAg-NPs Effects on 2D Neural Field Oscillations

the referred thalamic cells.

3.3 cAg-NPs Effects on 2D Neural Field Oscillations

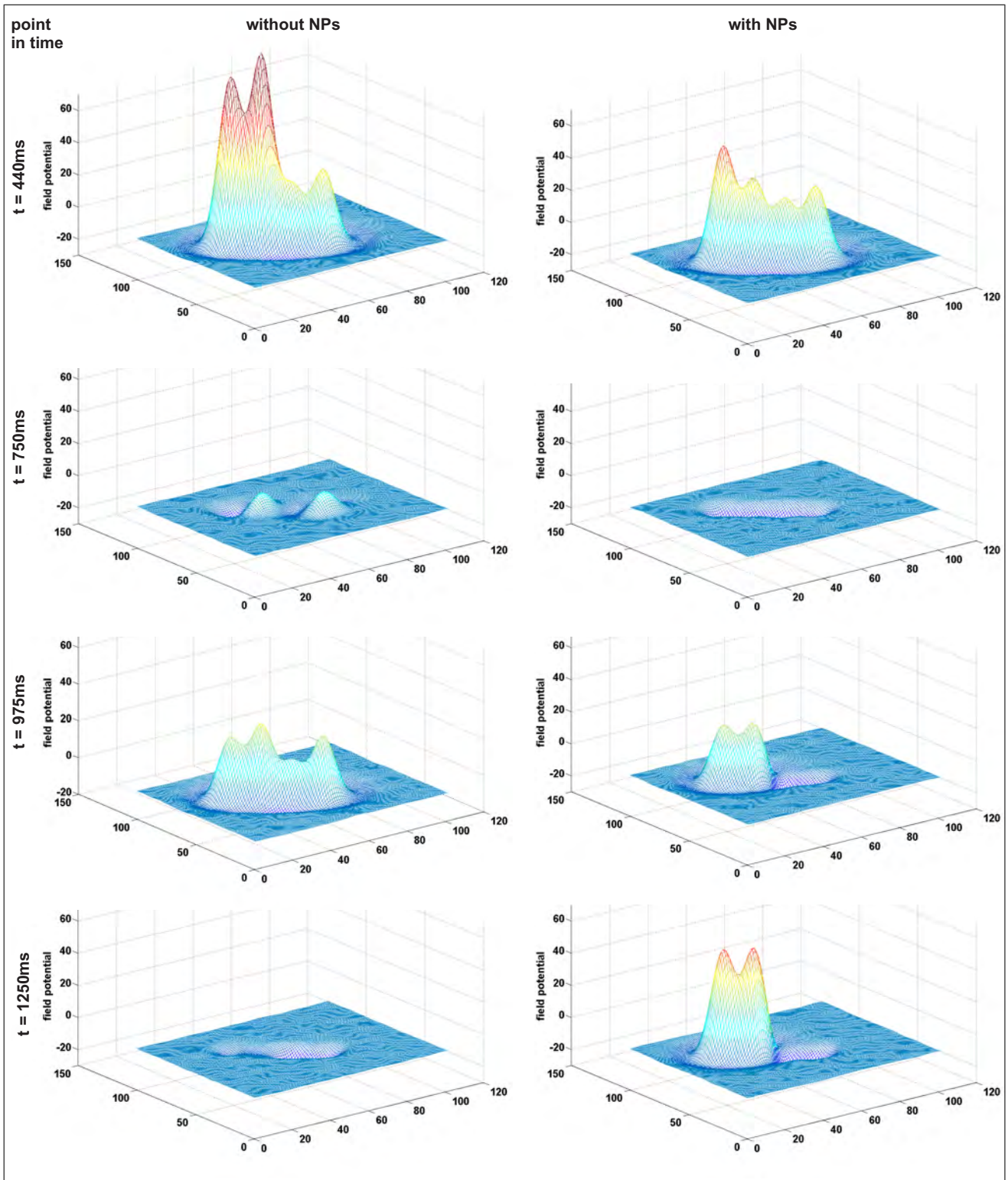


Figure 3.13: Comparison of the generated neural field potentials (1st layer) at four randomly chosen points of time including field potential feedback with and without the application of Ag-NPs on thalamic neurons. All field potentials are in $10^1 \mu V$.

3.3 cAg-NPs Effects on 2D Neural Field Oscillations

Table 3.3: Changes in neuronal bursting after cAg-NPs application.

neuron type	interburst interval (ms)	σ_a interburst interval (ms)	\sim interburst frequency (Hz)	intraburst frequency (Hz)	σ_a intraburst frequency (Hz)
PY1 before cAg-NPs app.	120	19	6.7	291	1
PY1 after cAg-NPs app.	110	32	7.5	278.5	4.5
PY2 before cAg-NPs app.	96	33	6.5	271	4
PY2 after cAg-NPs app.	93	33	7.75	266.5	6.5
PY4 before cAg-NPs app.	139	56	4.75	296	1
PY4 after cAg-NPs app.	125	57	6.7	691.5	2.5
IN before cAg-NPs app.	103	23	7.5	201	15.5
IN after cAg-NPs app.	89	27	8	139	2.5
RTN1 before cAg-NPs app.	68	15	7.5	348.5	49.5
RTN1 after cAg-NPs app.	65	8	7.75	366	72
RTN2 before cAg-NPs app.	75	15	7.5	293.5	35.5
RTN2 after cAg-NPs app.	69	12	7.75	332.5	19.5

^a σ = standard deviation.

Chapter 4

Discussion

4.1 cAg-NPs Effects on Neuronal Cells *in vitro* and *in silico*

The patch-clamp measurements show that the application of cAg-NPs to chromaffin-cells reduces the amplitude of sodium-currents. The changes were rapid, partially reversible and dose-dependent. Based on the Hodgkin-Huxley-fitting, the cAg-NPs may affect the electrically charged h -particles by the alteration to the non-inactivating (towards open) state at changed transfer rate coefficient α_h . Additionally, the m -particles are influenced by the transition to the open and closed state as α_m plus β_m is altered.

However, the lack of a rightward shift of the I-V curves (Figure 3.1) indicate that any effects on voltage sensors or gating lead to failure to gate or a decreased channel conductance, which are not overcome by stronger depolarization. A shift in null potential, which might result from a change in ion selectivity, also cannot explain the reduced I_{Na} . It was not possible to distinguish between these two possibilities based on the present data. It is possible that cAg-NPs may produce mechanical effects on the ion-channels leading to lower conductivity or fewer channels which reach the open state. An interaction of cAg-NPs with the reference-electrode can be ruled out since the holding current was not affected by cAg-NPs addition.

4.2 cAg-NPs Effects on the Neuronal Feedback Circuit

In any case, the net effects of cAg-NPs on neuronal feedback circuits will be reduced excitability of affected cells and such effects could have been simulated. The simulation indicates that application of cAg-NPs in the thalamus will result in dramatic changes in thalamocortical activity. This could occur, for instance, if cAg-NPs used as a drug carrier crossed the round window membrane of the cochlea and were retrograde transported. Praetorius et al. 2007 evaluated the safety and distribution of *Cy3*-labeled Silica-NPs in *in vivo* experiments by placing them on the round window membrane of adult mice. After 4 days, SiO_2 -NPs signals could be found in the superior olivary complex. Their observation proposes a retrograde axonal transport for the applied NPs. The developed *in silico* model enables investigation of potential effects of NPs which enter the CNS.

The simulations committed examine the systemic influences of cAg-NPs in neuronal systems. Though the computational model of the thalamocortical network is highly simplified and does not consider inputs or projections to other involved brain regions, it indicates that reduced excitability of a few neurons in such a circuit has distinct effects on network activity. Such was observable in Figure 3.6, Figure 3.7 and compendious in Table 2. The model is able to predict possible consequences of cAg-NPs introduction to neuronal feedback circuits.

The *in vivo* effects of such NPs on any network will likely be complicated by additional effects of NPs. The author introduced changes in voltage dependent sodium currents in the developed model. NPs induced changes in mechanisms affecting excitability such as other ion channels were not examined though effects on potassium channels have been reported (Liu et al. (2011)).

4.3 cAg-NPs Effects on 2D Neural Field Oscillations

After the membrane potentials of the involved cortical and thalamic neurons could have been calculated and illustrated as bursting activity over simulation time (Figure 3.6 and Figure 3.7), the neural field potentials that were generated by the

4.3 cAg-NPs Effects on 2D Neural Field Oscillations

pyramidal neurons on a very small cortical patch (Figure 3.10) could have been successfully modeled. Thereafter, the motivation was to employ this model to investigate how the neural field potentials in turn affect the single neurons' signaling behavior (i.e., closing the feedback loop). By first inspection of possible differences in the modeled firing behavior between '*including field feedback*' and '*not including field feedback*', it can be noted in Figure 3.8 and Figure 3.9 that changes in burst timing and duration emerged after feeding the field potentials back to the neuron models. The firing behavior of all PY neurons (Figure 3.8) is found to be changed after field effect consideration. In some cases the action potential generation was also found to be weaker in the '*no feedback*' model (e.g. PY3). A statistical review (Table 4.3) offers that for the PY neurons the frequency of the oscillating activity has decreased around $15 - 30Hz$ for intraburst frequencies and again around $0.7 - 2.0Hz$ for interburst frequencies. The cortical IN responses behave similar:

Table 4.1: Average intra- & interburst frequency in cortical neurons.

	intraburst frequency (Hz)		interburst frequency (Hz)	
	without feedback	with feedback	without feedback	with feedback
PY1	300	270	12	10
PY2	299	270	10	10
PY3	370	298	5	5.3
PY4	295	280	6.33	5.66
IN	237.23	179.8	10.67	10.00

here, the difference in intraburst frequency is $\sim 57Hz$ and for the interburst frequency only $\sim 0.67Hz$. Regarding the thalamic neurons and the cortical IN, it is observable in Figure 3.9 that the spiking activity is also diversified after field effect consideration. With respect to the statistical values of Table 4.3, in contrast to cortical neurons, the thalamic interburst frequencies are found to be slightly increased where the intraburst frequencies remain almost the same.

By comparison of the generated neural field potentials at randomly chosen time points (Figure 3.11 and Figure 3.12) with and without feeding back the field potentials to the single neuron models, it is clearly observable that the generated neural

4.3 cAg-NPs Effects on 2D Neural Field Oscillations

Table 4.2: Average intra- & interburst frequency in thalamic neurons.

	intra-burst frequency (Hz)		interburst frequency (Hz)	
	without feedback	with feedback	without feedback	with feedback
RTN1	221.7	308.7	10.50	10.33
RTN2	261.3	318.45	10.50	10.33
STC	336.13	404.68	10.30	10.00
NSTC	416	416	3.33	2.60

field potentials are extensive diversified in all chosen example time points. This was found to be the case for all time-points throughout the whole simulation.

The final task was then to compare the emerging field potentials (including feedback) with and without the absence of cAg-NPs. Figure 3.13 reveals that cAg-NPs brought into contact with thalamic cells of the circuit actually lead to diversified neuronal field activity of much higher spatial domains. This was also found for all time-points throughout the whole simulation.

- **Compendious**, the study was able to expand the model introduced by Llinás et al. to additionally observe related field potentials that spread over a spatial cortical patch. Incorporating the idea of NPs acting as neuromodulators to this new model, the emerging field potentials of the two-dimensional two-layer approach is found to be extensive diversified after presuming the application of NPs to thalamic neurons. In a single neuron model study (Busse et al. 2010, 2013), the author was able to identify the impact of Ag-NPs on the cells ionic currents. This little change was adopted to model the potential effects of those particles on small sized neuronal feedback circuits (Busse et al. 2011b, 2013). Even though the observed NPs induced diversifications in the feedback networks signaling behavior was quite small, when integrating the thalamocortical model from a functional column into the dynamics of spatiotemporal neural field potentials (Busse et al. 2011a), entirely altered field potentials could be observed after particle distribution on few thalamic cells. NPs in thalamic tissue may cause distortions in cortical field potentials, where especially the NSTC cause a spread of these modulatory effects over multiple cortical areas in consequence. This model may subserve as basic approach to estimate the

4.3 cAg-NPs Effects on 2D Neural Field Oscillations

spatiotemporal dynamics of cortical field potentials that may be electrophysiological measurable.

Chapter 5

Conclusion

The *in vitro* measurements that served as basis for this study have shown that the application of cAg-NP to chromaffin cells reduce the amplitude of sodium currents without an appreciable shift in either activation voltage or null potential. Those changes were found to be rapid, partially reversible and dose-dependent. It was not possible to figure out if cAg-NP may produce mechanical effects on the ion channels leading to lower conductivity nor if there are fewer channels that reach the open state. In any case, the net effects of cAg-NP on neuronal feedback circuits will be reduced excitability of affected cells, and we have simulated these effects.

Transferring those findings to neuronal circuits via modeling of the thalamocortical network resulted in the possibility to make initial predictions as to what effects coated silvernanoparticles' suppression of sodium currents will have on thalamocortical circuits. This model extension predicted that an alteration of the properties of RTN, STC or NSTC neurons, as they were found by the HH-model fits of I_{Na} after treatment with cAg-NPs, end in large alterations of network signalling behavior. It can be expected that NPs brought into contact with few cells of a neuronal feedback circuit will extensively alter network rhythms of large neuronal populations *in vivo*. Next, the *in silico* thalamocortical circuit model was additionally expanded to observe related field potentials spreading over a spatial cortical patch. Incorporating the idea of back propagating the field potentials effecting single neuron activity to this new model, the emerging field potentials of a basic two-dimensional two-layer approach was also found to be widely diversified after assuming cAg-NP presence in network thalamic neurons. The field potentials seem to have strong effects on the action potential generation of neurons that are exposed to those fields as well. The

Bibliography

results presume that as a consequence of cAg-NPs affected thalamocortical network cells, the emerging *in vivo* neural field potentials will be found to be extensively diversified. This model may also subserve as basic approach to estimate the spatiotemporal dynamics of cortical field potentials on a very small cortical patch that may be electrophysiologically measurable.

In future, two-dimensional multi-electrode array as well as voltage sensitive dye measurements with high spatiotemporal resolution will be carried out on rat auditory cortex. The experimental data will be applied to validate and also to extend the model with the focus on underlying neuronal mechanisms. Besides, cAg-NPs effects on other aspects of membrane excitability will be investigated and these findings will be included into the model. The experimental data will be applied to compare and also to extend the model with the focus on recovering estimates of the underlying mechanisms by means of excitable cells exposed to NPs. Furthermore, different NPs types, sizes, as well as their coatings' material and surface structure will be investigated in respect of their stability and impact on neuronal cells and tissues.

Bibliography

- Amari, S. (1977). Dynamics of pattern formation in lateral inhibition type neural fields. *Biological Cybernetics*, 27:77–87.
- Anastassiou, C. A., Perin, R., Markram, H., and Koch, C. K. (2011). Ephaptic coupling of cortical neurons. *Nature neuroscience*, 14(2):217–223.
- Aram, P., Freestone, D. R., Dewar, M., Scerri, K., Jirsa, V., Grayden, D. B., and Kadiramanathan, V. (2013). Spatiotemporal multi-resolution approximation of the amari type neural field model. *NeuroImage*, 66:88–102.
- Bazhenov, M., Timofeev, I., Steriade, M., and Sejnowski, T. J. (1998). Cellular and Network Models for Intrathalamic Augmenting Responses During 10-Hz Stimulation. *J. Neurophysiol.*, 79:2730–2748.
- Bazhenov, M., Timofeev, I., Steriade, M., and Sejnowski, T. J. (2002). Model of Thalamocortical Slow-Wave Sleep Oscillations and Transitions to Activated States. *The Journal of Neuroscience*, 22(19):8691–8704.
- Beurle, R. L. (1956). Properties of a mass of cells capable of regenerating pulses. *Philosophical Transactions of the Royal Society of London B.*, 240:55–94.
- Brumberg, J. C., Nowak, L. G., and McCormick, D. A. (2000). Ionic mechanisms underlying repetitive high-frequency burst firing in supragranular cortical neurons. *J Neurosci.*, 20:4829–4843.
- Busse, M., Kraegeloh, A., Arzt, E., and Strauss, D. (2011a). Modeling the influences of nanoparticles on neural field oscillations in thalamocortical networks. *Conf Proc IEEE Eng Med Biol Soc.*, pages 136–139.
- Busse, M., Kraegeloh, A., Stevens, D., Cavelius, C., Rettig, J., Arzt, E., and Strauss, D. J. (2010). Modeling the effects of nanoparticles on neuronal cells:

Bibliography

- From ionic channels to network dynamics. *Conf Proc IEEE Eng Med Biol Soc.*, 1:3816–3819.
- Busse, M., Stevens, D., Kraegeloh, A., Cavelius, C., Vukelic, M., Arzt, E., and Strauss, D. (2013). Estimating the modulatory effects of nanoparticles on neuronal circuits using computational upscaling. *Int J Nanomedicine.*, pages 3559–72.
- Busse, M., Vukelic, M., Kraegeloh, A., Stevens, D., Rettig, J., Arzt, E., and Strauss, D. (2011b). On the possible effects of nanoparticles on neuronal feedback circuits: A modeling study. *Conf Proc IEEE EMBS NER*, pages 136–139.
- Catterall, W. A., Goldin, A. L., and Waxman, S. G. (2005). International union of pharmacology. xlvii. nomenclature and structure-function relationships of voltage-gated sodium channels. *Pharmacological Reviews.*, 57:397–409.
- Chithrani, B., Ghazani, A., and Chan, W. (2006). Determining the size and shape dependence of gold nanoparticle uptake into mammalian cells. *Nano Lett.*, 6:662–668.
- Crick, F. (1984). Function of the thalamic reticular complex: the searchlight hypothesis. *Proceedings of the National Academy of Sciences*, 81(14):4586–4590.
- da Silva, F. H. L., Rotterdam, A. V., Barts, P., Heusden, E. V., and Burr, W. (1976). Models of neuronal populations: the basic mechanisms of rhythmicity. *Progress in Brain Research*, 45:281–308.
- David, O. and Friston, K. J. (2003). A neural mass model for meg/eeg: coupling and neuronal dynamics. *NeuroImage*, 20(3):1743–1755.
- Dayan, P. and Abbott, L. F. (2001). *Theoretical Neuroscience: Computational and Mathematical Modeling of Neural Systems*. The MIT Press, Cambridge, Massachusetts London, England.
- Deco, G., Jirsa, V., Robinson, P., Breakspear, M., and Friston, K. (2008). The dynamic brain: from spiking neurons to neural masses and cortical fields. *PLoS Comput Biol.*, 4(8):e1000092.
- Destexhe, A., Bal, T., McCormick, D. A., and Sejnowski, T. J. (1996a). Ionic Mechanisms Underlying Synchronized Oscillations and Propagating Waves in a Model of Ferret Thalamic Slices. *J. Neurophysiol.*, 76(3):2049–2070.

Bibliography

- Destexhe, A., Contreras, D., Sejnowski, T. J., and Steriade, M. (1994a). A Model of Spindle Rhythmicity in the Isolated Thalamic Reticular Nucleus. *J. Neurophysiol.*, 72(2):803–818.
- Destexhe, A., Contreras, D., and Steriade, M. (1998a). Mechanisms Underlying the Synchronizing Action of Corticothalamic Feedback Through Inhibition of Thalamic Relay Cells. *J. Neurophysiol.*, 79:999–1016.
- Destexhe, A., Contreras, D., Steriade, M., Sejnowski, T. J., and Huguenard, J. R. (1996b). In Vivo, In Vitro, and Computational Analysis of Dendritic Calcium Currents in Thalamic Reticular Neurons. *J. Neurosci.*, 16:999–1016.
- Destexhe, A., Mainen, Z. F., and Sejnowski, T. J. (1994b). An Efficient Method for Computing Synaptic Conductances Based on a Kinetic Model of Receptor Binding. *Neural Computation*, 6:14–18.
- Destexhe, A., Mainen, Z. F., and Sejnowski, T. J. (1998b). Kinetic Models of Synaptic Transmission. *in: Methods in Neuronal Modeling (2nd Edition)*, C. Koch and I. Segev (Eds.), The MIT Press, Cambridge.
- Dobrovinski, K. and Herrmann, J. M. (2009). Stability of localized patterns in neural fields. *Neural computation*, 21(4):1125–1144.
- El-Ansary, A. and Al-Daihan, S. (2009). On the toxicity of therapeutically used nanoparticles: an overview. *J Toxicol.*
- Faber, J. (2011). Computational neuroscience. *National Bernstein Network Computational Neuroscience*, 2.Edition:1–42.
- Fenwick, E. M., Marty, A., and Neher, E. (1982). A Patch-Clamp Study of Bovine Chromaffin Cells and of Their Sensitivity to Acetylcholine. *J. Physiol.*, 331:577–597.
- Ferguson, K. A. and Campbell, S. A. (2009). A two compartment model of a cal pyramidal neuron. *Can Appl Math Q*, 17(2):293–307.
- Freestone, D. R., Aram, P., Dewar, M., Scerri, K., Grayden, D. B., and Kadiramanathan, V. (2011). A data-driven framework for neural field modelling. *NeuroImage*, 56(3):1043–1058.
- Goldin, A. L. (2001). Resurgence of sodium channel research. *Annu. Rev. Physiol.*, 63:871–894.

Bibliography

- Goldin, A. L., Barchi, R. L., Caldwell, J., Hofmann, F., Howe, J. R., and et al., J. C. H. (2000). Nomenclature of voltage-gated sodium channels. *Neuron*, 28:365–368.
- Golomb, D. and Amitai, Y. (1997). Propagating Neuronal Discharges in Neocortical Slices: Computational and Experimental Study. *J. Neurophysiol.*, 78:1199–1211.
- Golomb, D., Shedmi, A., Curt, R., and Ermentrout, G. B. (2006). Persistent Synchronized Bursting Activity in Cortical Tissues With Low Magnesium Concentration: A Modeling Study. *J. Neurophysiol.*, 95:1049–1067.
- Golomb, D., Wang, X. J., and Rinzel, J. (1994). Synchronization Properties of Spindle Oscillations in a Thalamic Reticular Nucleus Model. *J. Neurophysiol.*, 72(3):1109–1126.
- Golomb, D., Wang, X. J., and Rinzel, J. (1996). Propagation of Spindle Waves in a Thalamic Slice Model. *J. Neurophysiol.*, 75(2):750–769.
- Gray, C. M. and McCormick, D. A. (1996). Chattering cells: superficial pyramidal neurons contributing to the generation of synchronous oscillations in the visual cortex. *Science.*, 274:109–113.
- Gray, C. M. and Singer, W. (1989). Stimulus-specific Neuronal Oscillations in Orientation Columns of Cat Visual Cortex. *Proc. Nati. Acad. Sci. USA*, 86:1698–1702.
- Gregoriou, G. G., Gotts, S. J., Zhou, H., and Desimone, R. (2009). High-frequency, long-range coupling between prefrontal and visual cortex during attention. *Science.*, 324:1207–1210.
- Gupta, A. (2003). *Structure, Function and Plasticity of Neocortical Microcircuits*. Weizmann Institute of Science, Rehovot.
- Gupta, A. and Gupta, M. (2005). Synthesis and surface engineering of iron oxide nanoparticles for biomedical applications. *Biomaterials.*, 26:3995–4021.
- Gupta, A., Wang, Y., and Markram, H. K. (2000). Organizing principles for a diversity of gabaergic interneurons and synapses in the neocortex. *Science*, 287:273–278.

Bibliography

- Hadipour-Niktarash, A. (2006). A Computational Model of how an Interaction between the Thalamocortical and Thalamic Reticular Neurons Transforms the Low-Frequency Oscillations of the Globus Pallidus. *J. Comput. Neurosci.*, 20:299–320.
- Herz, A. V. M., Gollisch, T., Machens, C. K., and Jaeger, D. (2006). Modeling Single-Neuron Dynamics and Computations: A Balance of Detail and Abstraction. *SCIENCE*, 314:80–85.
- Hodgkin, A. L. and Huxley, A. F. (1952). A quantitative description of membrane current and its application to conduction and excitation in nerve. *J Physiol.*, 117:500–544.
- Hughes, S. W., Errington, A., Lorincz, M. L., Kkesi, K. A., Juhsz, G., Orbn, G., Cope, D. W., and Crunelli, V. (2008). Novel modes of rhythmic burst firing at cognitively-relevant frequencies in thalamocortical neurons. *Brain Res.*, 1235:12–20.
- Huguenard, J. R. and McCormick, D. A. (1992). Simulation of the Currents Involved in Rhythmic Oscillations in Thalamic Relay Neurons. *J. Neurophysiol.*, 68:1373–1383.
- Izhikevich, E. M. (2004). Which Model to Use for Cortical Spiking Neurons? *IEEE TRANSACTIONS ON NEURAL NETWORKS*, 15(5):1063–1070.
- Izhikevich, E. M. (2007). *Dynamical Systems in Neuroscience: The Geometry of Excitability and Bursting*. The MIT Press, Cambridge, Massachusetts London, England.
- Jansen, B. H. and Rit, V. G. (1995). Electroencephalogram and visual evoked potential generation in a mathematical model of coupled cortical columns. *Biological Cybernetics*, 73(4):357–366.
- Jiang, W., Kim, B. Y., Rutka, J. T., and Chan, W. C. (2008). Nanoparticle-mediated cellular response is size-dependent. *Nat Nanotechnol.*, 3:131–132.
- Jones, E. G. (2002). Thalamic circuitry and thalamocortical synchrony. *Philosophical Transactions of the Royal Society of London. Series B: Biological Sciences.*, 357(1428):1659–1673.

Bibliography

- Kishimoto, K. and Amari, S. I. (1979). Existence and stability of local excitations in homogeneous neural fields. *Journal of Mathematical Biology*, 7(4):303–318.
- Knight, B. W. (1972). Dynamics of encoding in a population of neurons. *The Journal of General Physiology*, 59(6):734–766.
- Kobayashi, H., Shiraishi, S., Yanagita, T., Yokoo, H., Yamamoto, R., Minami, S., Saitoh, T., and Wada, A. (2002). Regulation of Voltage-Dependent Sodium Channel Expression in Adrenal Chromaffin Cells: Involvement of Multiple Calcium Signaling Pathways. *Ann N Y Acad Sci.*, 971:127–134.
- Lamarre, B. and Ryadnov, M. G. (2011). Self-assembling viral mimetics: one long journey with short steps. *Macromol Biosci.*, 11(4):503–13.
- Liu, Z., Ren, G., Zhang, T., and Yang, Z. (2011). The inhibitory effects of nano-ag on voltage-gated potassium currents of hippocampal ca1 neurons. *Environ Toxicol.*, 26(5):552558.
- Liu, Z., Ren, G., Zhang, T., and Yang, Z. L. (2009). Action potential changes associated with the inhibitory effects on voltage-gated sodium current of hippocampal ca1 neurons by silver nanoparticles. *Toxicology.*, 264:179–174.
- Llinás, R., Leznik, E., and Urbano, F. J. (2002). Temporal Binding via Cortical Coincidence Detection of Specific and Nonspecific Thalamocortical Inputs: A Voltage-dependent Dye-imaging Study in Mouse Brain Slices. *Proc. Natl. Acad. Sci.*, 99(1):449–454.
- Llinás, R. and Ribary, U. (1993). Coherent 40-Hz Oscillation Characterizes Dream State in Humans. *Proc. Natl. Acad. Sci. USA*, 90:2078–2081.
- Llinás, R., Ribary, U., Contreras, D., and Pedroarena, C. (1998). The Neuronal Basis for Consciousness. *Philos. Trans. R. Soc. Lond. B*, 353:1841–1849.
- Llinás, R., Ribary, U., Joliot, M., and Wang, X. J. (1994). Content and Context in Temporal Thalamocortical Binding. *in: Temporal Coding in the Brain*, G. Buzski et al. (Eds.), Springer-Verlag Berlin Heidelberg.
- Lorincz, A. and Nusser, Z. A. (2010). Molecular identity of dendritic voltage-gated sodium channels. *Science.*, 328(5980):906–909.
- Luck, S. J. (2005). *n introduction to the event-related potential technique (cognitive neuroscience)*. MIT Press, Cambridge.

Bibliography

- Malmivuo, J. and Plonsey, R. (1995). *Bioelectromagnetism*. New York: Oxford University Press, New York.
- McCormick, D. A. and Huguenard, J. R. (1992). A Model of Electrophysiological Properties of Thalamocortical Relay Neurons. *J. Neurophysiol.*, 68:1384–1400.
- Natschläger, T., Markram, H., and Maass, W. (2003). *Computer models and analysis tools for neural microcircuits*. In: R. Ktter, editor. *Neuroscience Databases*. Springer, New York.
- Nelson, M. E. (2004). *Electrophysiological models*. In: S. Koslow, S. Subramaniam, editors. *Databasing the Brain: From Data to Knowledge*. Wiley, New York.
- Oberdörster, G. (2010). Safety assessment for nanotechnology and nanomedicine: concepts of nanotoxicology. *J Intern Med.*, 267:89–105.
- Otis, T. S., Konink, Y. D. D., and Mody, I. (1993). Characterization of Synaptically Elicited GABA_B Responses Using Patch-Clamp Recordings in Rat Hippocampal Slices. *J. Physiol. (London)*, 463:391–407.
- Pellegrino, T., Manna, L., Kudera, S., Liedl, T., Koktysh, D., Rogach, A. L., Keller, S., Rdlar, J., Natile, G., and Parak, W. J. (2004). Hydrophobic nanocrystals coated with an amphiphilic polymer shell: A general route to water soluble nanocrystals. *Nano Lett.*, 127:703–707.
- Pinsky, P. F. and Rinzel, J. (1994). Intrinsic and network rhythmogenesis in a reduced traub model for ca3 neurons. *Journal of computational neuroscience*, 1(1-2):39–60.
- Potthast, R. and beim Graben, P. (2009). Dimensional reduction for the inverse problem of neural field theory. *Frontiers in computational neuroscience*, 3:17:1–14.
- Praetorius, M., Brunner, C., Lehnert, B., Klingmann, C., Schmidt, H., Staecker, H., and Schick, B. (2007). Transsynaptic delivery of nanoparticles to the central auditory nervous system. *Acta Otolaryngol.*, 127:486–490.
- Price, K. V., Storn, R. M., and Lampinen, J. A. (2005). *Differential Evolution: A Prictical Approach to Global Optimization*. Springer-Verlag, Berlin/Heidelberg.

Bibliography

- Ribary, U., Cappel, J., Yamamoto, T., Suk, J., and Llinás, R. (1991a). Anatomical localization revealed by meg recordings of the human somatosensory system. *Electroencephalogr. Clin. Neurophysiol.*, 78:185–196.
- Ribary, U., Ioannides, A. A., Singh, K. D., Hasson, R., Bolton, J. P. R., Lado, F., Mogilner, A., and Llinás, R. (1991b). Magnetic Field Tomography of Coherent Thalamocortical 40-Hz Oscillations in Humans. *Proc. Natl. Acad. Sci. USA*, 8:11037–11041.
- Rinzel, J. and Ermentrout, G. B. (1989). *Analysis of neural excitability and oscillations*. In: C. Koch, I. Segev, editors. *Methods in neuronal modelling*. MIT Press, Cambridge.
- Roxin, A., Brunel, N., Hansel, D., Mongillo, G., and van Vreeswijk, C. (2011). On the distribution of firing rates in networks of cortical neurons. *The Journal of Neuroscience*, 31(45):16217–26.
- Royeck, M., Horstmann, M., Remy, S., Reitze, M., Yaari, Y., and Beck, H. A. (2008). Role of axonal nav1.6 sodium channels in action potential initiation of ca1 pyramidal neurons. *Journal of Neurophysiology.*, 100(4):2361–2380.
- Shepherd, G. M. (2001). *The Synaptic Organization of the Brain; Fifth Edition*. Oxford University Press, Inc., Oxford New York.
- Singer, W. (1993). Synchronization of Cortical Activity and its Putative Role in Information Processing and Learning. *Annu Rev Physiol*, 55:349–374.
- Singer, W. (1999). Neuronal Synchrony: A Versatile Code for the Definition of Relations? *Neuron*, 21(1):49–65.
- Stemmler, M. and Koch, C. (1999). How voltage-dependent conductances can adapt to maximize the information encoded by neuronal firing rate. *Nature neuroscience*, 2(6):521–527.
- Steriade, M., Timofeev, I., Drmler, N., and Grenier, F. (1998). Dynamic properties of corticothalamic neurons and local cortical interneurons generating fast rhythmic (30-40 Hz) spike bursts. *J Neurophysiol.*, 79:483–490.
- Thomson, A. M., West, D. C., Wang, Y., and Bannister, A. P. (2002). Synaptic connections and small circuits involving excitatory and inhibitory neurons in lay-

Bibliography

- ers 25 of adult rat and cat neocortex: triple intracellular recordings and biocytin labelling in vitro. *Cerebral Cortex*, 12(9):936–953.
- Tischler, A. S. (2002). Chromaffin cells as models of endocrine cells and neurons. *Ann N Y Acad Sci.*, 971:366–370.
- Toledo-Aral, J. J., Moss, B. L., He, Z., Koszowski, A. G., Whisenand, T., and et al., S. R. L. (1997). Identification of pn1, a predominant voltage-dependent sodium channel expressed principally in peripheral neurons. *Proceedings of the National Academy of Sciences of the United States of America.*, 94:1527–1532.
- Traub, R. D. and Miles, R. (1991). *Neural Networks of Hippocampus*. Cambridge University Press, Cambridge.
- Unfried, K., Albrecht, C., Klotz, L. O., Mikecz, A. V., Grether-Beck, S., and Schin, R. (2007). Cellular responses to nanoparticles: Target structures and mechanisms. *Nanotoxicology.*, 1:52–71.
- Vukelic, M. (2010). Intrinsic Oscillations in the Thalamocortical Circuit: A Computational Modelling Approach. *Computational Diagnostics and Biocybernetics Unit, Hochschule fr Technik und Wirtschaft des Saarlandes und Universitätsklinikum des Saarlandes, Master Thesis*, pages 1–129.
- Wang, X. J. (1998). Calcium Coding and Adaptive Temporal Computation in Cortical Pyramidal Neurons. *J Neurophysiol*, 79:1549–1566.
- Wang, X. J. and Buzsáki, G. (1996). Gamma Oscillation by Synaptic Inhibition in a Hippocampal Interneuron Network Model. *The Journal of Neuroscience*, 16(20):6402–6413.
- Wang, X. J., Golomb, D., and Rinzel, J. (1995). Emergent Spindle Oscillations and Intermittent Burst Firing in a Thalamic Model: Specific Neuronal Mechanisms. *Proc. Natl. Acad. Sci. USA*, 92:5577–5581.
- Wang, X. J. and Rinzel, J. (1992). Alternating and Synchronous Rhythms in Reciprocally Inhibitory Model Neurons. *Neural Computation*, 4:84–97.
- Wijnhoven, S. W., Peijnenburg, W. J., Herberts, C. A., Hagens, W. I., Oomen, A. G., Heugens, E. H., Roszek, B., Bisschops, J., Gosens, I., Meent, D. V. D., Dekkers, S., Jong, W. H. D., van Zijverden, H., Sips, A. J., and Geertsma, R. E.

Bibliography

- (2009). Nano-silver - a review of available data and knowledge gaps in human and environmental risk assessment. *Nanotoxicology.*, 3:109–138.
- Wilson, H. R. and Cowan, J. D. (1973). A mathematical theory of the functional dynamics of cortical and thalamic nervous tissue. *Kybernetik*, 13:55–80.
- Xu, L., Zhao, J., Zhang, T., Ren, G., and Yang, Z. L. (2009). In Vitro Study on Influence of Nanoparticles of CuO on Ca1 Pyramidal Neurons of Rat Hippocampus Potassium Currents. *Environ Toxicol.*, 24:211–217.
- Zhang, Y., Satterlee, A., and Huang, L. (2012). In vivo gene delivery by nonviral vectors: overcoming hurdles? *Mol Ther.*, 20(7):1298–304.
- Zhao, J., Xu, L., Zhang, T., Ren, G., and Yang, Z. (2009a). Influences of nanoparticle zinc oxide on acutely isolated rat hippocampal ca3 pyramidal neurons. *Neurotoxicology.*, 30:220–230.
- Zhao, J., Xu, L., Zhang, T., Ren, G., and Yang, Z. L. (2009b). Influences of Nanoparticles Zinc Oxide on Acutely Isolated Rat Hippocampal Ca3 Pyramidal Neurons. *Neurotoxicology.*, 30:220–230.

List of Publications

Publications

Original Journal Papers

- M. Busse, D. Stevens, M. Vukelic, A. Kraegeloh, C. Cavelius, E. Arzt, and D.J. Strauss. Estimating the Modulatory Effects of Nanoparticles on Neuronal Circuits Using Computational Upscaling, *International Journal of Nanomedicine*, 2013; 8: 35593572.
- X.Q. Pei, R. Bennewitz, M. Busse, and A.K. Schlarb: Effects of single asperity geometry on friction and wear of PEEK, *Wear* 304, 2013, pp. 109-117.
- M. Busse, L. Josch, and A.K. Schlarb. Artificial Neural Network Facilitated Tribo-Maps - A Procedure to Compare Materials' Tribological Characteristics in a Wide pv-Range, *Wear*, in press.
- M. Busse, N. Salafzoon, E. Gonzalez-Trejo, D. Stevens, E. Arzt, and D.J. Strauss. From Single Neuron to Neural Field Potentials: Linking the Hodgkin-Huxley Model to Amari's Equation in a Multiscale Modeling Approach, in preparation.

List of Publications

Book Chapters

- M. Busse, A.K. Schlarb, A novel Neural Network approach for modeling tribological properties of polyphenylene sulphide reinforced on different scales. In: K. Friedrich, A.K. Schlarb, Tribology of Polymeric Nanocomposites: Friction and Wear of Bulk Materials and Coatings, 2nd Edition, Elsevier, 779-793, 2013.

Original Papers in Proceedings, Medline listed

- M. Busse, Y. F. Low, F. I. Corona-Strauss, W. Delb, and D.J. Strauss. Neurofeedback by Neural Correlates of Auditory Selective Attention as Possible Application for Tinnitus Therapies, In Proceedings of the 30th Annual International Conference of the IEEE Engineering in Medicine and Biology Society, Vancouver, Canada, August 2008, pp. 5136-5139.
- M. Busse, L. Haab, M. Mariam, C. Crick, T. Weis, W. Reith, and D.J. Strauss. Assessment of Aversive Stimuli Dependent Attentional Binding by the N170 VEP Component, In Proceedings of the 31th Annual International Conference of the IEEE Engineering in Medicine and Biology Society, Minneapolis, USA, August 2009, 3975-3978.
- M. Busse, A. Kraegeloh, D. Stevens, C. Cavelius, J. Rettig, E. Arzt, and D.J. Strauss. Modeling the Effects of Nanoparticles on Neuronal Cells: From Ionic Channels to Network Dynamics, In Proceedings of the 32th Annual International Conference of the IEEE Engineering in Medicine and Biology Society, Buenos Aires, Argentina, September 2010, pp. 3816-3819.

List of Publications

- M. Busse, M. Vukelic, A. Kraegeloh, D. Stevens, J. Rettig, E. Arzt, and D.J. Strauss. On the Possible Effects of Nanoparticles on Neuronal Feedback Circuits: A Modeling Study, In Proceedings of the 5th International IEEE EMBS Conference on Neural Engineering, Cancun, Mexico, April 2011, pp. 136-139.
- L. Haab, M. Busse, M. Mariam, T. Weis, and D.J. Strauss. Detection of a Novelty Event in the Identification of Faces in a Passive VEP Task, In Proceedings of the 5th International IEEE EMBS Conference on Neural Engineering, Cancun, Mexico, April 2011, pp. 679-682.
- M. Busse, A. Kraegeloh, E. Arzt, and D.J. Strauss. Modeling the Influences of Nanoparticles on Neural Field Oscillations in Thalamocortical Networks, In Proceedings of the 34th Annual International Conference of the IEEE Engineering in Medicine and Biology Society, San Diego, September 2012, 1230-1233.

Conference Papers, Peer-Review, not in Medline

- M. Busse, Y. F. Low, F. I. Corona-Strauss, W. Delb, and D.J. Strauss. Future for Tinnitus Therapies: Neurofeedback by Neural Correlates of Auditory Selective Attention, In Proceedings of the X. International Conference in Cognitive Neuroscience (ICON X), Bodrum, Turkey, September 2008, pp. 394.

Published Conference Abstracts

- W. Delb, D.J. Strauss, D. Hecker, M. Busse, and B. Schick. Entwicklung eines durch Neurofeedback kontrollierten Aufmerksamkeitstrainings beim Tinnitus, In Proceedings of the 12. Jahrestagung der Deutschen Gesellschaft für Audiologie e.V., Innsbruck, Austria, March 2009.

Danksagung

”We are made up of thousands of others. Everyone who has ever done a kind deed for us, or spoken one word of encouragement to us, has entered into the makeup of our character and our thoughts, as well as our success.” (*George Matthew Adams*)

Die Anfertigung dieser Dissertationsschrift war nur durch die vielfältige Unterstützung verschiedener Personen möglich. An erster Stelle gebührt in diesem Zusammenhang mein besonderer Dank meinem Doktorvater und Mentor

Prof. Dr. Dr. D. J. Strauss, der es mir ermöglichte, als Ingenieur eine Promotion auf dem Gebiet der theoretischen Medizin zu unternehmen. Ihm danke ich für die freundliche Überlassung des hochinteressanten Themas sowie der familiären Aufnahme in sein Team. Insbesondere danke ich Herrn Prof. Dr. Dr. Strauss für die in einer Vielzahl von Gesprächen gewährte fachliche sowie warmherzige Betreuung.

Prof. Dr. J. Rettig danke ich aufrichtig für sein Interesse an dem Thema und der dazu bereitgestellten Infrastruktur für mein Vorhaben - ungeachtet zeitweilig beengter Räumlichkeiten und der hohen Auslastung von Personal und Messapparaturen hat er mich herzlich in seinem Labor aufgenommen.

Prof. Dr. E. Arzt und **Dr. A. Kraegeloh** gebührt ebenfalls Dank für Ihr Interesse an der numerischen Modellierung von Nanopartikel-Zell Interaktionen und der dadurch entstandenen fruchtbaren Kooperation als Basis zur Bearbeitung dieses Themas.

Dr. D. Stevens - ein Meister seiner Zunft - verdient besonderen Dank für die unermüdlich geduldige und professionelle Einführung in die Theorie und schließlich in das Handwerk der elektrophysiologischen Messung einzelner Ionenkanäle. Ich danke ihm für seine konstruktiven Ideen, die zu hervorragenden Ergebnissen führten, für seine einfühlsame, aufbauende Art und seine vorbildliche Gelassenheit im anstrengenden Forschungsalltag. Vielen Dank auch für die zahlreichen produktiven Gespräche zur Auswertung des untersuchten Materials und der konstruktiven Unterstützung bei der Erstellung meiner Veröffentlichungen.

Lars Haab, mein langjähriger und geschätzter Studiengefährte, hat mit mir alle Höhen und Tiefen des Doktorandendaseins mitgemacht. Du warst mir wahrlich ein toller Kollege, ich hätte mir keinen besseren Leidensgenossen wünschen können. Danke für Deine außerordentlich sachkundige, erfahrene und wertvolle Unterstützung. Ohne die motivierenden Kaffeepausen mit der gemeinsamen Erspinnung kreativer Ideen - von nichtlinearer dynamischer Systeme über Amari- & Kuramoto Modelle bis hin zu schwarzer Materie und einem auf Support Vector Machines basierendem Gartenzwergimperium - hätte mir der Laboralltag nur halb soviel Freude bereitet. Ich danke allen anderen "Spinnern", die für eine Weile mit mir gesponnen haben, **Corinna Bernarding**, **Farah Corona-Strauss**, **Yin Fen Low**, **Ernesto Gonzalez-Trejo**, **Novaf Özgün**, **Kristof Schubert** und **Alejandro Romero Santiago**.

Allen Kaffemaschinenaufstellern, Cafété- und Mensa-Gängern, *UdSlern*, *TU-KLlern*, *INMlern*, *Doktorandenzirklern* und all meinen betreuten Studenten bin ich sehr dankbar für die vielen schönen Stunden und die tolle Atmosphäre.

Ich Danke meinen *SDSlern*, *Garageluischern*, den **Hubigs** und nicht zuletzt **meinen Schwestern** für Ihre Warmherzigkeit, Liebe, Geduld; für Beratung und Diskussionen und sicherlich auch für die tolle Gesellschaft während Zeiten der Zerstreuung.

Der wohl größte Dank gebührt jedoch **meinen Eltern** für ihre uneingeschränkte Unterstützung in allen meinen ausbildungsspezifischen Lebensabschnitten.

Ihr habt immer Euer Äußerstes dafür getan mir alle Möglichkeiten zu eröffnen, daß ich mir meine Träume erfüllen kann.

Ohne meine **Christina** wäre ich sicher früher oder später verzweifelt. Danke für Deine Liebe und Geduld in den vergangenen zehn bewegten Jahren.

Sankt Ingbert im April 2014,

Michael Busse